

**EFFECTIVE FINITE ELEMENT MODELLING OF
MICRO-POSITIONING SYSTEMS**

A Thesis Submitted to
the College of Graduate Studies and Research
in Partial Fulfilment of the Requirements for a
Degree of Master of Science in the
Department of Mechanical Engineering
University of Saskatchewan
Saskatoon, Canada

By
Benjamin A. Zettl

PERMISSION TO USE

In presenting this thesis in partial fulfilment of the requirements for a Master of Science degree from the University of Saskatchewan, the author agrees that the Libraries of this University may make it freely available for inspection. The author further agrees that permission for copying of this thesis in any manner, in whole or in part, for scholarly purposes may be granted by the professors who supervised the thesis work or, in their absence, by the Head of the Department or the Dean of the College in which the thesis work was done. It is understood that any copying or publication or use of this thesis or parts thereof for financial gain shall not be allowed without the author's written permission. It is also understood that due recognition shall be given to the author and to the University of Saskatchewan in any scholarly use which may be made of any material in this thesis.

Requests for permission to copy or to make other use of the material in this thesis in whole or in part should be addressed to:

Head of the Department of Mechanical Engineering,
University of Saskatchewan
Saskatoon, Saskatchewan, Canada, S7N 5A9

ABSTRACT

The goal of this thesis is to develop an efficient finite element model of a particular micro-positioning(MP) system, known as the 3RRR Mechanism. MP systems are capable of delivering accurate and controllable motion in the micro-metre to sub-micrometre range. Conventional mechanisms, which are often composed of rigid links with pinned connections are prone to friction, backlash and stiction, which are magnified at small displacements. As such MP systems utilize a new structure known as the compliant mechanism. The structure of most compliant mechanisms is based on conventional mechanisms; however they are monolithic devices which utilize flexible elements, instead of pins, to transform the input to a useful output position.

One common flexible element found in compliant mechanisms is the right circular flexure hinge. The seminal work on flexure hinges was done by Paros and Weisbord [1965], the basis of which was to calculate compliance (the reciprocal of stiffness) in order to characterize the behaviour of the hinge when loaded. However they essentially modelled the flexure hinge as a 1-D beam, when it is in fact 3-D in nature. Researchers completing finite element models of MP systems and flexure hinges have extended the model to 2-D elements, still resulting in poor results when compared to experimental data.

The task of completing a full 3-D finite element model of a MP system, let alone a right circular flexure hinge, is a major computational effort. For instance, a full 3-D model of the 3RRR mechanism would require over 1,000,000 degrees of freedom(DOF) dedicated to the flexure hinges alone. A 2-D model requires approximately 45,000 DOF in total; however, this number is still regarded as large.

Given these facts, a new technique called the Equivalent Beam Methodology(EBM) has been developed to model the 3-D stiffness of any right circular flexure hinge with a low number of DOF. This method essentially maps the 3-D stiffness of the hinge to a number of 1-D beam elements. For comparison, the finite element model of the 3RRR mechanism which incorporates the beams of the EBM has under 300 DOF in total, and is more accurate than the 2-D model. This method is extremely accurate, easy to use, and has a very low number of DOF, which makes it suitable to many advanced finite element modelling analyses such as topographic optimization, dynamic and modal analysis.

ACKNOWLEDGEMENTS

I would like to thank the many people who have helped me along this journey. First to my supervisor, Professor Chris Zhang, for his financial and academic support as well as giving me academic freedom in research direction. To my co-supervisor, Professor Walerian Szyszkowski, for his academic contributions, for challenging me to be thorough, and for his patience. I would also like to thank the Department of Mechanical Engineering for its financial support through both scholarship and employment and the opportunity to gain valuable teaching experience. I would like to also thank my academic teaching mentors: Professor Allan Dolovich, Professor Colin Sargent, and Dr. Jennifer MacLennan.

Many thanks also go out to friends and family for being there through the good and the bad times. In particular I would like to thank Mom and Dad, my many brothers and sisters (Brent, Lynne, Blair, Mary Anne, Bradley, Gerina, Naomi, Sarah, Nadine and Julie), my friends and colleagues Jeff Dobchuk and Ruska Paton, the Huxxtabulls, and DJ Charlie Hustle.

To Mom and Dad

Table of Contents

PERMISSION TO USE	i
ABSTRACT	ii
ACKNOWLEDGEMENTS	iii
DEDICATION	iv
Table of Contents	v
List of Figures	ix
List of Tables	xii
1 Introduction	1
1.1 Background	1
1.2 Introduction of the 3RRR Mechanism	2
1.3 Scope	5
1.4 Research Motivation	6
1.5 Research Objectives	7
1.6 Organization of Thesis	8
2 Literature Review	10
2.1 Introduction	10
2.2 Compliant Mechanisms	11
2.2.1 Flexure Hinges	12
2.2.2 Compliant Mechanisms — Design and Analysis	20
2.3 Early Micro-positioning Systems	23
2.4 The Piezo Driven 3RRR Micro-positioning Stage	27

2.4.1	Introduction	27
2.4.2	3RRR MP Stage — Physical Description and Behaviour . . .	27
2.4.3	Work of Bi et al. [1997]	28
2.4.4	Work of Zou [2000]	30
2.5	Concluding Remarks	32
3	Theoretical Foundations	33
3.1	Introduction	33
3.1.1	Fundamentals of the Theory of Elasticity	33
3.1.2	Uniaxial Loading and Poisson’s Ratio	35
3.1.3	Multiaxial Loading: Generalized Hooke’s Law(GHL)	36
3.1.4	2–D Applications: Plane Stress and Plane Strain	38
3.2	Beam Theory(2–D plane stress simplified to 1–D problem)	41
3.2.1	Statics – Equilibrium	43
3.2.2	Internal Force – Stress Relationship	44
3.2.3	Geometry of Deformation (Kinematics)	45
3.2.4	Internal Force – Stress: Revisited	48
3.3	Finite Element Method	50
3.3.1	Derivation of Structural Matrices	51
3.3.2	General Comments about the Finite Element Method	54
4	Flexure Hinge Stress Behaviour	56
4.1	Introduction	56
4.2	Purpose	57
4.3	Flexure Hinge Model	57
4.3.1	Physical Model	57
4.3.2	3–D Finite Element Model	60
4.4	Flexure Hinge Results	64
4.4.1	Test for Convergence	64

4.4.2	3–D Behaviour of the Right Circular Flexure	65
4.4.3	Stiffness Comparison of 3–D Models with 2–D Models	72
4.4.4	Classification of Thick and Thin Hinges	75
4.5	Flexure Hinge Conclusion	77
5	The Equivalent Beam Methodology	78
5.1	Introduction	78
5.2	Development	80
5.3	Comparison to 3–D Finite Element Results	84
5.3.1	Sizing Beams for the EBM	84
5.3.2	Result Comparison	85
5.4	Conclusion and Recommendations	90
6	Simulation Experimentation of the Equivalent Beam Methodology	91
6.1	Introduction	91
6.2	Model Description	92
6.2.1	2–D Planar 3RRR Model	93
6.2.2	EBM 3RRR Model	94
6.3	Method of Analysis	96
6.4	Results and Discussion	97
6.5	Recommendations and Conclusions	100
7	Conclusion and Proposed Future Work	102
7.1	Research Objectives	102
7.2	Literature and Theory Review	103
7.3	Flexure Hinge Study	104
7.4	Equivalent Beam Methodology	105
7.5	Comparing the 1-D EBM model to the 2–D Plane Finite Element Models of the 3RRR Mechanism	105
7.6	Proposed Future Work	106

References	107
A Flexure Hinge Models	110
A.1 Introduction	110
A.2 3-D Hinge Model	110
A.3 2-D Plane Hinge Model	115
B EBM Verification Models	119
B.1 Introduction	119
B.2 3-D Verification Model	119
B.3 EBM Verification Model	124
C 3RRR Models	126
C.1 Introduction	126
C.2 2-D 3RRR Planar Model	126
C.3 EBM 3RRR Model	133

List of Figures

1.1	3RRR MP Stage	3
1.2	Magnified Displacement Pose of 3RRR Mechanism — Actuating 1 Actuator	4
1.3	Magnified Displacement Pose of 3RRR Mechanism — Actuating 2 Actuators	4
1.4	Magnified Displacement Pose of 3RRR Mechanism — Actuating 3 Actuators	5
1.5	Magnified depiction of a Flexure Hinge of the 3RRR Mechanism . . .	6
2.1	Right Circular Fillet Flexure Hinge	12
2.2	Types of Single Axis Flexures	13
2.3	Flowchart of the Design Methodology [Howell and Midha, 1994] . . .	22
2.4	Complex Flexure used in Para-flex Stage[Teague et al., 1988]	24
2.5	Exploded View of 3RRR MP Stage	28
2.6	Poor Meshing of the Flexure Hinges of the Original 3RRR Model [Zou, 2000]	31
3.1	An element subjected to loading in the x direction	35
3.2	A unit element subjected to loading in the x, y and z directions . . .	36
3.3	A Thin Element in Bending	39
3.4	A Body Subjected to Loading in the x and y Directions	40
3.5	General Geometric Parameters of Generic Beam	42
3.6	Flow Chart of Elasticity	43

3.7	Notation used in Beam Theory Derivation	43
3.8	Free Body Diagram of Beam Element	44
3.9	Statics of Beam Section Relating Stress to Internal Moment	45
3.10	Arc-like Deflection of a Beam Element in Pure Bending	46
3.11	Equilibrium of a Layer of Elements in a Beam subjected to Pure Bending	47
3.12	Cross Section of Beam depicting the sum of the stress equivalency to the applied moment	49
4.1	The Standard Geometric Parameters which define a Flexure Hinge . .	59
4.2	3-D Model of Flexure Hinge	61
4.3	The Grid of Small yet Stiff Beam Elements Imposed to the Top of the 3-D Model	62
4.4	2D Planar Model of Flexure Hinge	64
4.5	Continuous Nature of the Field of Stress in y -direction of the 3-D Flexure Model	65
4.6	Estimated Stress Distribution using a Beam Bending Approach . . .	67
4.7	Stresses Calculated at the Nodes along Path AB	67
4.8	Strains Calculated at the Nodes along Path AB	68
4.9	Stress in the y -direction Calculated at the Nodes along Paths OA and CB	69
4.10	Stresses in the x - and z -direction Calculated at the Nodes along Paths OA and CB	70
4.11	Strains Calculated at the Nodes along Paths OA and CB	70
4.12	Deformation of the xz -plane of the Centre of the Hinge	71
4.13	Deflection of the Hinge: Defining v_x and α	72
4.14	Deflection of the Hinge: Defining v_x and α	73
4.15	Plot of k_α versus b/t ratio	75
4.16	Plot of Percent Error k_α versus b/t ratio	76
5.1	Parameters used to define the beam geometry of the EBM	81

5.2	Modified model set-up to test the validity of EBM	86
5.3	Comparing the angular rotation of the 3-D model to the EBM, plane stress and plane strain models	89
6.1	Mapped Meshing of the Hinges of the Planar Models	94
6.2	The graphical representation of the planar 3RRR finite element model	95
6.3	Discontinuous nature of beam element model	96
6.4	The graphical representation of the EBM 3RRR finite element model	97
6.5	Same Modes of Deflection of the EBM and Plane Strain 3RRR Model	98

List of Tables

4.1	Defining Hinge Parameters of the Flexure Model	58
4.2	Rotational and Lateral Bending Stiffnesses of the 3-D finite element model, the 2-D finite element models assuming plane strain and plane stress, and the Paros and Weisbord Simplifications	74
5.1	Calculation of the EBM geometry from the 3-D finite element data	85
5.2	A comparison of the EBM model to the 3-D model of a right circular hinge, with a $0.2 N \cdot m$ couple moment load in the z -direction	87
5.3	A comparison of the EBM model to the 3-D model of a right circular hinge, with a $0.1 N \cdot m$ couple moment in the z -direction and a $-12 N$ load in the x -direction	88
5.4	A comparison of the EBM model to the 3-D model of a right circular hinge, with a $-24 N$ load in the x -direction	88
6.1	Comparison of Displacement and Rotation of End Effector and Maximum Equivalent Stress in each Respective Model	99

Chapter 1

Introduction

1.1 Background

There is a growing need to have precise controllable positioning in many facets of engineering. For instance, a process of miniaturization has been occurring in the past decade on many tool and consumer goods; most notably, computers and cellular telephones. The majority of the miniaturization has been greatly attributed to the reduction of the size of electronics. The reduction in size of electronics cannot take place without precise control of the tools used to create them. The size of a given component is directly related to the resolution of the production tool, while quality is directly related to the accuracy.

Micro-positioning (MP) systems are also playing large roles in other technical fields. For instance, in the field of micro-biology there is an increasing need for high precision sensing, positioning and manipulation of cells and other biological entities. In the field of medicine, positional accuracy greater than that which is humanly possible is required in some surgeries. Micro-technology also increases the opportunity to create fine surgical tools for minimal evasive surgeries. In the field of optics, micro-positioning systems are being used in optical switches in fibre optic applications.

Micro-positioning is the study of devices capable of delivering controllable motion in the micro-metre and sub-micro-metre range. This field, also referred to as ‘micro-motion’, will be referred to as ‘micro-positioning’ in this thesis, as it implies controllability. Further, Micro Motion is a registered trade-name of a company which produces flow meters, which has little to do with the field of micro-positioning.

Following this section, Chapter 1 will include the following sections: the introduction of the Micro-positioning system studied in this thesis, the scope of the thesis, the research motivation, the research objectives, and the organization of this thesis.

1.2 Introduction of the 3RRR Mechanism

The subject of this thesis is the finite element modelling of a micro-positioning system. The MP system in this study is called the ‘Piezo’ Actuated 3RRR Mechanism. It is composed of four main parts: piezoelectric actuators, a compliant mechanism, an end-effector, and the control system. The compliant mechanism portion is symmetric about 120° ; each symmetric portion contains a linkage composed of three compliant revolute joints.

These three linkages are actuated independently by the piezoelectric actuators, as shown in Figure 1.1. The linkages are also connected to the end-effector, the component responsible for delivering the controlled positional output. Note that the end-effector is application specific; its shape and structure are ideally unlimited, as long as it interfaces with the compliant mechanism at the end-effector mounts. For the sake of visualization the end-effector is represented by a circular plate with a concentric thru hole.

The name 3RRR is composed of two main parts, the number 3 refers to the number of symmetric portions, while the RRR refers to the three main revolute joints in each arm of the mechanism.

Output position of the end effector is achieved by actuating one or combinations of

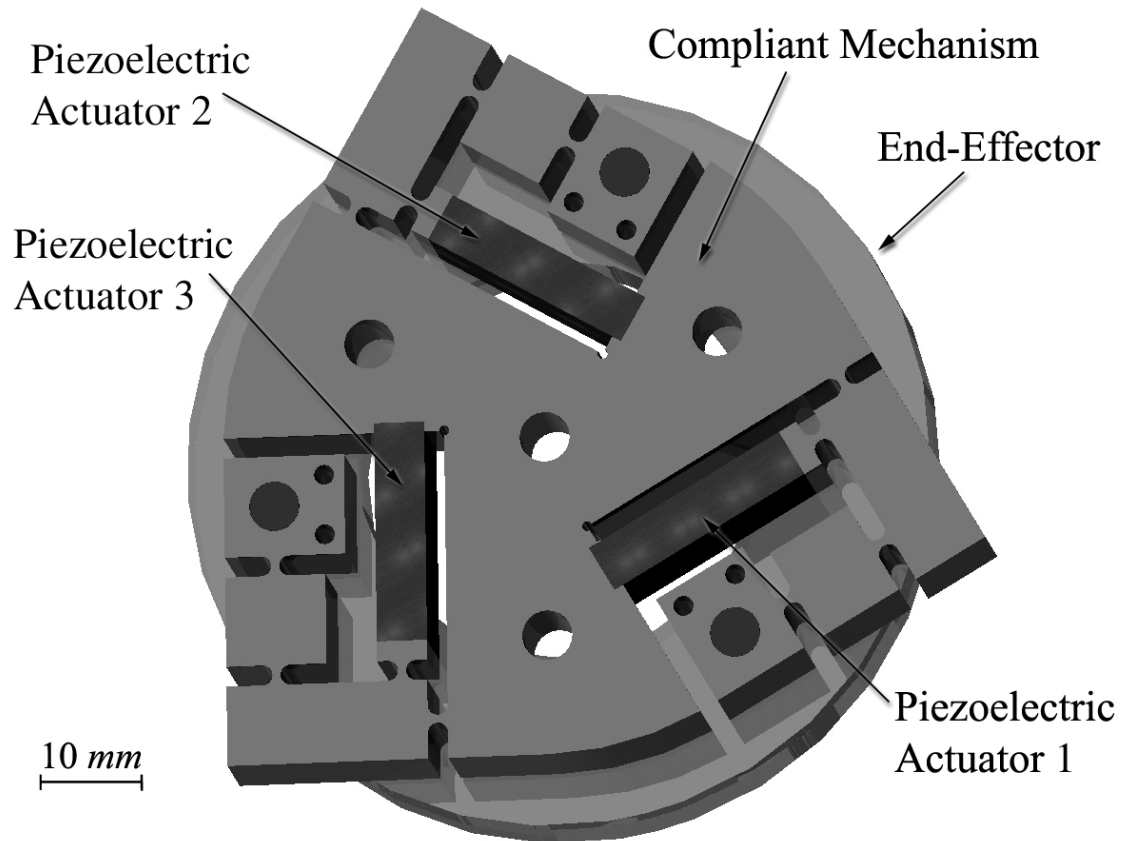


Figure 1.1 3RRR MP Stage

the three piezo electric actuators. The resulting motion of the end-effector is capable of three degrees of freedom, namely x , y and yaw rotation θ . To clarify this point, Figures 1.2, 1.3, and 1.4 show the effect of actuating several combinations of the actuators. These poses are magnified in the finite element software ANSYS to aid in their realization. The undeformed outline of the 3RRR mechanism can be seen in all of the above mentioned figures. Note that the end-effector in these figures is now triangular in nature.

Figure 1.2 depicts the pose when one actuator is extended. Notice that the motion of the end effector is approximately in the same direction as piezo extension and that it undergoes a small rotation.

Figure 1.3 shows the pose when two actuators are extended in combination. In this case the direction of the end effector is in the direction of the resultant of the

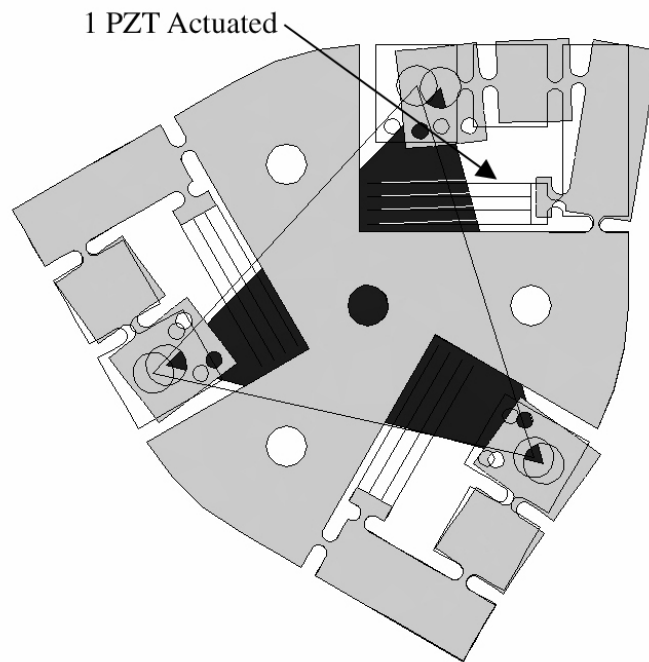


Figure 1.2 Magnified Displacement Pose of 3RRR Mechanism — Actuating 1 Actuator

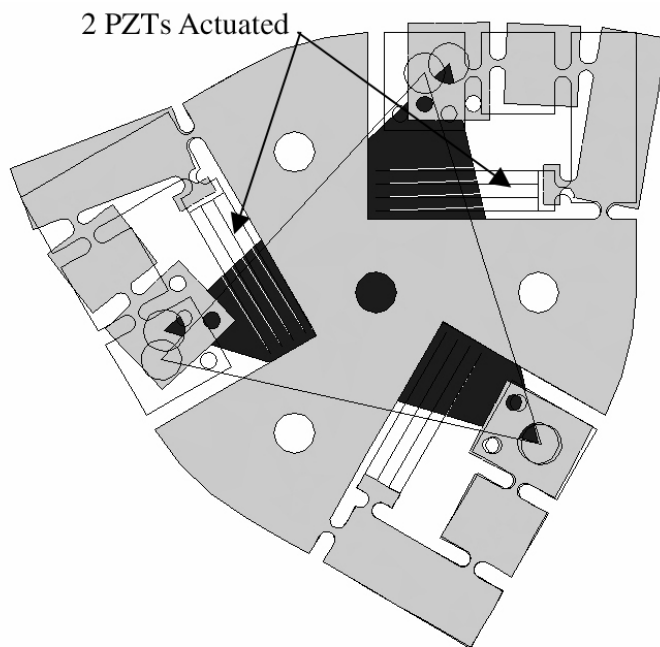


Figure 1.3 Magnified Displacement Pose of 3RRR Mechanism — Actuating 2 Actuators

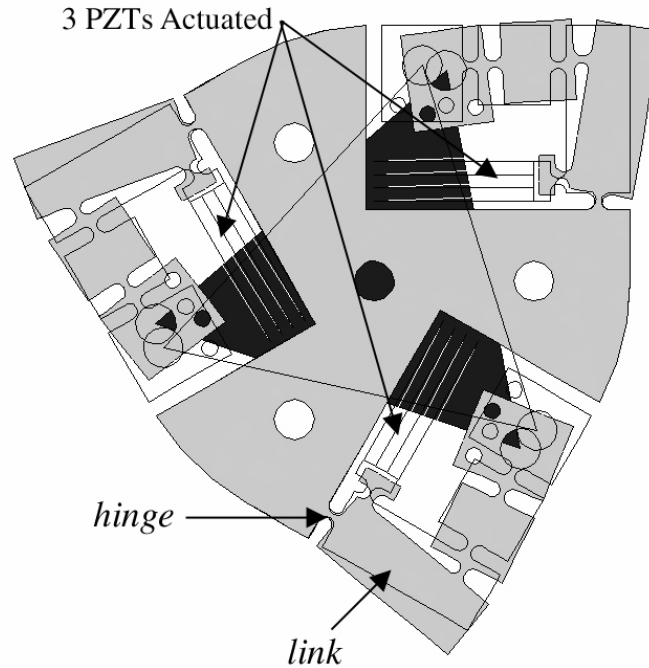


Figure 1.4 Magnified Displacement Pose of 3RRR Mechanism — Actuating 3 Actuators

piezoelectric actuator extension, and the end effector rotation is almost doubled.

Figure 1.4 is the effect of actuating all of the actuators simultaneously. Notice that there is no perceivable translation in the x or y -direction; however, the end effector rotation is almost tripled when compared to the pose shown in Figure 1.2. Also in Figure 1.4, two parts of the compliant mechanism, labelled hinge and link are identified now for clarification in future discussion.

1.3 Scope

The field of micro-positioning is very extensive; however, it can be divided into four sub-fields, specifically: Actuation (*input*), Mechanical Amplification and/or Transformation (*output*), Control and System Integration tailored toward a specific application. The parts can be further subdivided into several other areas such as design, modelling, synthesis, and optimization.

The main focus of this thesis is the mechanics of materials modelling of the mechanism responsible for the Mechanical Transformation of the 3RRR MP System, namely the compliant mechanism. The modelling in this study will be mostly implemented using the finite element method and completed using the software ANSYS.

1.4 Research Motivation

As shown in Figures 1.2 through 1.4, the motion of the 3RRR mechanism is planar in nature. Because of this fact, it may be considered logical to assume that all aspects of behaviour of the mechanism are in the plane of motion, including the stress–strain analysis. However this is not the case for one of the key parts of the mechanism called the flexure hinge as shown in Figure 1.5.

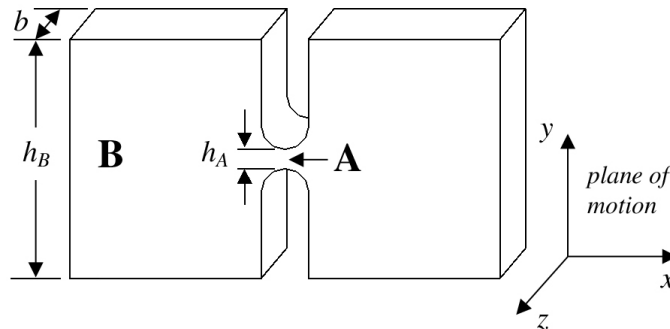


Figure 1.5 Magnified depiction of a Flexure Hinge of the 3RRR Mechanism

From the view point of mechanics and bending of structural members, portion A of the hinge is ‘thick’ for its height(h_A) is much smaller than the depth in the z -direction(b). On the other hand the portion B can be considered ‘thin’ because its height(h_B) is greater than or equal to the depth.

More precisely, a bent member can be considered ‘thin’ if the stress in the z -direction

is negligible and 'thick' if strain in the z -direction is negligible. The calculated bending stiffness of the member classified as 'thin' will be about $1 - \nu^2 \approx 0.9$ lower than the same member classified as 'thick'. Using 2-D elasticity the 'thick' elements can be approximated by the plane strain state, while the 'thin' elements by the plane stress state. Such a 2-D approximation is done to avoid the 3-D analysis that requires a great numerical effort, and usually works well if the whole structure can be considered either 'thin' or 'thick'. In the hinge, however, the seemingly 'thick' portion gradually become 'thin' (or vice versa) which essentially necessitates an 'exact' 3-D analysis.

It should be emphasized that the plane stress state has been used in the past for modelling the 3RRR mechanism, and is the most common assumption used for flexure hinge research. However, the results of this thesis will show that stress-strain behaviour of the flexure hinge is 3-D in nature. Further, to model it in a 2-D space, assuming either the plane stress or plane strain state, is acceptable only for particular ranges of the b/h_A ratio.

1.5 Research Objectives

It will be shown in this thesis that the stress-strain behaviour of the hinges of the 3RRR mechanism is in fact entirely 3-D. To model the entire mechanism in 3-D requires a problematically high number of elements. Since the 3RRR Mechanism operates in a planar fashion, it is tempting to model it with the use of 2-D elements; however, doing so corresponds to the assumption that the material behaves identical through the depth of the mechanism (i.e. the stress/strain components in the interior of structure are the same as those on the surface). Should this assumption fail, accuracy of the model is degraded.

On the other hand the links of the mechanism are quite 'thin' and essentially behave like beams. These portions could, in turn, be modelled as 1-D elements; which are

very efficient numerically. Additionally they are relatively rigid compared to the hinges, which would add to the accuracy of their 1-D modelling.

Given these facts, the objective of this thesis is to create an accurate finite model of the 3RRR Mechanism with a reasonably small number of degrees of freedom(DOF). The number of DOF affects substantially the ability of performing the dynamic and optimization analysis.

In order to accomplish this objective the following goals will be attempted:

Goal 1: Complete a 3-D finite element study on a flexure hinge to understand its true behaviours (only one hinge is modelled).

Goal 2: Develop an accurate model of a hinge made of 1-D beam elements, which accurately accounts for the hinge's physical behaviour, namely that when loaded it will result in the same maximum stress, and slope and deflection at the endpoint.

Goal 3: Create a finite element model of the 3RRR Mechanism based on the model developed in Goal 2, and test the model against experimental and other computational data.

1.6 Organization of Thesis

This thesis consists of six chapters. In Chapter 2, a literature review will be presented. In this chapter the nomenclature and past research of micro-positioning systems will be summed up in a concise manner. Also in this chapter, previous work done on the 3RRR Mechanism will be presented.

In Chapter 3 the theoretical foundations employed in the thesis are summarized to aid in the reader's understanding of the results and challenges of the project.

In Chapter 4 an investigation of the governing stress behaviour of flexure hinges is presented. Flexure hinges are a key component in the 3RRR Mechanism. Several models of a flexure hinge will be compared to one another, namely a 2-D plane stress, a 2-D plane strain, and a 3-D model. This will show under what conditions the 2-D modelling of flexure hinges is acceptable.

In Chapter 5, the development of the equivalent beam method will be presented. It will be shown in this chapter that the behaviour at the endpoints of a flexure hinge can be modelled with equivalent beams.

In Chapter 6, the equivalent beam model will be incorporated into a full 3RRR model. This model will be compared to a 2-D model of the 3RRR mechanism assuming either a plane strain state or plane stress state.

In Chapter 7, a summary of results, conclusions, and proposed future work will be presented.

Chapter 2

Literature Review

2.1 Introduction

The purpose of this chapter is to give the reader a brief outline of previous research done in the field of micro-positioning. The scope of the material presented is broad in nature. Before the purpose of this thesis was conceptualized, a thorough literature review was completed to learn specifically, what types of studies have been done, the general history of this relatively new field, and what has been done with regard to the 3RRR Mechanism.

As mentioned in the preceding chapter a micro-positioning system (MPS) is one capable of delivering accurate and controllable motion in the micro-metre range. However, they do not necessarily have to be 'micro' in size. The mechanical design of MPSs has gone in several directions.

Conventional positioning systems, which are often composed of electrical servo or stepper motors, hydraulic or pneumatic actuators, as well as gears or ball and lead screw mechanisms have not been, for the most part, incorporated into micro-positioning systems. Effects such as dead-band, friction and stiction are magnified as these components are made smaller [Ryu et al., 1997].

With this in mind, designers of micro-positioning systems have embraced relatively new concepts and technologies to model MP systems and components to deliver accurate motion. With the implementation of these new technologies, new design and analysis techniques have been introduced. However, in the area of elasticity, many designers of MPSs have failed to utilize or misinterpreted verified modelling techniques.

As mentioned earlier, the physical embodiment of a micro-positioning system can be divided into three main parts: actuation, transformation, and output. Piezoelectric actuators are almost universally used to deliver force/displacement to MPSs. They offer many advantages including: fast response time, fine resolution and high force generation capabilities. Though they are incorporated into the 3RRR mechanism, they are not a major concern with regards to the scope of this thesis.

Transformation of the actuation is almost universally accomplished using compliant mechanisms and will be covered extensively in this chapter. The transformed position/force is delivered to an end effector. The end effector can be anything from a simple platform to a wide variety of tools, such as cutting tools, surgical devices, and so on. Because they tend to be so application specific, they are not discussed at length in this thesis.

This chapter is broken up into a number of sections. First, compliant mechanisms from the micro-positioning standpoint are reviewed, then a brief history of micro-positioning systems is presented, and finally previous research with regard to the 3RRR Mechanism is presented.

2.2 Compliant Mechanisms

As mentioned in the previous section, micro positioning systems are created using relatively new devices. Compliant mechanisms are used to form the delivery system to change or magnify the motion/force from the actuator, to the end effector.

Compliant Mechanisms are monolithic (one-piece) structures that employ flexible elements to give desired motion, rather than rigid body joints. A concise intro into the classification of compliant mechanisms was presented by Midha et al. [1994]. In many compliant mechanisms the flexible element often used is the flexure hinge.

2.2.1 Flexure Hinges

A flexure hinge, as seen in Figure 2.1, is generally made of a blank of material with fillets machined or punched out of it.

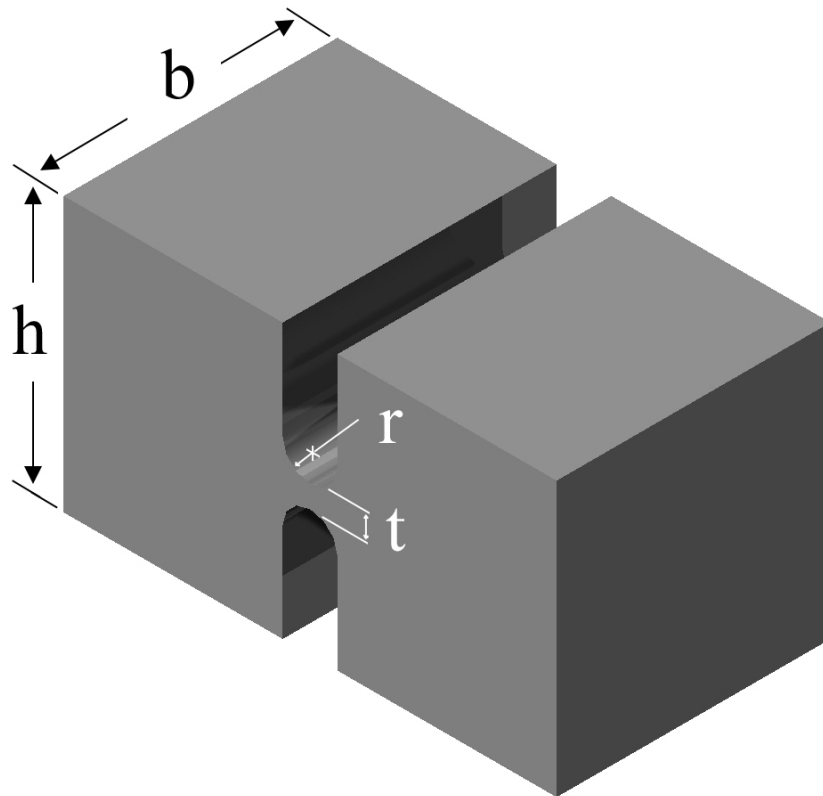


Figure 2.1 Right Circular Fillet Flexure Hinge

The parameters which define the geometry of a flexure hinge are h , t , b and r . The above hinge is referred to as a right circular flexure hinge or flexure. Other types of hinges include the corner filleted, leaf, and elliptically filleted. These, like the right circular flexure, have dominant compliance in one direction. The differences in

geometry of these hinges can be seen in Figure 2.2.

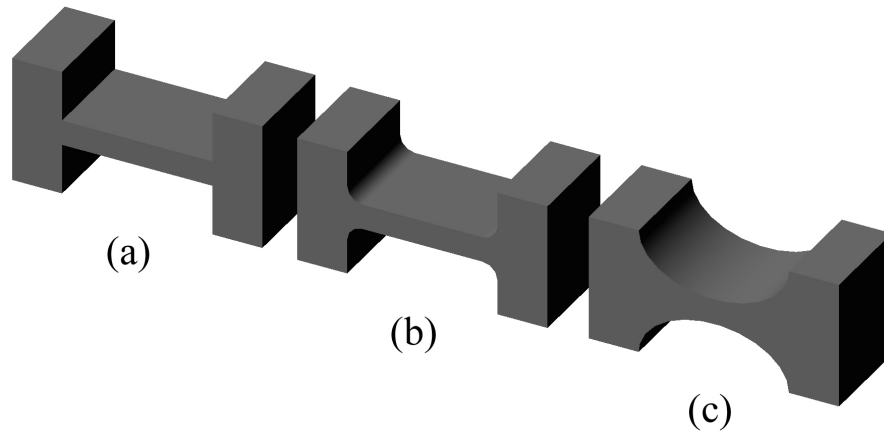


Figure 2.2 Other Types of Single Axis Flexures:
(a) Corner Filleted, (b) Leaf, and (c) Elliptically
Filleted

These hinges fall into the classification of compliance known as single axis revolute flexures (or joints/hinges) [Midha et al., 1994]. There are other types of compliant flexures; for instance, Goldfarb and Speich [1999] have developed a split tube revolute joint, which is not based on the flexure principle. Also, there are several types of non-revolute joints including the spherical flexure (also called universal) and prismatic flexure [Hara and Sugimoto, 1989]. For the sake of brevity, they will not be discussed here.

The physical differences in geometry of the single axis revolute flexures manifest themselves in different behaviours. The type of hinge used in a mechanism is dictated by its intended application. For instance, right circular hinges due to their nature are in general very “well behaved”.

To clarify this point, the term “well behaved” is expressed in the kinematic sense. Designers often assume the links of compliant mechanism are rigid, and that the flexure hinges are joints with a known bending stiffness, much like a torsional spring. “Well behaved” in this context means that the hinge always bends in the same place,

that is the thinnest portion of the hinge. This simplifies the kinematic models, such that the compliant mechanism can be modelled as a “rigid” body mechanism.

Leaf or corner filleted hinges are generally more flexible (up to 6 times) for similar t , b , and h dimensions. Corner filleted flexures are also subject to a reduced level of stress, as the stress concentration factors for this hinge are typically lower than all other hinges. The trade off is the loss of the well-behaved centre of rotation. Elliptical flexures are a middle ground between these two extremes, having slightly less flexibility than corner filleted flexures and less well behavioural nature of the centre of rotation[Lobontiu et al., 2001].

The Work of Paros And Weisbord

Paros and Weisbord [1965] wrote the first published work on flexure hinges. The majority of their paper is a development of the model of compliance for several axes of a right circular flexure. Compliance is the reciprocal of stiffness, and is sometimes referred to as flexibility. Using the Euler Bernoulli(E-B) beam equation they developed a model for the compliance of a single axis right circular flexure.

Note that the E-B Beam Equation was formulated to predict the deflection of thin beams for a given moment loading, in which any shear deformation is negligible. Further the E-B Beam Equation implies a 1-D stress state throughout the length of the beam. Because the equation was developed for beam analysis, it has some inherent assumptions imposed on it. Two predominant assumptions are that the beam in question is greater in height than depth (to ensure a 1-D stress state), and that the beam is prismatic (of constant cross-sectional area).

Clearly not all flexure hinges maintain these assumptions. Nevertheless, the E-B Equation, which is typically extended to beams of ‘slightly’ varying areas, was used to evaluate the hinge’s performance. The E-B Equation gives:

$$M_z(x) = \frac{EI_z(x)}{\rho} = EI_z(x) \frac{\frac{d^2y}{dx^2}}{\left[1 + \left(\frac{dy}{dx}\right)^2\right]^{\frac{3}{2}}}, \quad (2.1)$$

where $M_z(x)$ is the moment applied to the beam,

$I_z(x)$ is the area moment of inertia of the beams cross section,

and ρ is the radius of curvature of the beam during bending.

A valid assumption for small displacements is that the slope dy/dx is significantly smaller than 1 and therefore Equation 2.1 reduces to:

$$M_z(x) = EI \frac{d^2y}{dx^2}. \quad (2.2)$$

The slope of the beam dy/dx or deflection angle α_z is obtained from:

$$\alpha_z \approx \int_0^x \frac{d^2y}{dx^2} dx = \int_0^x \frac{M_z}{EI_z(x)} dx. \quad (2.3)$$

It should be noted that the E-B beam theory considers only one stress component.

The integral 2.3 is quite complex for the hinge shown in Figure 2.1, for which I_z is equal to:

$$I_z(x) = \frac{bh(x)^3}{12}, \quad (2.4)$$

where $h(x) = 2(r + t/2 - \sqrt{r^2 - x^2})$.

The integral for constant M_z as completed by Paros and Weisbord, takes the form:

$$\alpha_z = \frac{3M_z}{2Ebr^2} \left[\frac{1}{2\beta + \beta^2} \right] \left\{ \left[\frac{1 + \beta}{\gamma^2} + \frac{3 + 2\beta + \beta^2}{\gamma(2\beta + \beta^2)} \right] \left[\sqrt{1 - (1 + \beta - \gamma)^2} \right] + \left[\frac{6(1 + \beta)}{(2\beta + \beta^2)^{3/2}} \right] \left[\arctan \left(\sqrt{\frac{2 + \beta}{\beta}} \frac{(\gamma - \beta)}{\sqrt{1 - (1 + \beta - \gamma)^2}} \right) \right] \right\}, \quad (2.5)$$

where β is the ratio $t/2r$
and γ is the ratio $h/2r$.

Further, to simplify the solution they made several assumptions. The first assumption was that $\beta \ll 1$ (or $t \ll r$) and the second was that $\beta \ll \gamma$ (or $t \ll h$). Also, it was assumed that $\gamma = \beta + 1$ since h was assumed to be $t + 2r$. It is important to remember that because Equation 2.5 assumes only one stress component, it is only valid for hinges of thin depth (i.e. that $t \gg b$). This requirement is obviously violated for the hinge shown in Figure 2.1. That aside, they used these assumption and divided Equation 2.5 through by M_z , thus allowing them to express the compliance of the hinge as:

$$\frac{\alpha_z}{M_z} \approx \frac{9\pi}{2Ebr^2(2\beta)^{5/2}}. \quad (2.6)$$

The final simplification was achieved by substituting $t/2r$ for β to yield:

$$\frac{\alpha_z}{M_z} \approx \frac{9\pi r^{1/2}}{2Ebt^{5/2}}. \quad (2.7)$$

In a similar manner they also calculated the dominant lateral compliance for a given moment loading. For the sake of brevity the development is not shown here; however, the dominant lateral compliance simplification is as follows:

$$\frac{v_y}{M_z} \approx \frac{9\pi r^{3/2}}{2Ebt^{5/2}}, \quad (2.8)$$

where v_y is equal to the lateral deflection of the hinge's end-point when the hinge's length is assumed to be in the x-direction.

Note that this development presented above was for dominant compliance of a flexure. In their paper they also presented similar developments for less than dominant axes of compliance. Their goal was to give design engineers relatively simple rules of thumb and to aid them with flexure design and mechanisms containing flexures.

Today, many researchers still use this simplification, however special care and attention must be taken to ensure that the hinge in question falls within the assumptions of this approach. Specifically, it should be ensured that the hinge in question is suitably thin (i.e. that $t \gg b$), and also that the ratio β is in fact much less than unity. This is verified in the work of Smith et al. [1997].

Note that $t \approx b/12$ for the hinge used in the 3RRR mechanism, and the ratio β has a value of 0.4. This is the first indication that this seminal work may be invalid for the flexures used in the 3RRR mechanism.

It is believed that Paros and Weisbord's simplifications can generate compliance within 5% of experimental results given that the hinge in question is within the conditions of the assumptions and that it is in a 1-D stress state. The beam model and the 1-D stress state comply, in general terms, with the 2-D plane stress state, a formal explanation of which is given in Chapter 3.

Other Flexure Hinge Work

Ragulskis et al. [1989] presented a paper which focused on the finite element analysis of a right circular flexure. In their paper they eliminated Paros and Weisbord's original assumption that $\gamma = \beta + 1$ and hence referred to their hinges as Fillet Type Flexures. Using the finite element method in 2-D, presumably using a plane stress behaviour (no mention of stress state), they came up with a design criterion to size a Fillet Type Flexure based on design specifications such as maximum stress and required deflection.

Rong et al. [1994] developed a simple compliant stage incorporating right circular flexure hinges. As a precursor to the presentation of the stage, they recited the work of Paros and Weisbord, and then used the compliance equations for several axes of the hinge to develop compliance ratio equations. The compliance ratios were then used to select the best properties of a hinge, overall attempting to optimize the dominant compliance and minimize all others.

Xu and King [1995] presented their comparative work between elliptical and filleted (both right circular and corner filleted) flexures, and revisited the same topic in more detail in 1996 [Xu and King, 1996]. Using 2-D finite element analysis they showed the right circular hinges are the most accurate in the kinematic sense; however, they are the stiffest and therefore should not be used when large magnification of input is desired. They also found that right angle hinges (corner filleted with fillet radii approaching zero), are the most flexible but unpractical from a manufacturing point of view. Additionally, the accuracy of corner filleted hinges is directly related to corner radius to hinge length ratio. They found significant advantage to using elliptical hinges because they are more flexible than right circular hinges and yet better behaved than corner filleted hinges. Though they did not explicitly specify, plane stress was assumed as the behaviour of the studied hinges.

Smith et al. [1997] presented closed form equations for calculating compliance of elliptical flexure hinges, which was based on the work of Paros and Weisbord [1965]. Their closed form equation contained a ratio ' ϵ ' of the major to minor axes of an ellipse. The inclusion of such a ratio meant that it was applicable to any shape of ellipse. The closed form equations converged to the solution for right circular hinges when $\epsilon = 1$, and to that of leaf type hinges when $\epsilon \rightarrow \infty$, as presented by Ling [1952].

This paper also contained other contributions to the field, addressing such things as stress concentration factors and an error analysis of compliance as a function of β . As well they confirmed their closed form equations by completing a 2-D finite element analysis and an experiment. Good matching of their theoretical results to both

finite element and experimental results was realized. However, they used unusually thin hinges in their experiment. The good agreement was achieved because for such hinges the plane stress assumption inherent in the closed form solution and finite element analysis held.

Zhang and Fasse [2001] undertook a study into determining the Spatial Stiffness Properties of a Notch Hinge, which is very similar to a right circular hinge. They felt that from a design point of view it is inadequate to model the hinge as a single degree of freedom bending element. At the end of their paper they claim not to have characterized the spatial elastic behaviour of all notch hinges, but feel they have made progress toward such a characterization.

Lobontiu et al. [2001] developed simplified compliance equations for corner filleted flexures, again using the same approach Paros and Weisbord used. They completed 2-D plane stress finite element analysis and did an experimental comparison using thin hinges for which $t \gg b$. They found that results obtained using their theoretical equation were within 6% of the experimental results and 10% of the finite element results.

It became apparent that there was the need for research in the field of modelling flexure hinges. Many researchers used the work of Paros and Weisbord as the seminal work; however, the said work is based on assumptions that are easily violated in real hinges. The method has good agreement when the modelled hinge is sufficiently thin of depth. Although, to ensure a dominant compliance in a single direction and to reduce ‘parasitic’ deflections, hinges are often made thick of depth. This ensures that the compliance of each direction, except for the dominant one, is small and can be assumed to be negligible, hence realizing a kinematically well behaved hinge. The problem is that as hinges are made increasingly thick, the plane stress assumption becomes increasingly invalid. This point will be examined in greater detail in Chapter 4.

The next section will address compliant mechanisms from the design and analysis

point-of-view.

2.2.2 Compliant Mechanisms — Design and Analysis

Compliant mechanisms have several advantages and disadvantages as discussed by Goldfarb and Speich [1999]. The most notable advantage is the absence of Coulomb friction and backlash. Compliant mechanisms are also devoid of lubricant making them suitable for clean environments such as surgery and microchip assembly. Further, because they are monolithic in nature (made from one piece of material) there is a reduced cost of manufacturing as no assembly is required. Despite these advantages there are significant disadvantages when compared to conventional mechanisms.

Possibly the greatest disadvantage is the decreased range of motion. A compliant mechanism is limited by the elastic yield of the material used in their creation. Whereas conventional revolute joints have, in general, an unlimited range of motion about the desired axis and significant rigidity about all other axes and directions.

Also compliant mechanisms which contain elliptical and leaf/corner filleted flexures are kinematically problematic to model. The hinges used in mechanisms have centres of rotation that move along a locus of points about the length of the hinge. The range of the locus is dependant upon the type and quantity of loading. This makes kinematic modelling non-ideal as the assumed rigid lengths between flexures are rarely constant.

A large amount of research has already been done in this relatively new branch of mechanical engineering. The previously mentioned researchers focused primarily on a single component of compliant mechanisms (i.e. flexure hinges). While other researchers pour their efforts into attempting to model the kinematics, dynamics and physical behaviour of compliant mechanisms.

Because of the non-conventional nature of compliant mechanisms, non-conventional means of solving for deflection given an applied force/moment have been developed.

One method as cited by Howell and Midha [1994] involves a closed form solution to a second order non-linear differential as researched by Bisshop and Ducker in 1945, Frisch-Fay in 1969 and Gorski in 1976. Though a closed form solution exists, they are only practically found for simple cases.

Many researchers choose not to utilize the finite element method for compliant mechanism design. For instance Her and Chang [1994] call the finite element method a powerful tool, the foundation of which is based on Castigliano's First Theorem. They go on to say that the finite element method is too time consuming for complex mechanisms. Further, they say that the finite element method does not handle the analysis of rigid body motions. This thesis will address some of these issues in later chapters.

A good place to start when discussing compliant mechanisms design and analysis is the work of Midha et al. [1994]. In this particular work they presented the nomenclature and classification of compliant mechanisms. They discuss the differences between a linked compliant mechanisms (a mechanism with a compliant subassembly) and a fully compliant mechanism. Perhaps the greatest benefit of this work is the presentation of the language of compliant mechanisms.

Howell and Midha [1994] presented a design methodology for compliant mechanisms. The embodiment of the methodology is represented in the a flowchart as shown in Figure 2.3.

It is seen in Figure 2.3 that the Pseudo-Rigid-Body-Model(PRBM) is used to obtain a significant portion of the design. Then finite-element type algorithms, such as the chain algorithm, are used to fine tune the design.

The basis of the PRBM as discussed by Lyon et al. [1999] consists of representing a compliant mechanism as rigid links and torsional spring elements for the flexures. Often times the PRBM is based on a conventional mechanism.

Her and Chang [1994] also contributed the analysis of compliant mechanisms using the PRBM. They analyzing a stage, based on a 5 bar, 6 joint compliant linkage.

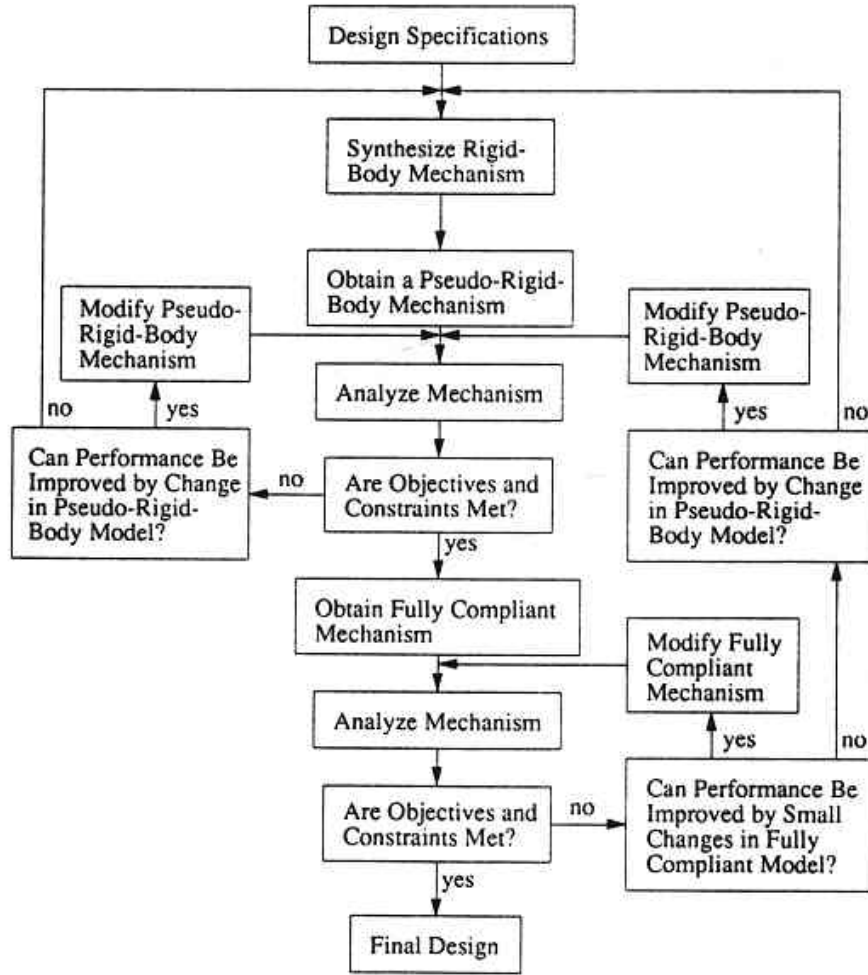


Figure 2.3 Flowchart of the Design Methodology [Howell and Midha, 1994]

The stage had three degrees of freedom (x , y and θ), which were coupled due to the physical nature of the stage. They calculated compliance using the Paros and Weisbord approach of the hinge they used in the MPS, and applied the PRBM to aid in their kinematic modelling of the stage. The kinematics of the PRBM for this case are statically indeterminate, however they overcame this problem by introducing a virtual work principle to completely solve the kinematics of the PRBM.

Further works pertaining to PRBM can be found in the following: Howell and Midha [1995], Howell et al. [1996] and Jensen et al. [1997].

The chain algorithm as discussed by Howell and Midha [1994] is a finite element type

method where a mechanism being analyzed is discretized into beam elements. Each element is considered to be cantilevered at the end of the previous beam. The first node in the beam chain is considered to be fixed.

Another work of note was written by Salamon and Midha [1998]. They used a method of Mechanical Advantage to describe Force/Displacement relationships. The method also accounts for the energy stored in the flexible links.

With these concepts in mind, attention is now turned to the early micro-positioning systems, which in general combine a compliant mechanism and piezoelectric actuators.

2.3 Early Micro-positioning Systems

It may be argued that the use of compliant mechanisms in MPSs is unnecessary. The simplest type of MPS would be one that simply contains an end effector attached to a piezo actuator. The role of a compliant mechanism is to change the input force/displacement in some meaningful way. For instance compliant mechanisms can often amplify the input force/displacement or convert it to a useful degree of freedom (i.e. changing linear displacement into rotation).

In this section MP stages will be discussed. A MP stage inherently implies the use of compliant mechanisms [Her and Chang, 1994]. The resolutions of a piezo-driven MP stage is directly related to the resolution of its input piezoelectric actuators (more specifically the resolution of the driving electronics). As such, unless otherwise stated, the resolution can be assumed to be in the nanometre range (i.e. the voltage source used has a resolution of around 1 mV).

Scire and Teague [1978] developed the first micro-positioning stage in 1978. Its displacement was in one direction only and had a range of 50 μm with a 'claimed' resolution of less than 1 nm . Because piezoelectric actuators were not readily available at that time, they created their own by stacking layers of piezoelectric ceramic.

The application for this device was intended for use with optical and electron microscopes.

Teague et al. [1988] presented a practical application for MP stage in 1988, which was called the Para-flex stage. Its use was for micro-topographic mapping, also referred to as surface roughness profile measuring. The stage was composed of a compliant mechanism and driven by two stepper motors. The end effector in this case was merely a platform that held a sample. The range of displacement for the Para-flex stage was 1 mm in x or y with an accuracy of 0.1 μm . However, the error tolerance for the controller must be larger than this to compensate for backlash and dynamics of the stepper motors.

Also, in their paper they used Paros and Weisbord's work to calculate stiffness. Then, using classical beam analysis they determined a theoretical force vs. displacement curve with apparently good agreement with experimental results. What makes this extraordinary is that Paros and Weisbord's simplification held for a hinge even more complex than the typical right circular fillet shown in Figure 2.4.

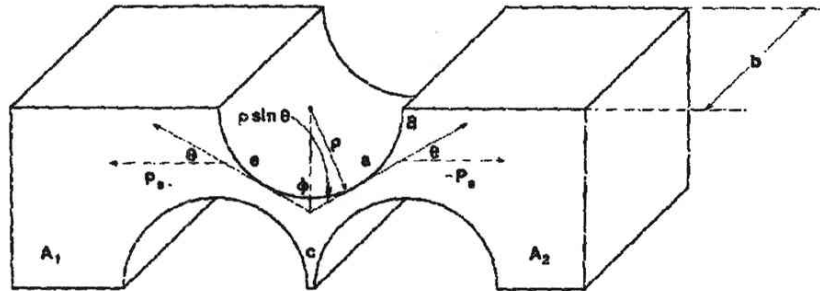


Figure 2.4 Complex Flexure used in Para-flex Stage[Teague et al., 1988]

In 1988, Moriyama et al. [1988] developed a 3-DOF MP stage that was intended for a micro-lithography system, which is used in semiconductor production. Their MP stage had a fine positioning stage and a coarse positioning system which were called the fine-table and the coarse-table, respectively. The fine-table was capable of producing a range of $\pm 8 \mu m$ in the x and y directions and a maximum rotation

of $160 \mu\text{rad}$ (33 arc-sec). The coarse-table had a 120 mm range in the x and y directions with a $5 \mu\text{m}$ resolution. The fine-table design was relatively simple as it was composed of three piezoelectric actuators mounted on flexure hinges and connected to a common end effector. Because of this design, no mechanical advantage or amplification was realized. However, the resolution of the fine-table becomes that of the piezoelectric actuators and also unmagnified. One disadvantage of this MP stage is the increased cost due to the 2 stage design.

Furukawa and Mizuno [1992] developed a new translation mechanism (one linear DOF) which utilized flexures and a single piezoelectric actuator. With the single stage mechanisms they were able to achieve $65 \mu\text{m}$ of deflection with an unspecified resolution. Their main goal was to optimize the stiffness of the mechanism using its natural frequency. One advantage of this device was its relative simplicity, which is beneficial when considering control and cost.

Furukawa et al. [1994] developed an X-Y stage which was an extension of their previous translation mechanism. Their mechanism, called the Twin-Type Translation Mechanism, received its name because of its two tier nature. The device had a range of $46 \mu\text{m}$ in the x and y directions with an unspecified resolution. It also had low parasitic yaw error of $0.1 - 0.3 \text{ arcsec}$. Due to their configuration they required four piezoelectric stack actuators which inherently increased the cost of the device.

Gosselin et al. [1996] presented a new architecture for a MP stage. Their stage called the PRR type is very similar to the 3RRR mechanism studied in this thesis. The difference is that one of the revolute joints is replaced with a prismatic joint. The PPR mechanism has 3-DOF, namely x, y, and θ . The majority of their paper dealt with kinematic analysis and calculating the workspace of this new mechanism.

In 1997, Bi et al. [1997] did accuracy analysis of a Serial-Parallel MP system. It was comprised of two 3DOF parallel mechanisms connected in series with each other. The lower platform was a 3RRR Mechanism, which is the same type of mechanism studied in this thesis. Its DOF are x, y, and θ_z . The upper platform is called

3RPS parallel mechanism. The letters RPS refer to the types of links used in this mechanism: Revolute, Prismatic and Spherical respectively. Its DOF are z , α_x and β_y . Because of the relevance of the 3RRR mechanism, further details regarding this work will occur in the next section.

In that same year, Ryu et al. [1997] developed a 3-DOF MP Stage (x , y and θ). It was a piezo actuated parallel structure similar to the 3RRR mechanism. Instead of the 3RRR configuration they used a double compound flexure pivoted lever. Their goal was to optimize the geometric parameters of the flexure in order to increase the yaw (θ) to correct for errors in current electron beam lithography systems. Through optimization their prototype achieved a total range of $41.5 \mu m$ and $47.8 \mu m$ in the x and y directions respectively, while the yaw range was 322.8 arcsec (1.565 mrad).

Chang and Du [1998] developed a large range MP mechanism with 1 degree of freedom. Their design was based on the Scott–Russell Mechanism which converts and amplifies motion from one direction to an in-plane orthogonal direction. They successfully used finite element tools in combination with Taguchi’s method to find near-optimal values for flexure geometry. By using two Scott–Russell Mechanisms in series they achieved a range of $112 \mu m$. This differed slightly from their theoretical estimate of $232 \mu m$, because they neglected to account for the force/displacement relationship of the piezoelectric actuators used in their device.

Gao et al. [1999] developed a new x - y stage which can be described as multi-levered amplified design. The stage was piezo-driven by two actuators and had a range of $45 \mu m$ and $40 \mu m$ in the x and y directions respectively. The respective resolutions of the stage were 20 nm in the x -direction and 18 nm in the y -direction. One interesting note about this stage is that in its design the parameters of each hinge were optimized separately.

2.4 The Piezo Driven 3RRR Micro-positioning Stage

2.4.1 Introduction

The focus of this section is the currently completed research done on the 3RRR MP Stage. This section has two main parts, in particular: The work of Bi et al. [1997], and the work of Zou [2000]. However, before delving into these particulars, a sub-section dedicated to the physical description of the 3RRR MP stage and its behaviour is presented.

2.4.2 3RRR MP Stage — Physical Description and Behaviour

The 3RRR MP Stage is a parallel actuated system. It is symmetric about 120° as shown in Figure 2.5.

In Figure 2.5 notice the main components: 3 piezoelectric actuators mounted in parallel, the compliant mechanisms and the end effector. Each arm of the compliant mechanism contains 3 revolute flexure hinges, which translate the input motion from the actuator to the end effector, plus an additional hinge near the interface of the piezo actuator and the compliant mechanism, which ensures that shear stress is minimized in the piezo actuator.

Figure 1.2 depicted the result of a single actuator extension; specifically, the resultant direction of the end effector is in approximately the same direction as the piezo extension, and the production of a yaw angle. The amount of end effector's translation and rotation is directly proportional to the amount of piezo extension.

When two of the actuators are extended in combination, the total translation of the end effector is approximately the resultant of the translation due to the extension of each piezo actuator. Meanwhile, the total rotation becomes the sum of the yaw angles induced by the actuators. This was the pose shown in Figure 1.3.

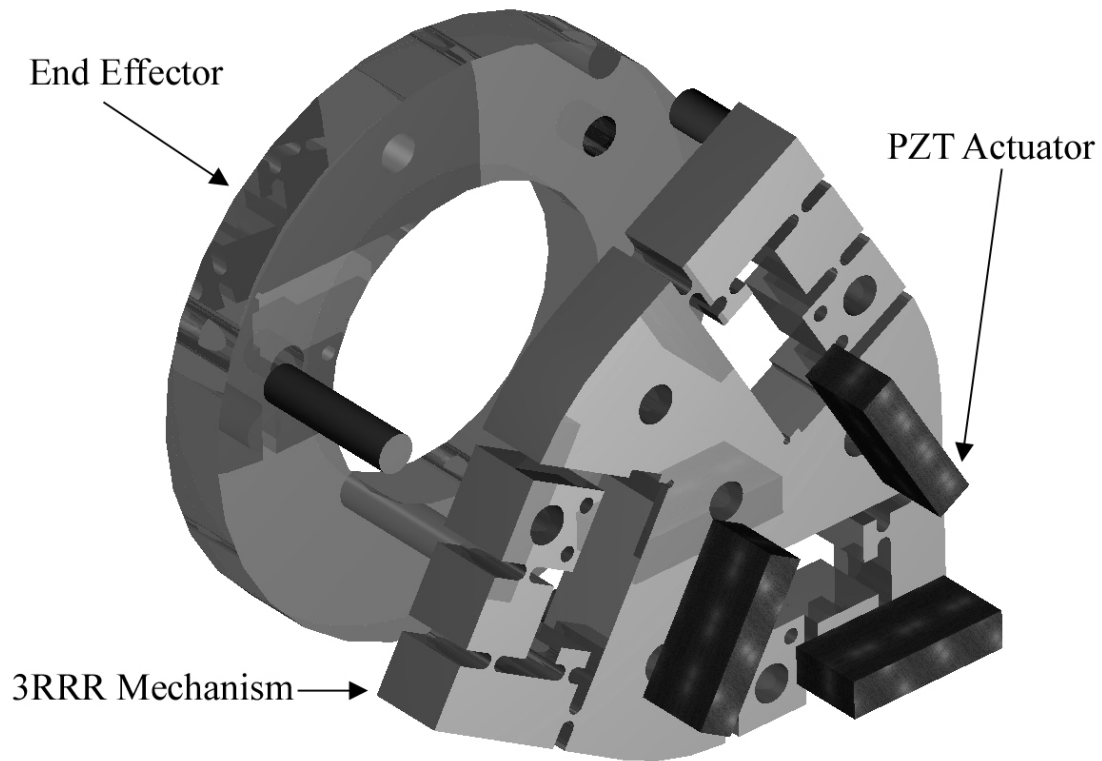


Figure 2.5 Exploded View of 3RRR MP Stage

Finally when all three piezo actuators are fully flexed, as in Figure 1.4, the end effector does not move in the x - or y -direction. However, maximum yaw rotation is achieved, approximately equal to 3 times the rotation of the yaw angle resulting from fully flexing one piezoelectric actuator.

Because the actuators deliver continuous motion. Any position(x,y) can be realized with the workspace of the MP stage. Workspace refers to the envelope the end effector can reach. These relationships in particular will be examined in subsequent sections.

2.4.3 Work of Bi et al. [1997]

To the author's knowledge, the first 3RRR MP Stage was created by the Beijing University of Aeronautics and Astronautics. Bi and his associates developed a hybrid

serial-parallel mechanism for micro-positioning, specifically aimed at manipulating cells. The device incorporated two 3 DOF micro-positioning systems in order to make the hybrid which had a total of 6 DOF.

The first MP system was the 3RRR mechanism studied in this thesis. It was responsible for delivering the x , y and $\theta(yaw)$ degrees of freedom. While the second, referred to as the SPU mechanism, was based on a “Stewart Platform” and was responsible for the z , $\alpha(pitch)$ and $\beta(roll)$.

The objective of their research was aimed at completing a kinematic analysis of the combined system. However, they mentioned there are four main difficulties when considering the design of a micro-positioning system. These are:

1. the optimal setting of design parameters in order to achieve the desired results,
2. the control system including interface with the end-user,
3. the instrumentation of the system, as micro-positioning systems are notoriously difficult to “sense”,
4. the sensitivity analysis of the MP system with specific attention to manufacturing tolerances and assembly accuracy.

By assuming a constant Jacobian matrix for all kinematic “poses”, they defined the forward kinematics of both the 3RRR mechanism and the SPU mechanism. Using their kinematic models they were able to calculate the hybrid’s workspace.

Further they realized that coupling between the two mechanisms was at a minimum. They supported their analysis by creating a working prototype, and concluded that the work-space was sufficient to accomplish cell manipulation, with promising development in the IC chip industry.

2.4.4 Work of Zou [2000]

Zou's research was aimed at developing an understanding and a design tool for the 3RRR planar mechanism. Her research had 3 main objectives, namely:

1. to develop an accurate and computationally efficient kinematic model for the RRR compliant mechanism based on the PRBM approach,
2. to develop a computationally efficient dynamic model for the 3RRR compliant mechanism based on the PRBM approach,
3. to perform a preliminary study of control methods for the 3RRR compliant mechanism.

Zou showed that the constant-Jacobian method for kinematic analysis shows satisfactory results. The benefit of the constant Jacobian method is that it can be solved explicitly compared to the mathematically exact forward kinematic model which requires an iterative solution.

She also said that conventional analysis methods, including the finite element method, are not capable of modelling manufacturing and measurement error. She mentioned that the constant Jacobian method, if tuned, can offer as accurate a solution as the finite element method.

To her credit, Zou also instituted a real-time controller for the 3RRR compliant mechanism. The dynamic model was based on the PRBM. The model was "sufficiently accurate" as it was based on an "experimentally verified constant-Jacobian method". Because of the constancy and approximations the resulting model was computationally efficient.

Also she found that the dynamic model was much more applicable to real-time control vs. the finite element method. Note that this is the case for the finite element model she developed, which had a large number of active degrees of freedom.

In general the greater number of active degrees of freedom in a model, the greater the computational time required to solve. That said, an accurate finite element model with a few active degrees of freedom, may be more applicable to real-time control.

Zou also developed a finite element model of the 3RRR mechanism. She considered it to be of high accuracy compared to the other methods she employed. She also noted that the finite element method is a useful tool for the design of compliant mechanisms.

However, her finite element model had some fundamental flaws. First, plane stress was assumed as the stress state for the entire compliant mechanism including the flexure hinges, which are not arguably ‘thin’. Second, as shown in Figure 2.6, the mesh of the model can be considered much too coarse for meaningful results, particularly at the flexure hinges.

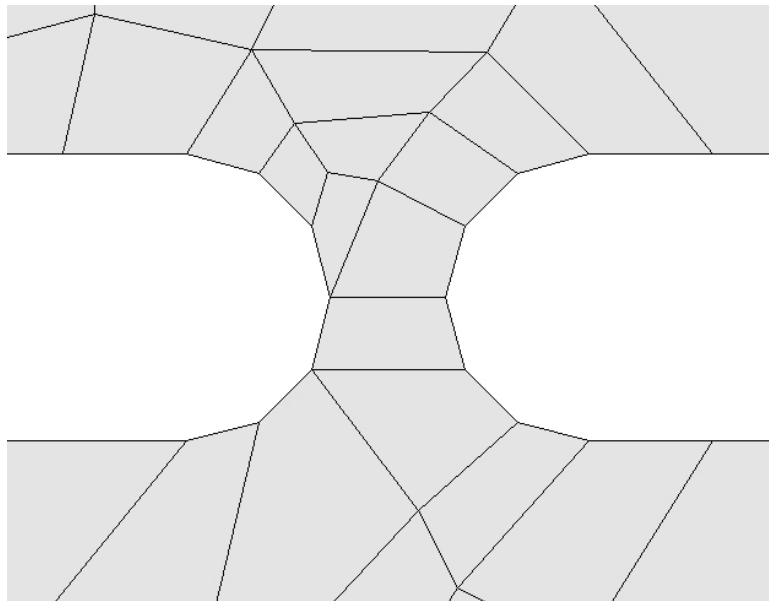


Figure 2.6 Poor Meshing of the Flexure Hinges of the Original 3RRR Model [Zou, 2000]

Another over simplified assumption is that the PZT actuators will deliver the input motion in the direction of their length. This results in over-stiffening of the model; further, she neglected to account for the reaction force vs. relation governing the

actuator behaviour. Assuming the piezo-extension could be modelled as pure input displacement implies that the actuator is infinitely stiff. Clearly this is not the case.

In Zou’s defence, her goal was to explore the finite element method as a tool for compliant mechanism design. Some of her predecessors, as shown in this thesis, viewed the finite element method to be “too cumbersome” for compliant mechanism design. Also, her original model was used as the “parent” for all models created by the author of this thesis. Further, Zou’s admittance that the model required refinements, spawned the research involved in this thesis.

2.5 Concluding Remarks

This literature review was broad in nature. After its completion, it was decided that there was need to further understand the solid mechanics of the flexure hinge. In the reviewed literature, it was apparent that finite element models of flexure hinges and compliant mechanisms were often out by errors greater than 5 per cent, when compared to experimental data. Because most of the models were done in a plane fashion, it was hypothesized that either the wrong plane state was used or that a plane state is not a valid assumption for some hinges.

Also, many researchers viewed the finite element method as “too cumbersome” for compliant mechanism design. A technique that eased the use of the finite element method would be beneficial. If the said technique could accurately model the behaviour of the flexure hinge using a low number of DOF, the models of compliant mechanisms and flexure hinges could be used with other analyses such as dynamic, modal, and optimization.

A review of the fundamentals of solid mechanics and the finite element method is completed in the next chapter.

Chapter 3

Theoretical Foundations

3.1 Introduction

The purpose of this chapter is to review the base foundations of the theory employed in this thesis. This will help to aid the reader in understanding the results presented in subsequent chapters.

This chapter will be broken up into a number of sections as follows: a review of the fundamentals of elementary plane theory of elasticity, a review of analytical beam theory, and a review of the finite element theory of solid mechanics. The discussion of this chapter is restricted to linearly elastic isotropic materials.

3.1.1 Fundamentals of the Theory of Elasticity

The theory of elasticity enables one to estimate the stress and strain inside a body subjected to external loads and constraints. The theory can be used either independently or in combination with simplifications derived using the mechanics of materials method to obtain the stress-strain field estimation, as well as the deformation, and /or deflection.

For clarification, the theory of elasticity is the theory which attempts to describe how solids behave when loaded within the linear elastic range of the structure's material. The theory is rigorous in its mathematics, however it is only practical for a limited number of problems. The basic idea behind the theory is to simultaneously satisfy [Cook and Young, 1985]:

1. the conditions of equilibrium at every point,
2. the continuity of the displacement field,
3. the loading and support conditions.

This method is the foundation of the finite element method. Because, this method requires that all conditions are met, it is often known as the exact solution. However, because it is based on some assumptions it is most often still an approximation.

Elastic Theory enables one to find mathematically unique solutions if the body has a linear load vs. displacement relationship. For problems with large displacement, buckling and material non-linearities there may be more than one state of stress and deflection that will support the applied load. Though the theory of elasticity is more complicated than the mechanics of materials method, it can yield solutions which cannot be obtained by the latter method.

In comparison, the Mechanics of Materials method requires an educated guess on how the body deforms. The deformation field may be exact, however in general it is likely an approximation. The deformation field yields a strain field, and then using elastic law a stress field can be obtained [Cook and Young, 1985]. Statics can then be used to relate the stress-field to the external loading. This process will be seen more in depth in the next section.

In the developments presented in this chapter, the following assumptions are made:

- strains and displacements are small,

- the material used is homogeneous, isotropic, and linearly elastic,
- loads do not vary with time,
- body forces, such as weight and those due to acceleration, are neglected.

With these assumptions and restrictions in mind, attention is now turned to the fundamentals of elastic law.

3.1.2 Uniaxial Loading and Poisson's Ratio

Hooke's Law states that a body of homogeneous isotropic material subjected to a uniaxial stress load will undergo a strain deformation in the form:

$$\epsilon_x = \frac{\sigma_x}{E}. \quad (3.1)$$

Any free surface not experiencing load or constraint will have zero stress in the direction normal to the free surface, as shown in Figure 3.1.

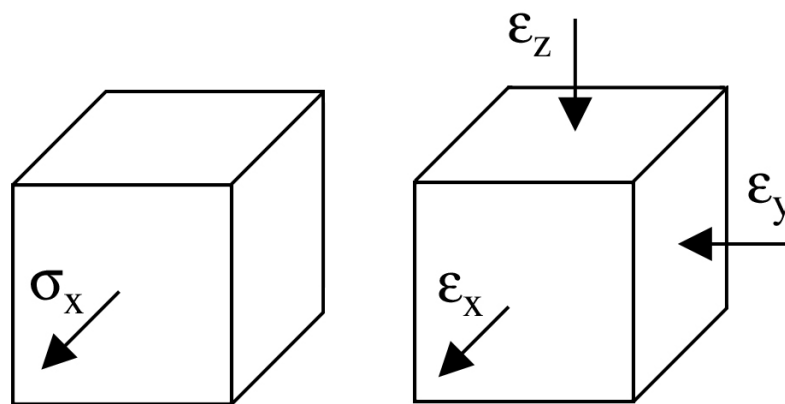


Figure 3.1 An element subjected to loading in the x direction

However the strains ϵ_y and ϵ_z are not zero, and are defined as:

$$\epsilon_y = \epsilon_z = -\nu\epsilon_x, \quad (3.2)$$

where ν is Poisson's ratio. In the next section multiaxial loading is examined.

3.1.3 Multiaxial Loading: Generalized Hooke's Law(GHL)

Consider a 3-D cube element with side lengths equal to 1 unit subjected to loading in x-, y- and z-direction, as shown in Figure 3.2.

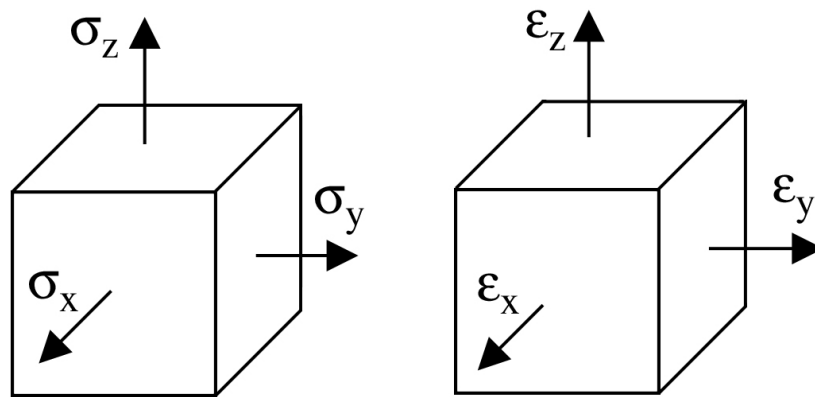


Figure 3.2 A unit element subjected to loading in the x, y and z directions

Notice after loading each side length has increased by the amount of strain in their respective directions. For instance the lengths parallel to the x-axis are now $1 + \epsilon_x$ in length. Note that this is deformation only and regardless of the translation the element may experience.

Using the principle of superposition the effect of the combined loading on the element may be obtained by determining separately the effects of various loads and combining the results obtained. This is possible provided that:

- Each effect is linearly related to the load which produces it, and so the material is not loaded past its proportional limit.
- The deformation resulting from any given load is small and does not affect the conditions of application of the other loads.

By examining the x-direction it is known that an axial load in this direction will cause a stress σ_x ($\frac{P_x}{A}$) and also a strain in the x-direction, $\epsilon_{x1} = \frac{\sigma_x}{E}$ (as well as strains in the y- and z-direction). Further an axial load in the y-direction will cause a stress and strain in that direction but also strain in the x-direction, $\epsilon_{x2} = \frac{-\nu\sigma_y}{E}$. Likewise in the z-direction, the resultant strain is $\epsilon_{x3} = \frac{-\nu\sigma_z}{E}$. Then by using the superposition method within the bounds of the assumptions, the following relation is realized:

$$\epsilon_x = \epsilon_{x1} + \epsilon_{x2} + \epsilon_{x3} \quad (3.3)$$

$$= \frac{\sigma_x}{E} - \frac{\nu\sigma_y}{E} - \frac{\nu\sigma_z}{E} \quad (3.4)$$

$$= \frac{1}{E} [\sigma_x - \nu(\sigma_y + \sigma_z)] \quad (3.5)$$

The expressions of strain in the y-direction and z-direction respectively, are derived in the same manner and are expressed as:

$$\epsilon_y = \frac{1}{E} [\sigma_y - \nu(\sigma_z + \sigma_x)], \quad (3.6)$$

and

$$\epsilon_z = \frac{1}{E} [\sigma_z - \nu(\sigma_x + \sigma_y)]. \quad (3.7)$$

The element will also experience angular deformation(γ) of the angles formed by the faces subjected to the shear stress. Shear stress in the x-y plane(τ_{xy}) is related to γ_{xy} by the following relation:

$$\tau_{xy} = G\gamma_{xy}. \quad (3.8)$$

Equation 3.8 is known as Hooke’s law for shearing stress and strain. The constant G is known as the modulus of rigidity or shear modulus of the material and is equal to:

$$G = \frac{E}{2(1 + \nu)} \quad (3.9)$$

Similarly the same element subjected to a shear in the yz and zx planes are:

$$\tau_{yz} = G\gamma_{yz}, \quad (3.10)$$

$$\tau_{zx} = G\gamma_{zx}. \quad (3.11)$$

3.1.4 2–D Applications: Plane Stress and Plane Strain

The group of equations which describe GHL can be simplified to either plane strain or plane stress behaviours. The simplifications for either behaviour are similar and yet the results are significantly different. This section details under what circumstances either of the two simplifications can occur.

Plane Stress

In order to demonstrate the plane stress state, consider a ‘thin’(or tall) element in bending as shown in Figure 3.3. Because of the free surface and the ‘thinness’ of the element it is reasonable to assume:

$$\sigma_z = \tau_{zx} = \tau_{yz} = 0. \quad (3.12)$$

This is the definition of plane stress and allows for the simplification of the equations which describe GHL. In terms of stress, these strain simplifications are expressed as:

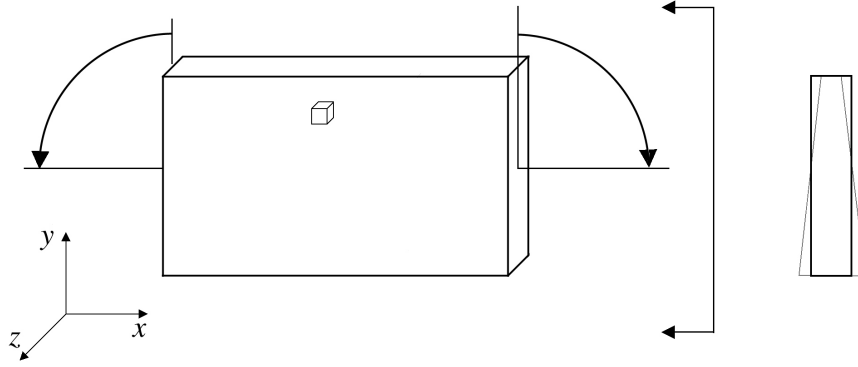


Figure 3.3 A Thin Element in Bending

$$\epsilon_x = \frac{1}{E} (\sigma_x - \nu \sigma_y) \quad (3.13)$$

$$\epsilon_y = \frac{1}{E} (\sigma_y - \nu \sigma_x) \quad (3.14)$$

$$\epsilon_z = \frac{1}{E} [-\nu (\sigma_x + \sigma_y)] \quad (3.15)$$

$$\gamma_{xy} = \frac{\tau_{xy}}{G} \quad (3.16)$$

$$\gamma_{yz} = \gamma_{zx} = 0 \quad (3.17)$$

Notice that although there is no z -component of stress there is a z -component of strain. This will cause deformation of the element as shown on the right-hand side of Figure 3.3

Plane Strain

In order to show the plane strain state, consider a ‘thick’ member fixed between two rigid blocks in bending as shown in Figure 3.4. The element A on the xy free surface of the member is in a plane stress state. However considering element B in the interior of the member it is clear that,

$$\epsilon_z = \gamma_{zx} = \gamma_{yz} = 0. \quad (3.18)$$

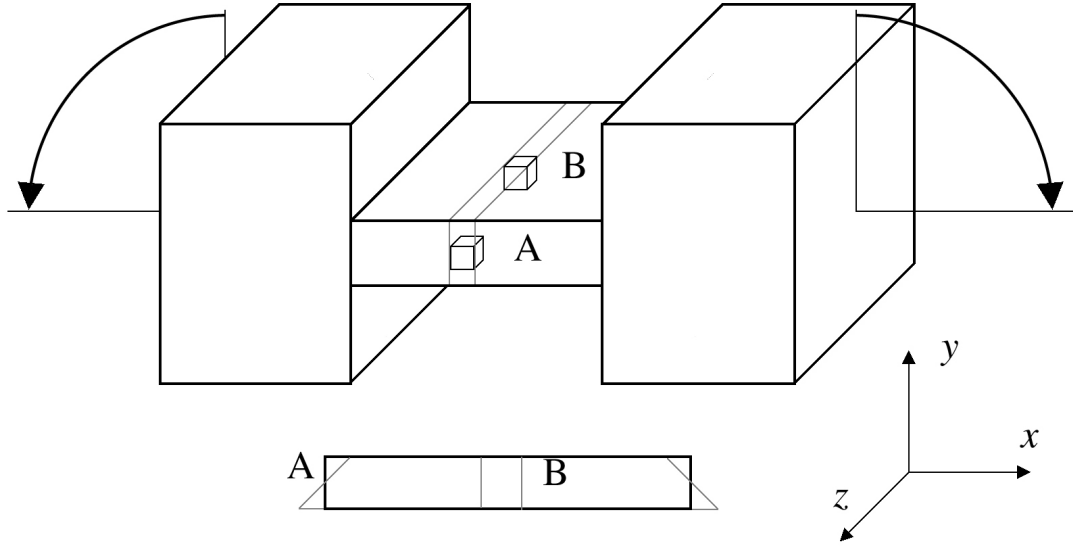


Figure 3.4 A Body Subjected to Loading in the x and y Directions

This is the definition of the plane strain state. This too results in simplifications to the equations which describe the generalized form of Hooke's Law. As stresses in terms of strain the simplifications are:

$$\sigma_x = \frac{E}{(1 - 2\nu)(\nu + 1)} [\epsilon_x(1 - \nu) + \nu\epsilon_y] \quad (3.19)$$

$$\sigma_y = \frac{E}{(1 - 2\nu)(\nu + 1)} [\epsilon_y(1 - \nu) + \nu\epsilon_x] \quad (3.20)$$

$$\sigma_z = \frac{E}{(1 - 2\nu)(\nu + 1)} [+ \nu(\epsilon_x + \epsilon_y)] \quad (3.21)$$

$$\tau_{xy} = G\gamma_{xy} \quad (3.22)$$

$$\tau_{yz} = \tau_{zx} = 0. \quad (3.23)$$

From this it is apparent that plain strain is valid when a planar body is thick.

Plane Behaviour Conclusions

The cases presented show that careful consideration must be taken when using either of the two planar simplifications. As a general rule plane stress is a good assumption

for planar bodies of thin depth. On the other hand, plane strain is a good assumption for planar bodies of thick depth.

Both of these plane assumptions can be seen as limits that the 3-D behaviour will tend to depending on its thickness (or thinness). There are thicknesses for which the behaviour of structures cannot be accurately modelled using either of these two plane assumptions. Chapter 4 will further discuss this point with the flexure hinges as the structure in question.

3.2 Beam Theory(2-D plane stress simplified to 1-D problem)

To add clarity to the material presented thus far, it is beneficial to review classical beam theory, from the view point of elastic theory. The development will show under what conditions application is possible, as well as the limitations and restrictions of the theory. Also in Chapter 5 beam elements, which are governed by beam theory, are used to simulate the behaviour of flexure hinges.

A beam is a 3-D body modelled as 1-D line with bending stiffness. In this development, a beam is considered to be homogeneous and prismatic (of constant cross-sectional area), as depicted in Figure 3.5. A beam is generally denoted by the geometric parameters: h for height, b for base, and l for length.

Before the 3-D Beam can be mapped into its 1-D counterpart, several assumptions are needed [Cook and Young, 1985]:

1. The beam width is less than the beam height, as this allows for the assumption that $\sigma_z = 0$ (it also distinguishes a beam from a plate),
2. Each differential layer in the z direction (parallel to the x - y plane) is in a uniaxial stress state,

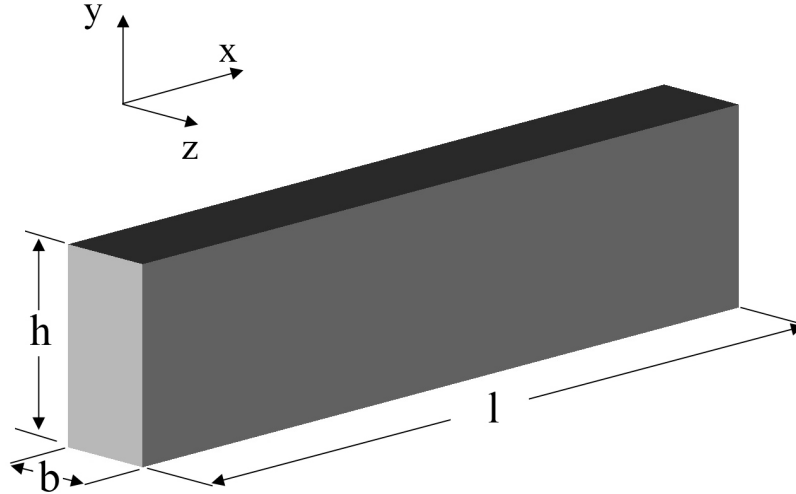


Figure 3.5 General Geometric Parameters of Generic Beam

3. The beam is prismatic (straight and constant cross sectional area) along its length and homogeneous,
4. Shear deformations are neglected,
5. The deflections that occur do so in the linear elastic regime of the material used, and
6. The deflections are small such that d^2v/dx^2 is a good approximation for curvature.

The displacement of a beam cannot be directly calculated from the applied external loads. Instead a number of steps must be followed to find the relationship. By examining the external loads, equilibrium is used to find the internal forces. The relationship between internal forces and stress is then found by integrating the various components of stress over the area which they act. Then the relationship between stress and strain is then found using Hooke's Law. And finally the relationship between strain and displacement is found using the geometry of deflection (kinematics). This process is better seen in Figure 3.6.

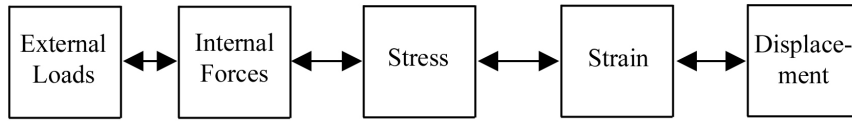


Figure 3.6 Flow Chart of Elasticity

Before discussing each of these steps, the typical notation in this derivation is given as seen in Figure 3.7. The beam has length in the x direction (l), height in the y (h) and depth (b) in the z -direction. A distributed load is specified by w_y , and dx is the differential length.

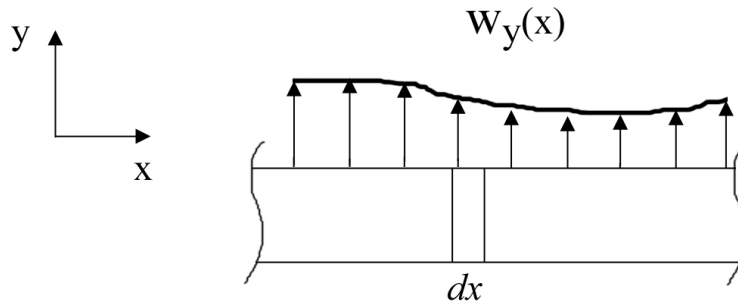


Figure 3.7 Notation used in Beam Theory Derivation

3.2.1 Statics – Equilibrium

By examining a free body diagram of a differential element of the beam, the sum of the forces in all directions should equal zero, as shown in Figure 3.8. Note that formally shear forces are also included; however, they are later ignored in this development.

Equilibrium in the y -direction after simplification is:

$$w_y = -\frac{dV}{dx}. \quad (3.24)$$

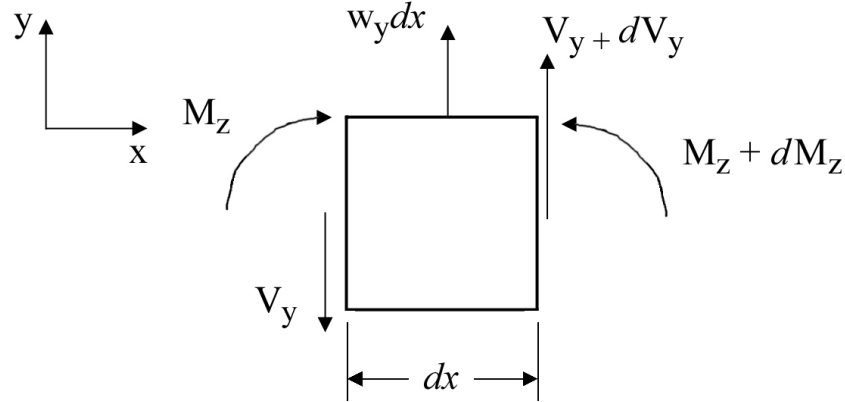


Figure 3.8 Free Body Diagram of Beam Element

While the moment equilibrium becomes:

$$V = -\frac{dM_z}{dx}. \quad (3.25)$$

By combining Equations 3.24 and 3.25 the differential relationship between external load and internal force is achieved:

$$w_y = \frac{d^2 M_z}{dx^2}. \quad (3.26)$$

3.2.2 Internal Force – Stress Relationship

Examine a section of the beam as shown in Figure 3.9. Note that only a constant bending moment is applied, which clearly implies that V and w_y are assumed to be zero. Such an assumption, in which the deformation due to V and w_y (or τ_{xy} and σ_y) are neglected, permits the derivation of simple bending formulae which are accurate for most uses.

From the above figure, the equilibrium of force in the x -direction and moments about the z -axis are respectively:

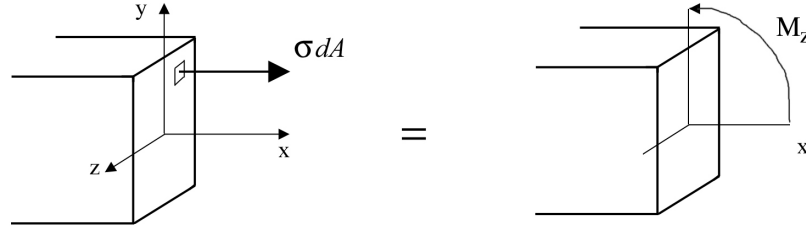


Figure 3.9 Statics of Beam Section Relating Stress to Internal Moment

$$\int_A \sigma_x dA = N = 0, \quad (3.27)$$

$$\int_A (-y \sigma_x dA) = M_z. \quad (3.28)$$

Several assumptions are needed to solve for the resulting deformation presented in the next section. These are that the beam is in pure bending ($M_z \neq 0$) and that there is one stress component ($\sigma_x \neq 0$).

3.2.3 Geometry of Deformation (Kinematics)

A prismatic beam subjected to a pure bending moment deflects in an arc-like fashion. Consider a differential element of such a beam as shown in Figure 3.10.

In order to simplify this analysis this differential element is considered to be perfectly square (all angles between sides are normal) before and after deflection (*Kirchhoff approximation*). This then implies that the shearing strain $\gamma_{xy} = \gamma_{xz} = 0$ and therefore $\tau_{xy} = \tau_{xz} = 0$, and consequently that $V = 0$ (or that the effects of shear force on deformation are ignored).

The stress components σ_z , τ_{xz} and τ_{yz} are zero along the free surfaces of the beam's sides. Because of the 'thinness' of the beam it is reasonable to consider these stress components negligible in the interior of the beam, and hence also zero. These assumptions coincide with the plane stress state in the xy plane, which again by definition states that σ_z , τ_{yz} and τ_{zx} are 0.

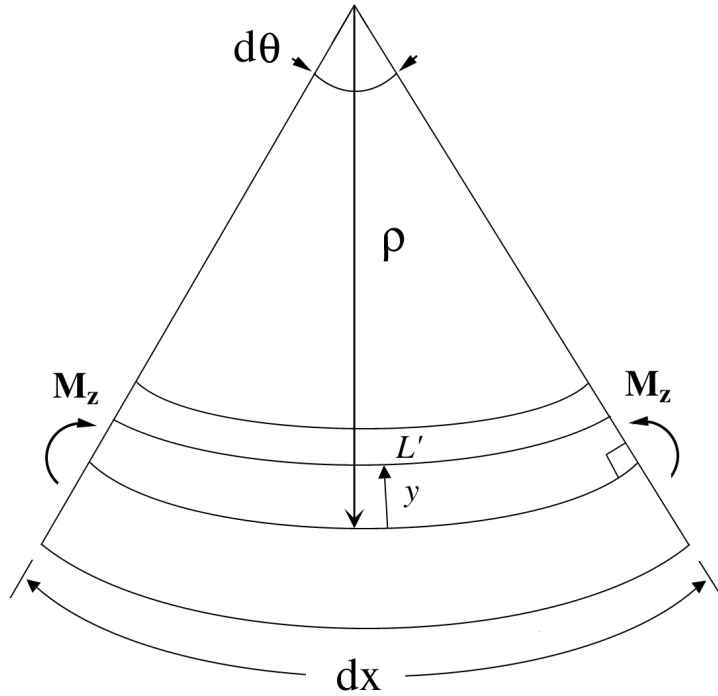


Figure 3.10 Exaggerated Arc-like Deformation of an Element of a Prismatic Beam Subjected to a Pure Bending Moment

The stress components σ_y and τ_{xy} are also zero to be consistent with the pure bending loading. Thus any element in the beam is considered to be in a uniaxially stress state. This point however leads to another assumption. By examining a strip of elements in a deformed configuration it can be clearly seen that a stress in the y -direction is required to keep the layer in equilibrium, as shown in Figure 3.11. It is assumed that for small deformations σ_y is negligible.

By again examining Figure 3.10, it is seen that under this loading condition ($M_z > 0$) the top and bottom of the beam, decrease and increase respectively in length. From this it can be assumed there is a zero strain, and hence stress, plane in the beam. This plane is referred to as the neutral surface, the length of which by definition does not undergo deformation. For the rest of this derivation it is useful to select the origin, such that it lies on the neutral surface.

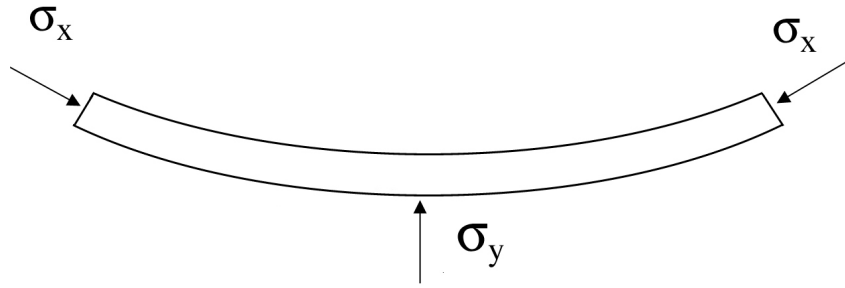


Figure 3.11 Equilibrium of a Layer of Elements in a Beam subjected to Pure Bending

Defining the radius of curvature (ρ) from the centre of curvature to the neutral axis allows the undeformed length of an element in the beam to be expressed as:

$$dx = \rho d\theta. \quad (3.29)$$

Then the arc-length of any line away from the neutral axis denoted by L' is:

$$L' = (\rho - y)d\theta. \quad (3.30)$$

The deformation of any line may then be expressed as:

$$d\delta = L' - dx = (\rho - y)d\theta - \rho d\theta = -y d\theta. \quad (3.31)$$

Then the strain of the elements belonging to the same layer may be found by:

$$\epsilon_x = \frac{d\delta}{dx} = \frac{-y d\theta}{\rho d\theta} = -\frac{y}{\rho}. \quad (3.32)$$

It is clearly seen from Equation 3.32 that the strain varies linearly throughout the height of the beam. By substituting the equation of curvature in terms of x and

vertical deflection v into Equation 3.32 the following relation is obtained:

$$\epsilon_x = -y \frac{\frac{d^2v}{dx^2}}{\left[1 + \left(\frac{dv}{dx}\right)^2\right]^{3/2}}. \quad (3.33)$$

By assuming small rotations (i.e. $\frac{dv}{dx} \ll 1$) the following relation is obtained:

$$\epsilon_x = -y \frac{d^2v}{dx^2}. \quad (3.34)$$

Equation 3.34 allows one to calculate strain at height y from the neutral axis if the deflection is known, or vice versa. With this development presented in the preceding two sections, the Internal Force - Stress relationships can be completed

3.2.4 Internal Force – Stress: Revisited

The first step in completing the Internal Force – Stress development is to combine Hooke’s Law for the 1-D stress state with Equation 3.32, which yields,

$$\sigma_x = -E \frac{y}{\rho}. \quad (3.35)$$

The location of the neutral axis is analyzed by expanding and analyzing Equation 3.27, defined mathematically as:

$$\int_A \sigma_x dA = - \int_A E \frac{y}{\rho} dA = - \frac{E}{\rho} \int_A y dA = 0. \quad (3.36)$$

From this it can be deduced that $\int y dA$ is zero, or that the first moment of the cross section about the neutral axis must be zero.

As shown in Figure 3.12, the sum of the stresses in a cross-section of the beam must be equivalent to the moment M_z (Internal Force).

Combining Equations 3.28 and 3.35 yield a relationship between the internal force, the deformation geometry and the cross sectional geometry of the beam:

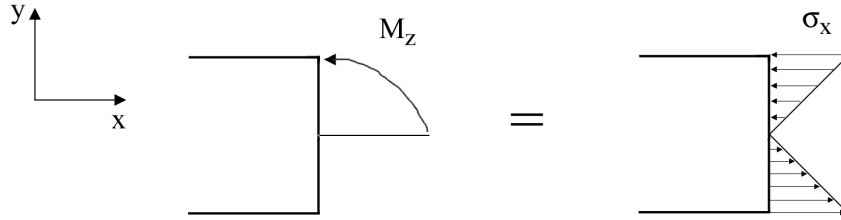


Figure 3.12 Cross Section of Beam depicting the sum of the stress equivalency to the applied moment

$$-\int_A y \frac{Ey}{\rho} dA = -M_z. \quad (3.37)$$

Introducing the moment of inertia of the beam's cross section defined as,

$$I_z = \int_A y^2 dA, \quad (3.38)$$

combining Equations 3.37 and 3.38, the following is obtained:

$$\frac{1}{\rho} = \frac{M_z}{EI_z}. \quad (3.39)$$

This of course is the famous Euler–Bernoulli beam equation. The final step is in combining Equations 3.35 and 3.39, which yields a relationship which relates stress to internal force at a given distance y from the neutral axis. This relationship can be seen in the following equation:

$$\sigma_x = -\frac{M_z}{I_z}y. \quad (3.40)$$

The stiffness of a beam is found by employing the E-B equation along the length of the beam, and is defined as:

$$\frac{M_z}{\alpha_z} = \frac{EI_z}{L}, \quad (3.41)$$

where α_z is the angle of rotation at the end of the beam approximated as dv/dx .

Though not explicitly shown here, if the structure is thick enough to be considered a plate and hence the plane strain state is dominant, the stiffness of the plate is defined as:

$$\frac{M_z}{\alpha_z} = \frac{EI_z}{(1 - \nu^2)L}. \quad (3.42)$$

For a Poisson's ratio of $\nu = 0.3$ the stiffness of a plate compared to the beam is 11 per cent greater, for equal I_z .

3.3 Finite Element Method

Application of the matrix method for structural analysis was first pursued in the late nineteen-forties and early nineteen-fifties. This interest was spawned by the necessity for lighter aircraft structures [Ross, 1990]. However it was not until the development of the integrated circuit in the nineteen-sixties and the microprocessor in the seventies, that the finite element method became relatively practical to implement.

The finite element method has grown from its static structural roots to encompass many physical phenomena including: heat transfer, vibration analysis, dynamic analysis, acoustics and electro-magnetic behaviour to name a few. However since this thesis deals only with structural statics, the finite element theory will be limited to this particular field.

Generally speaking, "the finite element method is particularly useful for solving a differential equation, together with its boundary conditions, over a domain of complex shape" [Ross, 1990]. That said, the general process is to discretize a complex structural geometry by elements of simple shape. Elements are the building blocks of any finite element model.

Elements are defined geometrically by nodes. The number of nodes which define an element is based on the complexity of the element type. This complexity is in general a function of the analysis sought (i.e. 1-D, 2-D, or 3-D). The finite element method employs the theory explained in the sections above in a very simple yet intense way. Many view the finite element method and analysis as a graphical based tool. Although the advent of the Graphical User Interface(GUI) has increased the ease of use in many commercially available packages, the engine of these software is designed to solve the equations which govern the behaviour of physical systems.

3.3.1 Derivation of Structural Matrices

The principle of virtual work states that any virtual work done on a ‘system’ due to applied loads, must be converted into an increment of internal strain energy of that ‘system’ as shown in Equation 3.43:

$$\delta U = \delta V, \quad (3.43)$$

where δU is the increment of virtual internal strain energy of the element,
and δV is the increment of virtual work done on the element.

The internal strain energy is defined as:

$$\delta U = \int_{vol} \{\delta\epsilon\}^T \{\sigma\} d(vol), \quad (3.44)$$

where $\{\delta\epsilon\}$ is the increment strain vector,
 $\{\sigma\}$ is the elements stress vector,
and vol is the volume of the element.

By replacing the stress vector in equation 3.44 with the equivalent matrix representation of generalized Hooke's law ($\{\sigma\} = [D]\{\epsilon\}$), the said equation takes the form:

$$\delta U = \int_{vol} \{\delta\epsilon\}^T [D] \{\epsilon\} d(vol), \quad (3.45)$$

where $[D]$ is the elasticity matrix that contains the coefficients of generalized Hooke's Law.

The strains in the above relation can be related to displacements using the relation:

$$\{\epsilon\} = [B]\{u\}, \quad (3.46)$$

where $[B]$ is the strain-displacement matrix based on the elements shape function,
and $\{u\}$ is the nodal displacement vector of the element.

Equations 3.45 and 3.46 are combined to yield:

$$\delta U = \{\delta u\}^T \int_{vol} [B]^T [D] [B] d(vol) \{u\} \quad (3.47)$$

The displacement of the body is defined as:

$$\{v\} = [N]\{u\}, \quad (3.48)$$

where $[N]$ is the matrix of shape functions of the element.

The virtual work term is due to nodal forces and is defined as:

$$\delta V = \{\delta u\}^T [F] \quad (3.49)$$

With the terms of the virtual work principle defined, Equations: 3.47 and 3.49 can be substituted into Equation 3.43 to yield:

$$\{\delta u\}^T \int_{vol} [B]^T [D] [B] d(vol) \{u\} = \{\delta u\}^T [F] \quad (3.50)$$

Often Equation 3.50 is presented as:

$$\{\delta u\}^T \int_{vol} [B]^T [D] [B] d(vol) \{u\} - [F] = 0, \quad (3.51)$$

or simply:

$$[K] \{u\} = [F]. \quad (3.52)$$

The advantage of the finite element method is that it can yield approximate solutions to problems too complicated to be solved exactly. It has the capability of using a 3-D constitutive law, at the expense of drastic increase to the number of DOF in a model. That said, the disadvantage of the finite element method is its unforgiving nature. Using an incorrect relation, assumption, loading condition, or constraints will result in incorrect results. The theory in itself is beautiful; however, employing the theory requires careful planning and execution, always ensuring the model is error free and that the results make sense. Structurally speaking, it is a tool only practically used by those who have a priori knowledge of elastic theory and strength of materials. It is not a short-cut and requires the user to be fully aware of what is happening behind the GUI.

3.3.2 General Comments about the Finite Element Method

There are several levels of abstraction available to the user of the FEM. Full 3-D models are extremely accurate; however, they come at the cost of increased complexity and DOF. This drastically increases the computational power required to solve the governing equations of a model, and also increases the amount of effort required to gather meaningful results and the time needed to build and ‘debug’ a model.

2-D models can greatly reduce the number of DOF in a model; however, depending on the mesh density the number can still be high. A 2-D model is bound to either a plane stress, a plane strain or an axis-symmetric assumption. It is up to the user to decide if the model can be accurately modelled in 2-D.

1-D models composed of either beam, spring or truss elements have the fewest number of DOF, and are the easiest to build and verify. Though they are called 1-D models, the system of elements is not bound to a single dimension. They are generally very fast and accurate if used within the assumptions of their respective 1-D theory.

Auto-meshing is a term which describes how the elements are automatically assigned to a model. In general 1-D models do not require auto-meshing, as the elements are easy enough to assign by hand between nodes. Free-meshing, a type of auto-meshing, of 2-D and 3-D models is often a convenient way to mesh areas and volumes respectively, in which an algorithm automatically defines the mesh.

Often a free mesh algorithm used with quad or brick elements, which are by far the most accurate of the 2-D and 3-D elements, cannot deal with complex geometries including holes and fillets. In general free meshing only works for triangular elements and tetrahedral elements, which due to their shape function are more stiff than required. In order to achieve an accurate model using triangular and tetrahedral elements, mesh densities have to be much higher than a mesh of quads or bricks.

The introduction of a mid-side node into an element often helps to combat this

over-stiffening. Elements with mid-side nodes are referred to as 'quadratic' which describes their shape function. The mid-side node increases the number of DOF and hence equations of a model; although, mesh densities do not have to be as high for comparable accuracy. Also with the inclusion of mid-side node, quads and bricks can be meshed to complex area and volumes using a 'mapped mesh'.

The mapped mesh algorithm still automatically meshes the area or volume in question; however, the user has more control and the resulting elements will mimic the shape of the modelled structure. In general a mapped mesh requires a lower mesh density for comparable accuracy to free mesh.

In this thesis, there is an underlying emphasis to keep the number of DOF in a model to a minimum. If the finite element method were only capable of static structural analysis, this would be more a point of elegance rather than prudence. However, the finite element method is capable of dynamic, modal, and optimization analyses. Because of the increased level of complexity required for these analyses, it is necessary to have a reasonable number of DOF in a model. Otherwise, results are often not only suspect, but impossible to obtain in some instances.

Chapter 4

Flexure Hinge Stress Behaviour

4.1 Introduction

In Chapter 3 it was shown that plane stress is a good assumption when dealing with bodies which are relatively unconstrained; this mostly applies to thin and tall bodies in bending. Also in Chapter 3, it was also shown that plane strain is a good assumption when dealing with constrained bodies, or those with significant thickness. Thick and thin in this context are relative terms which may be described as the ratio of depth (z -direction) to width (x - or y -direction).

The reviewed literature pertaining to flexure hinges mostly dealt with hinges that were assumed thin. However, to reduce the effects of parasitic deflections, hinges are often made thick so that the compliance in all the directions, other than the dominant direction, can be assumed to be negligible. Information as to what is thick and what is thin for flexure hinges is not currently available. Further, it was not known if the plane stress assumption used in the previous finite element models of the 3RRR Mechanism is valid.

The results of this chapter, are based on three finite element models: the first that assumes a plane stress state, the second that assumes a plane strain state, and the

third that is three dimensional in nature which does not imply any plane state. The models were created using the finite element software ANSYS. The 3-D finite element model was selected as the reference model for the comparison.

One significant advantage of using the finite element method is that stress, strain, and displacement are easily attained at any point of the model.

4.2 Purpose

As outlined in the above section, the purpose of this chapter has two parts:

1. To analyze the stress/strain state in flexure hinges used in the 3RRR Mechanism, and whether or not it can be accurately modelled with: plane stress, plane strain, or 3-D behaviour of the stress and strain fields.
2. To report at what thickness to depth ratio a hinge can be considered thin (valid plane stress assumption) and thick (valid plane strain assumption)

4.3 Flexure Hinge Model

4.3.1 Physical Model

In order to better understand the stress-strain behaviour of flexure hinges, a study was developed to compare the 3-D behaviour of a given hinge in bending to an assumed plane stress and plane strain behaviour of the same hinge. The model of the hinge is somewhat geometrically equivalent to those found in the 3-RRR mechanism.

Before delving into the specifics of the finite element models, an explanation of the physical hinge model is presented. It consists of a very flexible part(the hinge) of

width t , and a very rigid part(the link) of width h . The bending stiffness ratio of these two portions is approximately equal to $(t/h)^3$ and in practice is negligibly small. Therefore only a small portion of the link, denoted here by l need be considered. Also the width of the link (h) is irrelevant if this ratio is smaller than about 0.01.

As mentioned in Chapter 2, the standard parameters which describe a flexure hinge are: depth (b), radius (r), and thickness (t); however, two additional parameters, length(l) and height(h), are introduced to define the geometry of the link portion of the flexure hinge. For clarification, please refer to figure 4.1.

Note that for the presented research in this chapter: l is in the y-direction, h and t are in the x-direction, and b is in the z-direction. The values assigned to the defining parameters of the hinge are shown in table 4.1.

Table 4.1 Defining Hinge Parameters of the Flexure Model

Hinge Parameter	Value
b	10 <i>mm</i>
h	10 <i>mm</i>
l	8 <i>mm</i>
r	1 <i>mm</i>
t	0.8 <i>mm</i>

All of the parameters presented in Table 4.1 are based on the flexures found in the 3-RRR mechanism, except for l and to some degree h . The parameter l was selected so that the stress and strain fields occurring at the hinge centre are not interfering with the stress in the link. The parameter h was set to 10 *mm*; however in the 3-RRR mechanism its value can be 5, 8 or 10 *mm*, dependant upon the location of the link it defines in the 3-RRR mechanism.

This does not reduce the validity of the results because, the stiffness of the links is so much greater than that of the hinges, it can be assumed that the deformation of the link is negligible compared to that of the hinge.

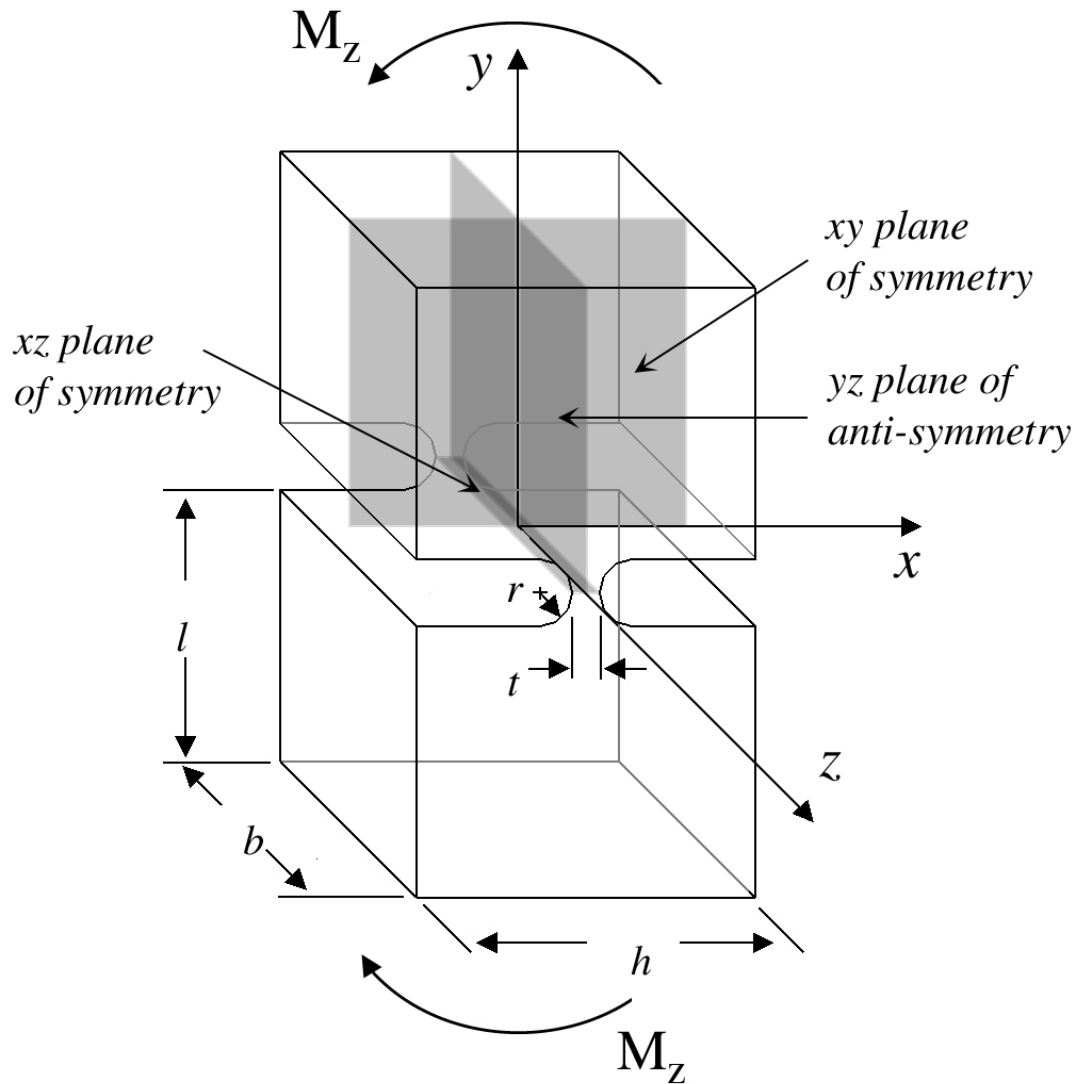


Figure 4.1 The Standard Geometric Parameters which define a Flexure Hinge

The material properties of the flexure model are modelled after the material used in the 3RRR compliant mechanism. The material used is a type of brass and its properties are as follows: Young's Modulus (E) is 105 GPa and a Poisson ratio of 0.33. The model assumes the material behaviour is linearly elastic, isotropic and homogeneous.

Flexure hinges are inherently designed to bend, and as such the model of the hinge is loaded with a couple moment parallel to z -axis. The moments of the couple are

specified at either end of the hinge as specified in Figure 4.1.

4.3.2 3-D Finite Element Model

The reference model of this study was a 3-D solid model and was based on the physical model described in the previous section. It was meshed with 20-node brick elements, which have 8 corner nodes, and 12 mid-side nodes. In general, the 20-node brick element is the most accurate of all the 3-D structural elements.

The model as shown in Figure 4.2 employed three planes of symmetry. The model has two planes of symmetry in the y- and z-directions, and anti-symmetry in the x-direction. The use of symmetry does not compromise the accuracy of the finite element model.

The use of symmetry greatly decreases the time to solution as there are approximately one eighth the number of equations to solve simultaneously. A full finite element model of the flexure hinge, given the converged mesh density, exceeds the 30,000 node limit imposed by ANSYS for academic use.

The values of deflection, rotation, and stiffness of the hinge calculated with respect to the xy-plane. Therefore they are one half(double for the stiffness) of the respective results one would attain if the hinge was fixed at its end-point.

Because of the 20-node brick element's geometric cubic nature, it is often problematic to free-mesh complex geometries including curves; however, the element's mid-side node helps to maintain the geometry of the structure being meshed. In the hinge model, most of the stress and strain occur at the radius of the hinge. As such the meshing in and around the radius is very fine. "Free-meshing" is often an attractive option for FEM users, but often the tool creates badly shaped elements, particularly when using quads and bricks in a complex area or volume. A "mapped" mesh mimics the shape of the geometry of the area or volume being meshed; as shown in Figure 4.2, when used correctly, it achieves a very fine mesh of nicely shaped elements.

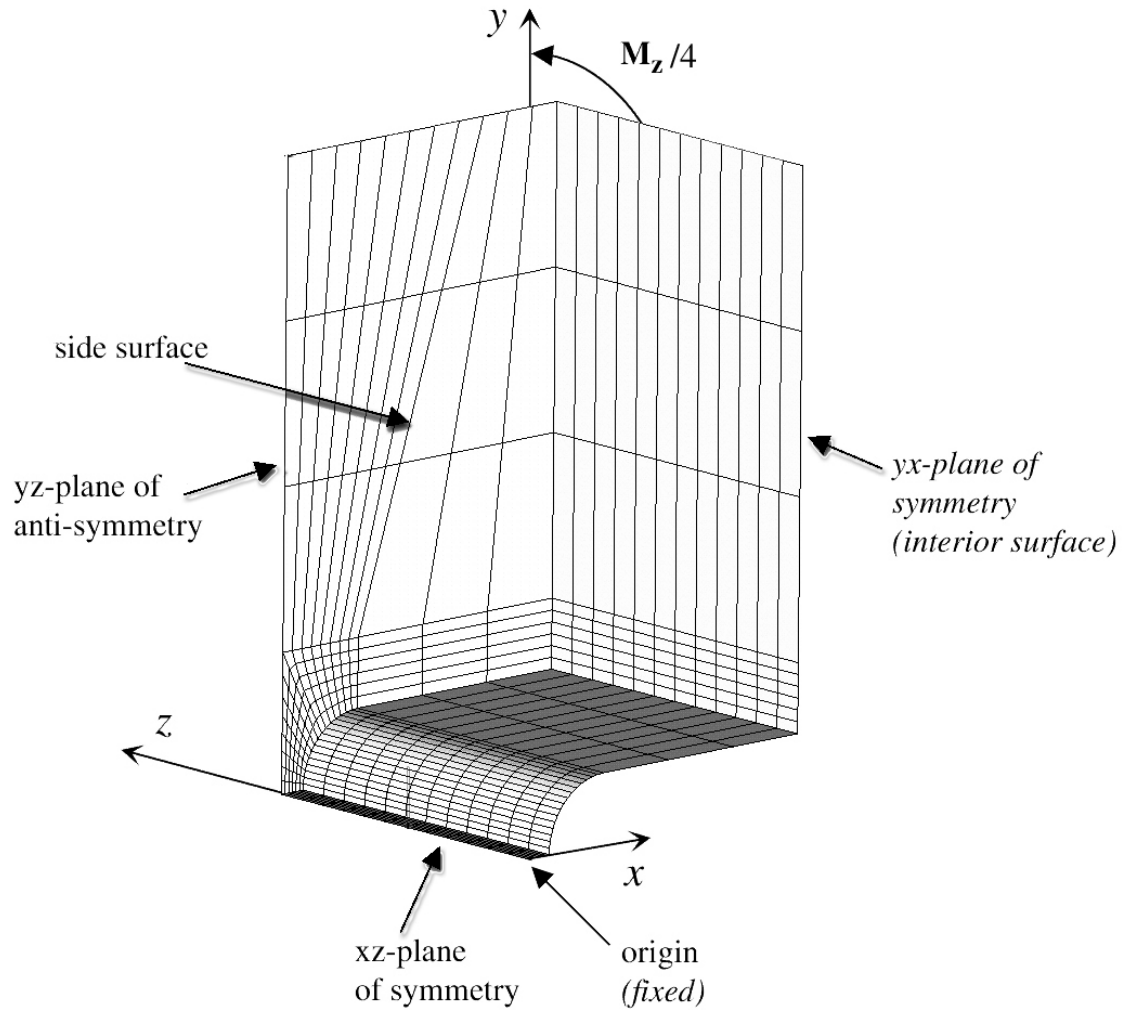


Figure 4.2 3-D Model of Flexure Hinge

Also in Figure 4.2, it is shown that the elements in the link portion of the model are coarse compared to the elements in the hinge portion. Almost all of the strain, and hence stress occurs in the lower portion, where the hinge has the least width. Though it would be visually appealing to have the entire model meshed with relatively the same size element, numerically speaking it is a waste of computational time. The elements of the link portion, can be more coarse, because they act as pure load carriers as the strain field developed in this portion is almost constant and negligible. In general, if the strain field is relatively small or constant in portion A compared to portion B of a model, the element size of portion A compared to portion B can be relatively larger with no appreciable decrease of accuracy.

Discussion is now turned to the details about the application of moment, M_z . Because the nodes of the brick elements have 3 degrees of freedom per node representing the displacements, it is impossible to apply a moment directly to the nodes. To overcome this problem fictitious beam elements are introduced to the model. The beam elements have rotational degrees of freedom, and thus a bending moment can be applied at their nodes. They transmit, if correctly used, the bending moment to proper stresses at the top surface of the hinge. The beam elements are attached to the top of the hinge, as shown in Figure 4.3.

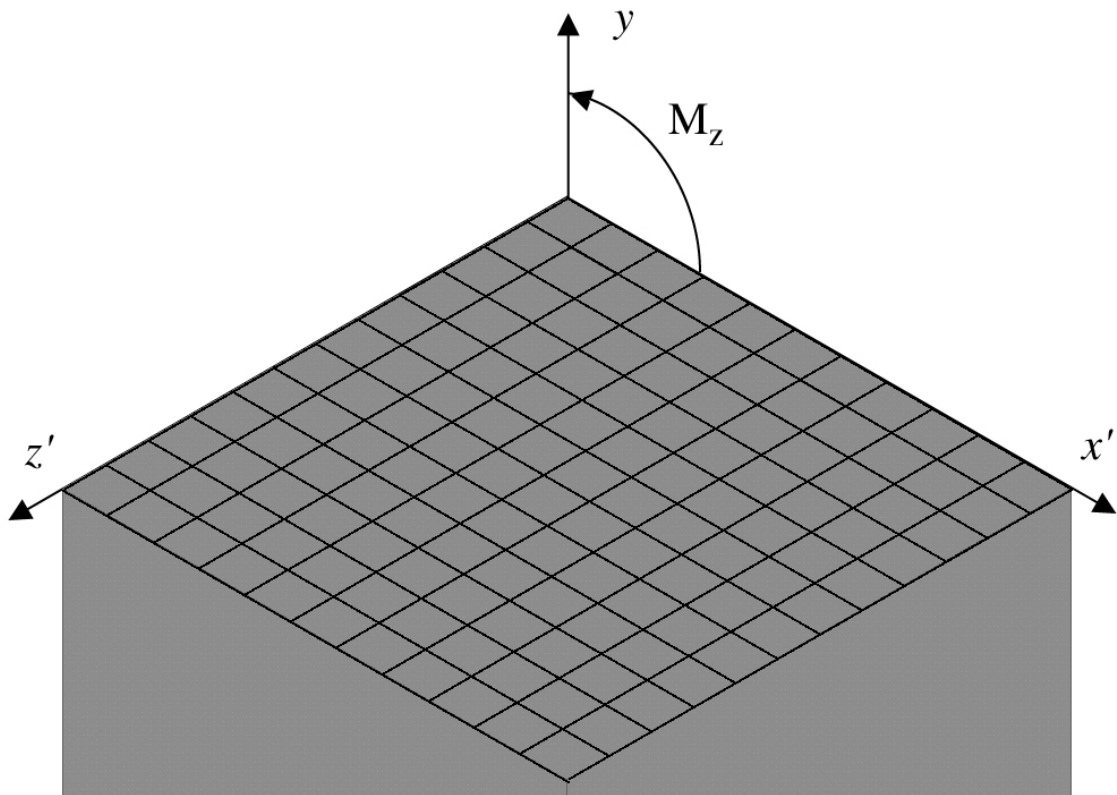


Figure 4.3 The Grid of Small yet Stiff Beam Elements Imposed to the Top of the 3-D Model

The stiffness of the beam elements was sized so that the top-most x-z plane of the hinge had constant rotation throughout the plane for a given moment loading. However, when the stiffness of these beams was set too high, numerical instability resulted. By trial and error, beams of circular cross-section of diameter of 0.01 *mm* and Young's Modulus (E) of 10×10^{24} were used.

The 3-D finite element model was coded in a parametric fashion, so that geometry of the hinge is readily changed, without having to manually re-mesh. This model has approximately 24,000 active DOF. The commented ANSYS script can be seen in Appendix A.

2-D Finite Element Models

The 2-D models are a planar representation of the x-y face of the 3-D model as shown in Figure 4.4. The main elements used in these planar finite element models were 8-node quadrilateral (quads), and they are the 2-D equivalent of the 20-node brick elements. The elements of the model have the option of using either a plane stress or plane strain stress state.

The 8-node quads have similar advantages and disadvantages compared to their 3-D counterparts; namely, the advantage of being the most numerically accurate in their 2-D class, and the disadvantage of being problematic when meshing complex areas. This disadvantage was dealt by again employing a mapped meshing strategy.

Symmetry was again used to decrease the number of degrees of freedom in the 2-D models. The models were constrained much in the same way as the 3-D model. Also, the small yet stiff beam elements were again applied to top-most nodes of the model to ensure loading was both distributed evenly to the top of the hinge and possible.

Also note that for the plane strain model, specifying a plane thickness (depth) is not possible. A unity plane thickness with regard to the length unit used in the model is assigned automatically. The stiffness of the model is then a linear function of depth. The true 2-D stiffnesses can be found by multiplying the modelled stiffness by the ratio of actual depth of the hinge to unity depth, in this case 0.01.

This model has approximately 1050 active degrees of freedom. The commented ANSYS code which defines these models is also presented in Appendix A.

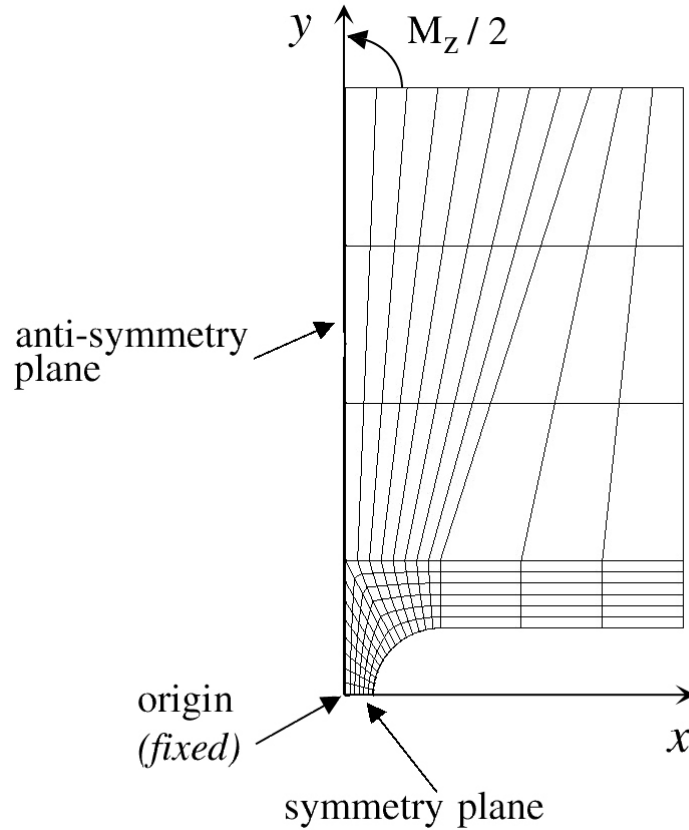


Figure 4.4 2D Planar Model of Flexure Hinge

4.4 Flexure Hinge Results

4.4.1 Test for Convergence

Because the models were coded in a parametric fashion, the density of the mapped mesh could be increased with relative ease. The convergence procedure involved increasing the mesh density until the change in the maximum deflection for a given moment loading was less than 0.1 per cent.

Another method to verify that convergence has been reached, is to visually examine a stress or strain field developed in the model elements for a given load. If the field is continuous in nature, then numerical stability has been achieved. This was the case for the three finite element models. Figure 4.5 shows the continuity of the field

for the y -component of stress.

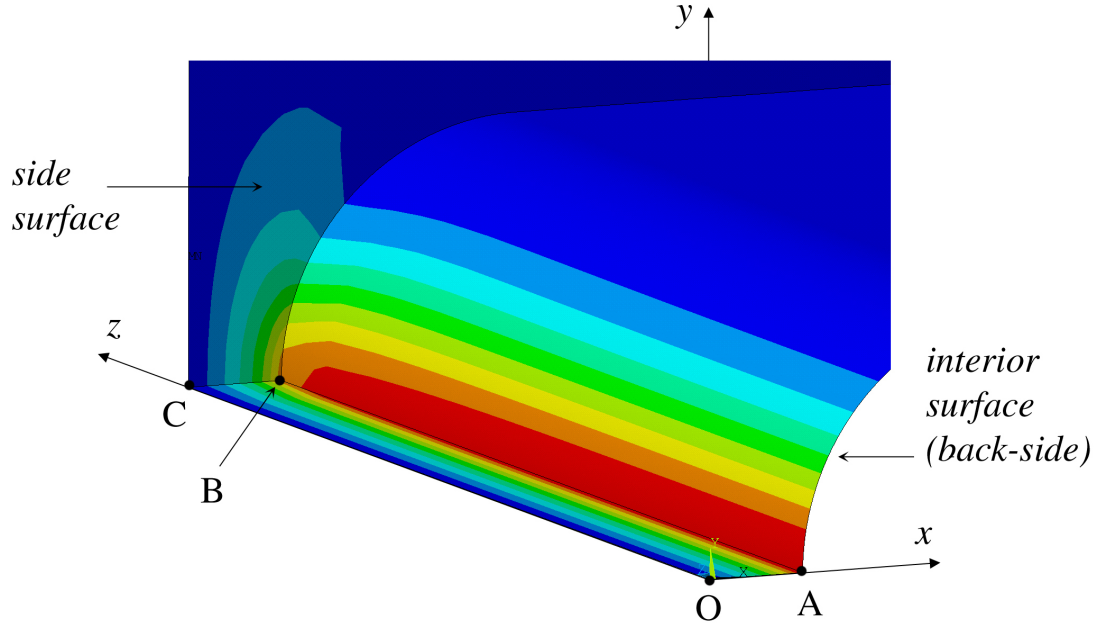


Figure 4.5 Continuous Nature of the Field of Stress in y -direction of the 3-D Flexure Model

The maximum stress in the above figure was 219.3 MPa , the contour of which is shown in red. Figure 4.5, also shows that all of the stress, and hence strain, occurs in the filleted portion of the hinge. This is further validation that it was acceptable to make the link portion of the hinge of a coarse mesh density.

4.4.2 3-D Behaviour of the Right Circular Flexure

In order to better understand the stress-strain behaviour of the flexure hinge, the key results of 3-D finite element model will be discussed in depth. Before delving into the specifics, an explanation is given of the results that would be obtained if beam theory was used to analyze the flexure hinge. By first using Equation 3.40 with the values of loading and geometry from the model, the maximum stress according to beam theory is estimated as,

$$\sigma_{max}^{BT} = \frac{M t}{I_z} \frac{1}{2} = \frac{200 \text{ Nmm}}{\frac{(0.8 \text{ mm})^3 (10 \text{ mm})}{12}} \frac{0.8 \text{ mm}}{2} = 187.5 \text{ MPa} \quad (4.1)$$

However, it is known that a strain concentration will exist around geometric irregularities such as the fillets of the flexure hinge. These strain concentrations give rise to stress concentrations. The maximum stress can be found by multiplying the bending stress by a stress concentration factor (K_T). K_T is usually estimated from empirical data in a graphical form. To do so the ratios h/t and r/t of the hinge must be known.

Unfortunately, both of the ratios of hinge used in the 3RRR have not been experimentally measured. For instance the ratio h/t for the 3RRR hinge ranges from 10 to 12.5, the maximum h/t ratio as presented in Beer and Johnston [1981] is 5. Likewise the ratio r/t for the 3RRR hinge is 1.25, while the maximum presented in the literature is 0.8.

An estimate of K_T is found by applying a curve fit to the graphs of K_T . By assuming the curves become a linear function of the ratio r/t for $h/t < 1$, K_T can be expressed as:

$$K_T = \frac{A}{r/t} + B, \quad (4.2)$$

where A and B are found to be 0.096 and 1.2 respectively. K_T for the ratio $r/t = 1.25$ is then estimated as 1.28, which gives a maximum stress ($\sigma_{max}^{K_T}$) of 240 MPa. This differs significantly from the maximum stress found in the 3-D finite element model of 219.3 MPa, the stress concentration factor of which is 1.17.

If beam bending is assumed as the behaviour then the stress increases linearly from the neutral surface to the maximum value as shown in Figure 4.6.

In beam theory the maximum stress is in the y-direction, and all other stress components are assumed to be zero. Now the 3-D finite element model is used to examine what really is occurring during the bending of the hinge.

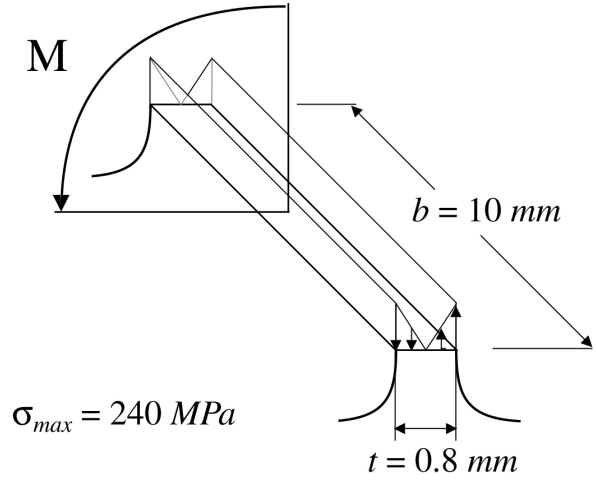


Figure 4.6 Estimated Stress Distribution using a Beam Bending Approach

By examining the stress and strain as they vary along the paths shown in Figure 4.5, the behaviour of the hinge is better understood. Paths AB, OA and BC are located on the tensioned half of the hinge. The stress and strain results were taken when a couple moment load of 0.2 Nm was applied. The stresses and strains attained from the nodal solution for Path AB, are plotted in Figures 4.7 and 4.8 respectively.

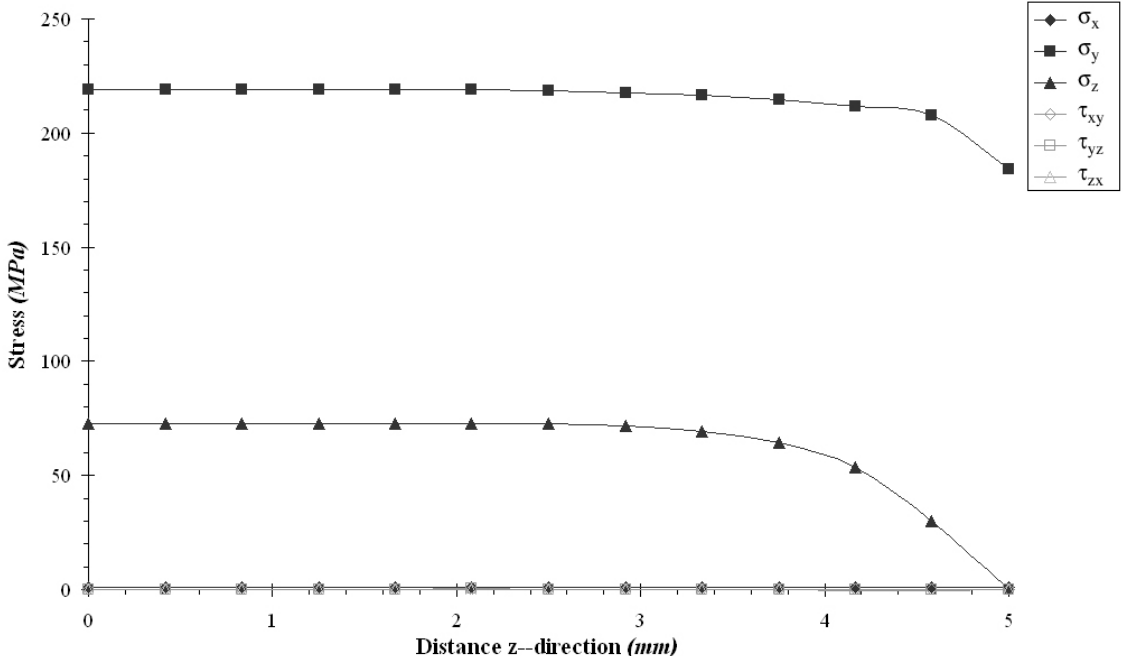


Figure 4.7 Stresses Calculated at the Nodes along Path AB

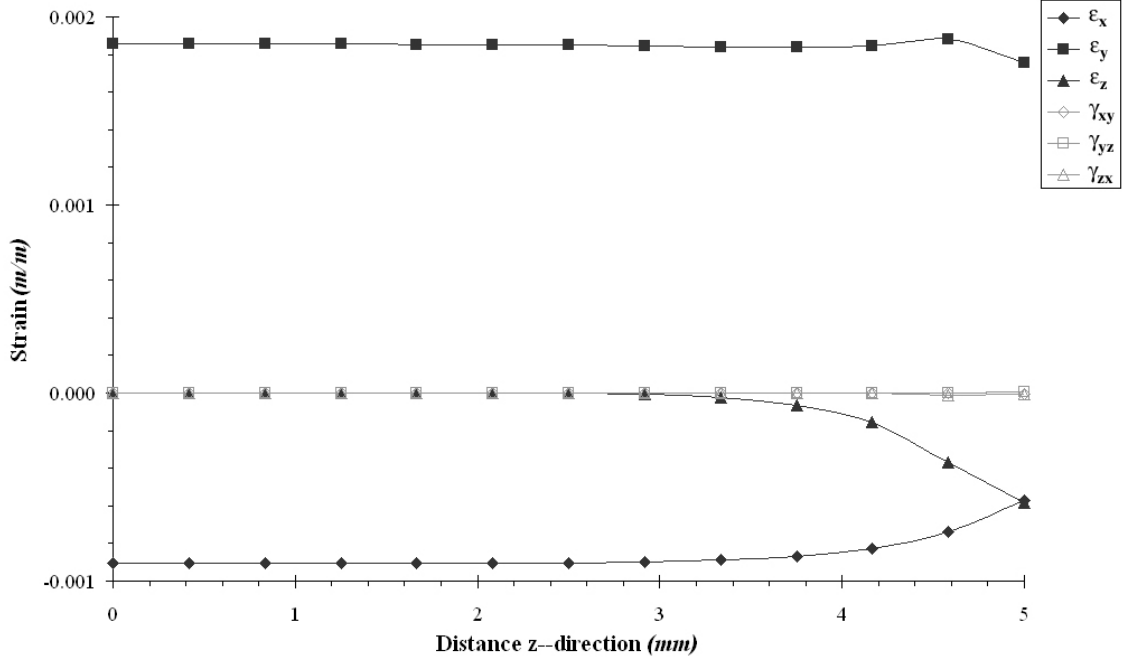


Figure 4.8 Strains Calculated at the Nodes along Path AB

It becomes immediately apparent that at the centre of the hinge (point A), when the distance in the z -direction is 0 mm , that the strains $\epsilon_z = \gamma_{xz} = \gamma_{yz} = 0$ and that $\sigma_z = \nu\sigma_y$ which respects the plane strain state condition. Also note that $\epsilon_x = -\nu\epsilon_y$. The plane strain conditions are preserved up to about 3.5 mm ($\approx 70\%$ of the bent section).

On the other hand, at point B, on the side surface, the stresses $\sigma_z = \sigma_{xz} = \sigma_{yz} = 0$, and that $\epsilon_z = -\nu\epsilon_y$, which is valid for the plane stress state. Note that the plane stress conditions disappear quickly when moving away from the side surface.

The stress σ_y remains relatively constant at 220 MPa along Path AB, and decrease to a value of 185 MPa at the side surface at B. Also the stress, σ_z is constant at 73 MPa for about 70% of the path, and decreases to zero as it approaches point B.

This suggests that the interior, and a significant portion, of the hinge is governed by the plane strain state, while the side surface(s) is governed by the plane stress state. There exists a portion of the hinge (about 25%), which is governed by 3-D elastic law, as the stress state changes from plane strain to plane stress.

The variation of the stresses and strains along Paths OA and BC verify that the interior of the hinge is in a plane strain state and that the side surface is in a plane stress state. The stress and strain data of these paths are shown in Figures 4.9, 4.10 and 4.11.

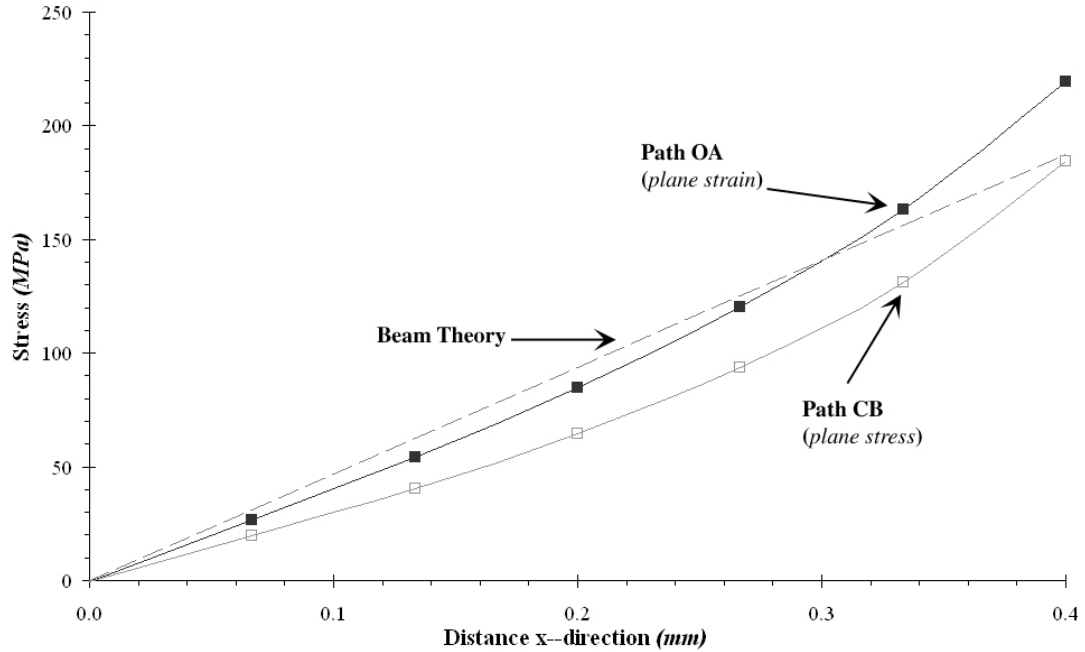


Figure 4.9 Stress in the y-direction Calculated at the Nodes along Paths OA and CB

Figure 4.9 shows how the dominant bending stress (σ_y) grows as the distance away from the neutral surface is increased. The curve labelled beam theory shows how σ_y would linearly increase if the hinge was governed by beam theory. The curves from both Path OA and CB show that this linear relationship does not exist, and hence the hinge cannot be considered to be uniaxial stress state. Notice that the maximum stress occurs in the interior of the hinge when it is governed by the plane strain state.

Figure 4.10 verifies that the side surface of the hinge (Path CB) is in the plane stress state, as σ_z is close to zero. The fact that σ_z for Path CB is not completely zero, suggests that the mesh was not as accurate as first expected. Because the plane stress state disappears so quickly, a higher mesh density in the z-direction near the

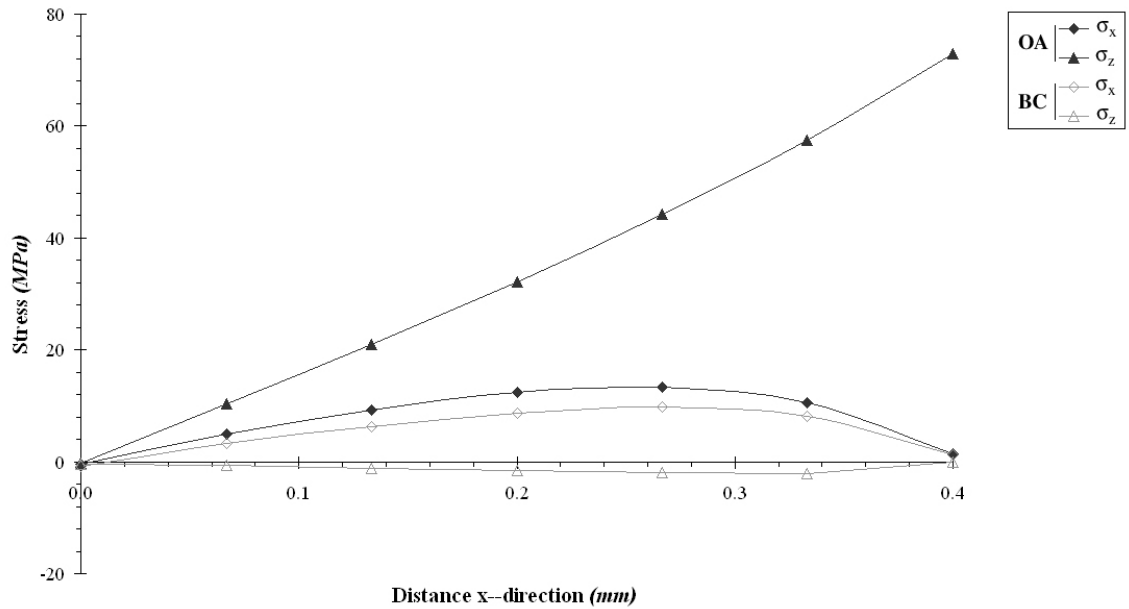


Figure 4.10 Stresses in the x- and z-direction Calculated at the Nodes along Paths OA and CB

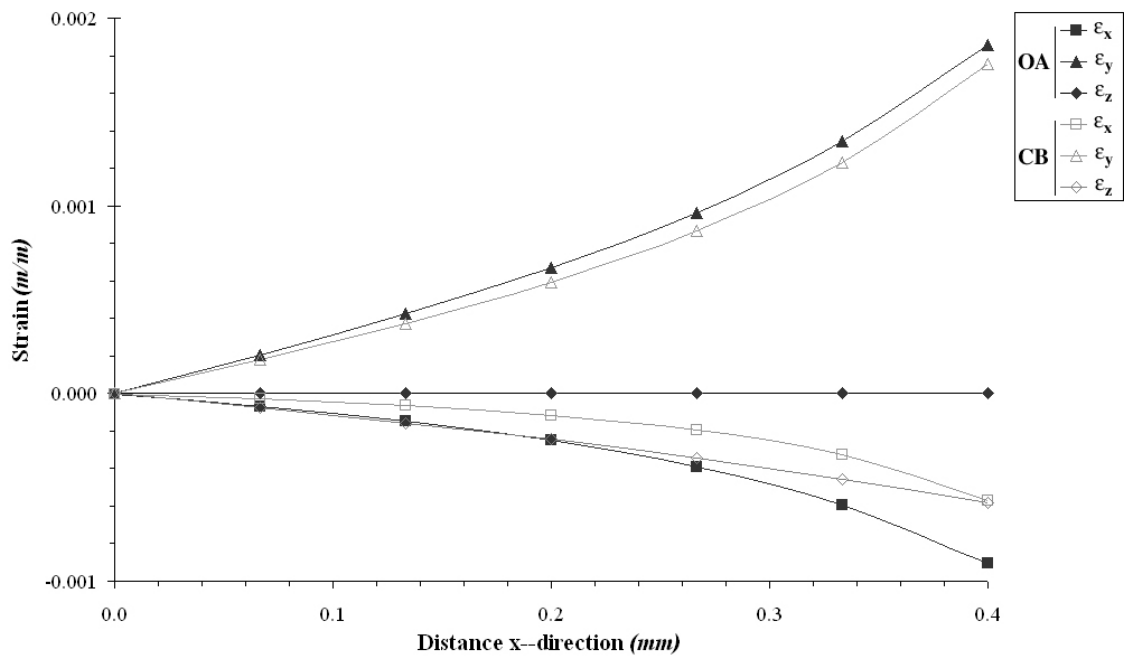


Figure 4.11 Strains Calculated at the Nodes along Paths OA and CB

free surface is required. Doing so, would ensure that σ_z was zero at the side surface, however the resulting stiffness of the model would hardly change, as the majority of

the hinge is dominated by the plane strain state.

Figure 4.11 shows that the strain in the z -direction in the interior of the hinge (Path OA) is zero, which shows that the plane strain state is in fact governing the entire interior of the hinge.

From the stress and strain plots of the paths, it is clear that the interior of the hinge is in the plane strain state, while the side surface is in the plane stress state. Further confirmation of this is found by examining the deformation of the x - z plane of the hinge centre. A graphical representation of the deformation is presented in Figure 4.12 that depicts the full x - z plane of the hinge centre for a moment loading of $0.2 Nm$ and a displacement scaling factor of 500.

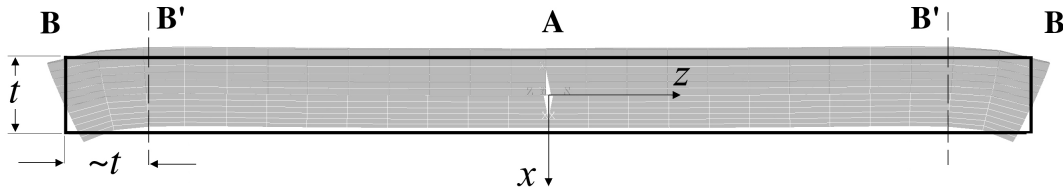


Figure 4.12 Deformation of the xz -plane of the Centre of the Hinge

Along $B'B'$ ($\sim 70\%$ of the cross section) the deformation is characteristic of the plane strain state. The strain ϵ_z in this section is completely constrained by the rigid links. Only close to the side surfaces at points B does the deformation become characteristic of the plane stress state.

There should be little doubt, that the behaviour of the hinge is 3-D in nature. May it, nevertheless, be approximated by either plane stress or plane strain with reasonable accuracy? This question is addressed in the next section, by a comparison of stiffnesses of the 2-D plane stress and plane strain models to the 3-D finite element model for a range of hinge width to thickness ratios.

4.4.3 Stiffness Comparison of 3-D Models with 2-D Models

The stiffness of hinges is the most important information required for accurate assessment of the 3RRR operations. Therefore, such information will be extracted first from the 3-D model (referred to as exact) and then from the possible 2-D approximations.

First consider the deflection of the hinge when subjected to a moment loading, as shown in Figure 4.13.

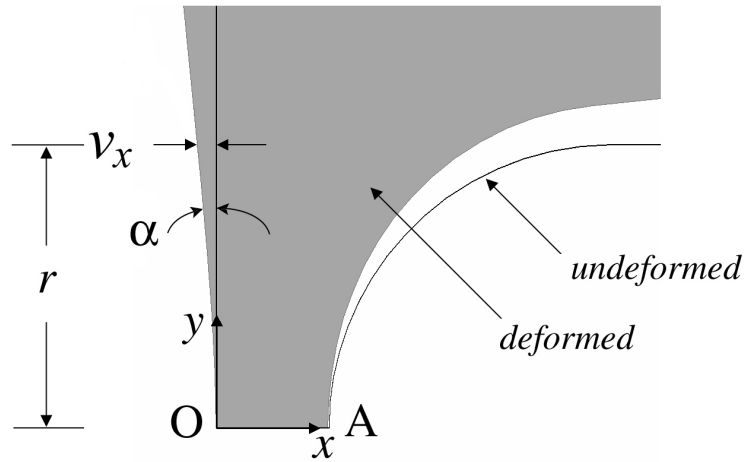


Figure 4.13 Deflection of the Hinge: Defining v_x and α

By plotting the lateral deflection v_x as a function of the distance along the length, it is easily shown that practically all of the deformation occurs at the hinge and that the link rotates as a rigid body, as shown in Figure 4.14.

This clearly shows that rotation angle of the link α can be considered constant, and hence obtained from any point of the link. The rotational bending stiffness of a hinge is given by the formula:

$$k_\alpha = \frac{M}{\alpha}, \quad (4.3)$$

where α is the rotation at the hinge end (*for* $y = r$). Similarly, the lateral bending

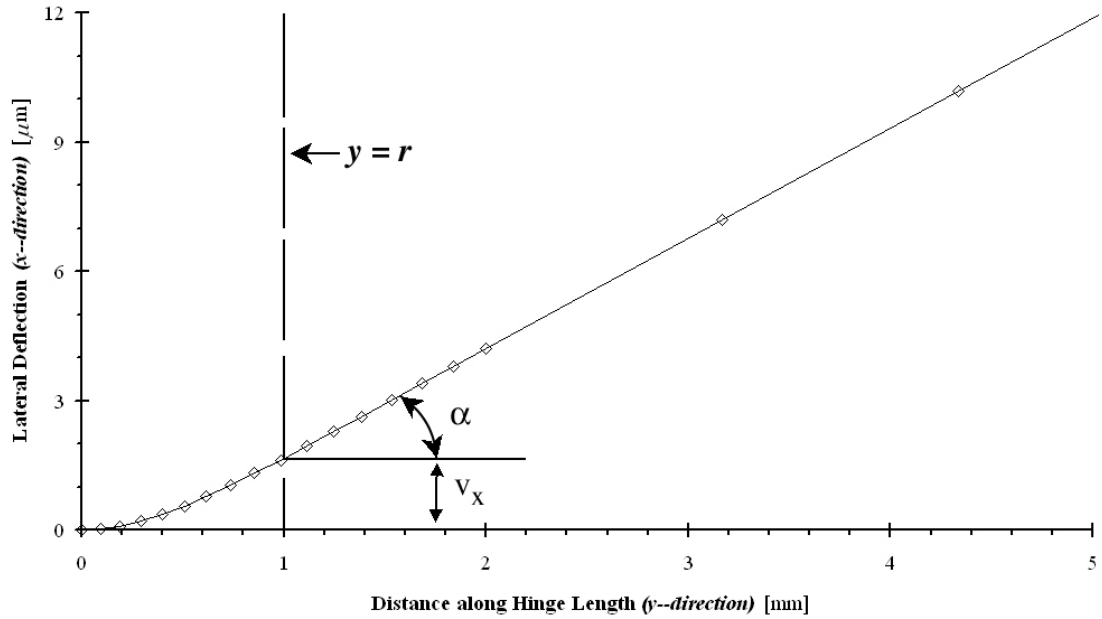


Figure 4.14 Deflection of the Hinge: Defining v_x and α

stiffness is defined as:

$$k_v = \frac{M}{v_x}, \quad (4.4)$$

where v_x is again calculated at the hinge end.

For the 2-D approximations the entire 2-D model was assumed to work either in the plane stress or plane strain condition. The geometries and loading for all models were identical. The equivalent Paros and Weisbord stiffnesses were also found by taking the inverse of the compliance as calculated by Equations 2.7 and 2.8.

The stiffnesses k_α and k_v were calculated and compared, the results of which are shown in Table 4.2.

From the results presented in Table 4.2 a number of things are apparent. As can be seen for this particular geometry, the rotational stiffness k_α for the plane strain approximation (k_α^ϵ) is 1.9% higher than the exact value, while k_α for the plane stress approximation (k_α^σ) is 9.2% lower than the exact value.

This first shows, that the 3-D stiffnesses k_α^{3D} and k_v^{3D} lie between the lower bounds of the respective plane stress stiffnesses, and the upper bounds of the respective

Table 4.2 Rotational and Lateral Bending Stiffnesses of the 3–D finite element model, the 2–D finite element models assuming plane strain and plane stress, and the Paros and Weisbord Simplifications

Model	$k_\alpha \frac{Nm}{rad}$	$k_v \frac{kNm}{m}$
Exact	78.2	120.1
Plane Strain	79.7 (+1.9%)	122.2 (+1.7%)
Plane Stress	71.0(−9.2%)	110.5 (−8.0%)
Paros and Weisbord	85.0 (+8.7%)	85.0 (−29.2%)

plane strain stiffnesses. This is to be expected as the 3–D finite element model has portions that are characterized by the plane stress state, and other portions that are characterized by plane strain. Second, it is clear that the 3–D stiffnesses are closer to the plane strain stiffnesses than the plane stress stiffnesses. This too, is expected as the plane strain behaviour is dominant for a larger span of the hinge’s depth, whereas the plane stress behaviour only holds for the two free surfaces normal to the direction of depth. In conclusion, it can be said with confidence that if either of the two plane behaviours must be selected for future modelling of the 3RRR mechanism, plane strain is a better assumption to use for the hinges of the said mechanism.

Third, the ratio of the stiffnesses for the 2–D models, $k\alpha^\sigma/k\alpha^\epsilon$ is 0.89. This completely agrees with the prediction based on elastic theory, in which this ratio should equal $(1 - \nu^2) = 0.89$. This is another sign that this finite element solution is correct.

Finally, with regard to the Paros and Weisbord stiffnesses, notice that k_α is greater than any of the other respective stiffnesses of the other models; however, it can be said that it is at least in the “ball–park” of the other respective stiffnesses. The value of k_v is significantly lower than any of the other respective stiffnesses. One of the reasons the Paros and Weisbord calculations are inaccurate is that the geometry of the hinge of the 3RRR mechanism does not comply with the assumptions used in the Paros and Weisbord development.

4.4.4 Classification of Thick and Thin Hinges

In order to verify when a 2-D model with either the plane stress or plane strain assumption can be used, the rotational bending stiffness of the hinge was compared to the respective stiffness of the plane stress and plane strain assumptions for varying b/t ratios. The depth b of the 3-D hinge was varied incrementally from ‘very thin’ to ‘very thick’, and at each increment the bending stiffness k_α was found.

For 2-D models, their stiffnesses are proportional to the depth b . Figure 4.15 shows the plot of the stiffness ratio k_α/b for increasing depth to thickness ratio (b/t).

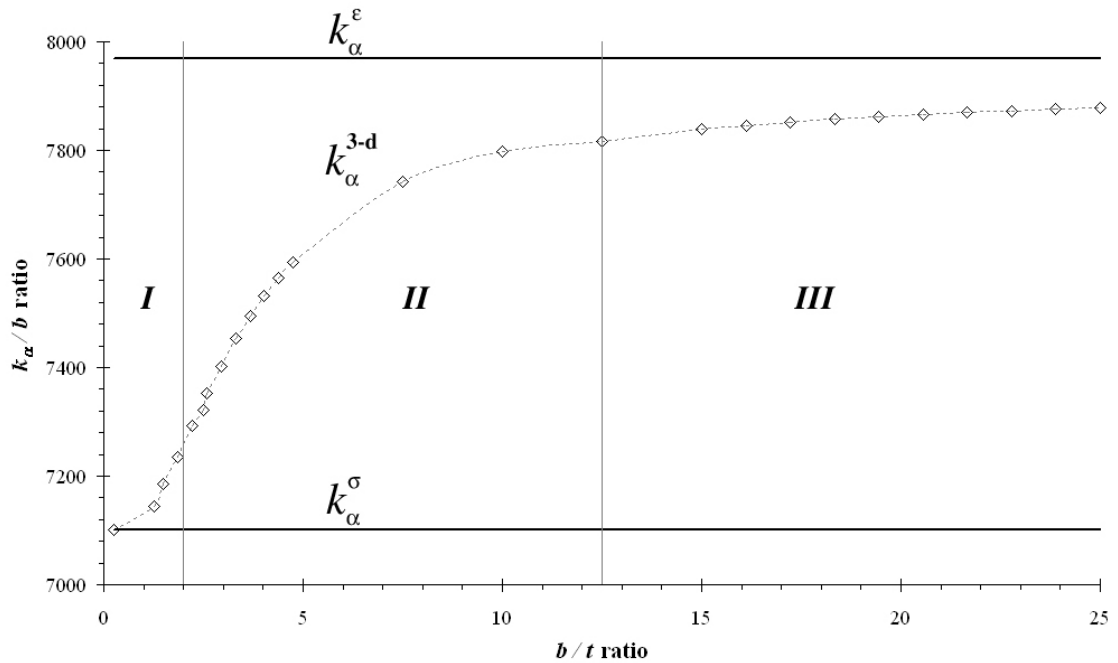


Figure 4.15 Plot of k_α versus b/t ratio

Figure 4.15 shows that the 3-D stiffness of the hinge is always bound between the plane stress(lower bound) and plane strain(upper bound) stiffnesses, for varying b/t ratios. In the domain labelled *I*, the 3-D bending stiffness of the hinge is approaching the plane stress stiffness. In domain *III*, the 3-D bending stiffness is approaching the plane strain stiffness.

These domains were actually selected by examining a plot of a relative errors Δk_α^ϵ and Δk_α^σ , as shown in Figure 4.16. These relative errors are computed using the

formulae:

$$\Delta k_{\alpha}^{\epsilon} = 100 \frac{k_{\alpha}^{\epsilon} - k_{\alpha}^{3D}}{k_{\alpha}^{3D}}, \quad (4.5)$$

and

$$\Delta k_{\alpha}^{\sigma} = 100 \frac{k_{\alpha}^{\sigma} - k_{\alpha}^{3D}}{k_{alpha}^{3D}}. \quad (4.6)$$

Using a threshold of 2 %, the domains are defined as:

I: plane stress if $b/t < 2$

II: mixed if $2 \leq b/t \leq 12.5$

III: plane strain if $b/t > 12.5$

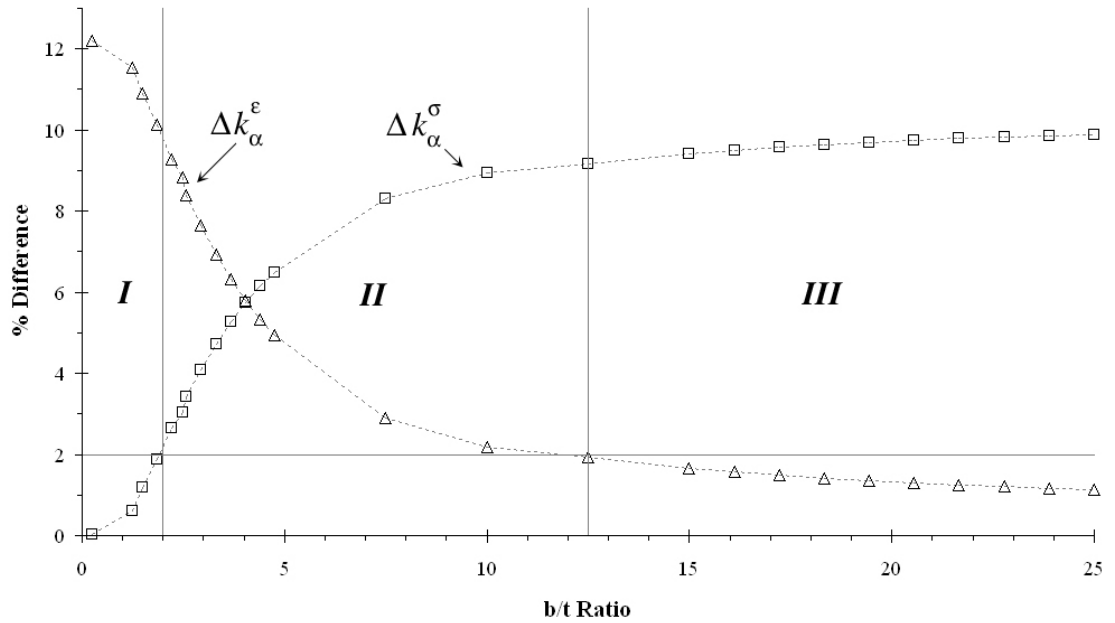


Figure 4.16 Plot of Percent Error k_{α} versus b/t ratio

In domain *II*, the stiffness of the hinge cannot be accurately approximated with either of the two plane assumptions. For a hinge in this domain, a 3-D analysis is required.

Note that almost identical results were obtained for k_{ν} .

4.5 Flexure Hinge Conclusion

It is apparent that the stress–strain behaviour of the flexure hinge used in the 3RRR mechanism is 3–D in nature. Through the hinge’s depth, the free surfaces at either end are governed by plane stress and a significant portion of the hinge is governed by plane strain. Between these two plane behaviours there lies a region which is governed completely by 3–D elastic theory.

By using 2–D analysis, either the upper limit (by assuming the plane strain state) or the lower limit (by assuming the plane stress state) of the hinge’s stiffness can be determined. The difference between these two limits is about 10 %. The stiffness of real hinge(from the 3–D model) depends on the b/t ratio.

For the hinge used in the 3RRR mechanism($b/t = 12.5$) the 2–D plane strain model, resulted in over–stiffening of about 1.9%. Thus for this particular hinge the plane strain assumption is much better than the commonly used 2–D plane stress assumption(9.2 % under–stiffened).

It was found that hinges can be considered ‘thin’ for b/t ratios less than 2 and ‘thick’ for b/t ratios greater than 12.5. Plane stress is then appropriate assumption for hinges which are ‘thin’, while plane strain is an appropriate assumption for hinges which are ‘thick’. Hinges with $2 \leq b/t \leq 12.5$ are governed by 3–D elasticity. Chapter 5 will address some alternate ways of handling such hinges.

Chapter 5

The Equivalent Beam

Methodology

5.1 Introduction

In the previous chapter it was concluded that a hinge with geometry such that $2 \leq b/t \leq 12.5$ requires a full 3-D analysis in order to obtain accurate results. The 3-D model used in Chapter 3, which utilized 3 planes of symmetry, contained over 24,000 DOF. The model was considered to be very accurate; however, it was also shown that it was not perfect. For instance σ_z along path AB was not zero, although it certainly should be.

An accurate 3-D model of the 3RRR mechanism would require over 1,000,000 DOF dedicated to its hinges alone, as two of the three planes of symmetry are no longer usable. Clearly this is too many DOF, especially if any dynamic or optimization analysis are required. Does this mean that mechanisms which contains ‘Domain II’ hinges cannot be feasibly modelled? The answer to this question is no. There are a number of conceivable ways to accurately model flexure hinges that fall into this domain, without having to complete a full 3-D analysis.

After a hinge is loaded, three points are of key interest: the maximum stress in the hinge, the end-point rotation and the end-point deflection. It is possible to shift the parameters of a hinge (i.e. E , b , t , or r) such that a 2-D model, using one of the plane state assumptions, would match the exact results. A model of this type for the 3RRR mechanism would still have almost 45,000 DOF dedicated to the hinges alone! This too is considered to be an unacceptable number of DOF.

It was shown in the previous chapter that the stress developed in the links is negligible compared to the stress in the hinge during loading. Further, the stress in the links is a 1-D plane stress state, as such they can be suitably and accurately modelled using beam elements. This would help to decrease the number of DOF in the model.

The stress behaviour of the hinge is 3-D in nature, containing elements in either the plane stress or plane strain state. Despite its 3-D stress-strain nature, its behaviour can be characterized quite accurately using the stiffnesses k_α and k_v for the end-point rotation and deflection prediction, and the beam centre's section modulus ($\mathcal{S} = M_z/\sigma_{max}$). A single beam can be sized such that one of these characteristics are equivalent to that of the real hinge. This would be similar to PRBM, where essentially k_α is modelled by a spring.

The Equivalent Beam Methodology (EBM) accurately models all of the above mentioned characteristics of a flexure hinge. It does so by replacing the real hinge with a number of fictitious beams of equivalent length, stiffness, and section modulus (at the hinge centre). The geometric parameters which define the fictitious beams give rise to the mathematical equivalence of the characteristics in a low DOF way. As such it will accurately predict the maximum stress, the displacement and the angle of rotation of a flexure hinge, regardless of its b/t ratio.

It was conceived to be used in conjunction with the finite element method, although it is not restricted to the finite element method. A full hinge then can be modelled with as few as 4 elements. For comparison purposes, a 3RRR model constructed in this way only requires 180 DOF for the hinges. The advantage of a model with

a small number of DOF is that it not only greatly decreases the time to solution, it also allows for more involved analyses such as dynamic, optimization and modal. Further, the governing equations are greatly simplified and conceivably applicable to a real-time control environment.

Following this section, this chapter is subdivided into three parts, namely: the development of the EBM, a comparison of the EBM and conclusions about the method.

5.2 Development

In this development the x-axis is the direction of hinge length, as such the angle of rotation after loading is α , and the lateral deflection is now v_y . The development of the EBM is based on half hinge stiffness and geometry.

In order to find the geometry of the fictitious beams in the EBM, information is required from the actual hinge being used in the compliant mechanism. Specifically, the depth of the hinge(b), the section modulus of the hinge(\mathcal{S}), Young's Modulus(E), the bending stiffnesses (K_v and K_α) and the hinge length (r). This information is used to find the geometric parameters of the fictitious beams required for deflection mapping at the endpoint, namely: the beams height (h_1 and h_2) and the beams lengths(L_1 and L_2). Figure 5.1, depicts the parameters used in the EBM.

The depths of the two beams are assumed to be constant and equal to the depth of the flexure hinge being modelled. As well, the beams are assumed to have the same proportional elastic limit (E), as the flexure hinge. Also, note that the sum of the lengths of the beams are equal to the radius of the hinge being modelled, as shown in Equation 5.1:

$$r = L_1 + L_2. \quad (5.1)$$

Because bending is the dominant deflection type of the flexure hinge, a pure bending moment in the z-direction (M_z) is used as the loading type. For small angles, the

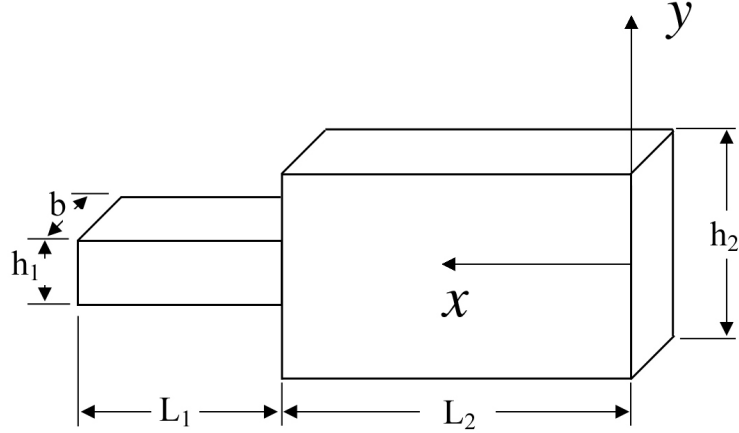


Figure 5.1 Parameters used to define the beam geometry of the EBM

slope is approximately equal to α . Under a plane stress assumption and by using Castigliano's Second Theorem α can be found using the integral:

$$\alpha = \int_0^{L_2} \frac{M_z m_z}{EI_2} dx + \int_{L_2}^{L_1+L_2} \frac{M_z m_z}{EI_1} dx, \quad (5.2)$$

where I_1 is the moment of inertial of beam 1 and equal to $bh_1^3/12$,

I_2 is the moment of inertial of beam 2 and equal to $bh_2^3/12$,

and m_z is the partial differential: $\partial M_z / \partial P_i$.

The partial differential m_z , is often referred to as the dummy moment. It describes the amount by which the moment, M_z changes throughout structure when P_i changes. For all linear elastic structures the partial m_z is independent of the magnitude of P_i ; hence P_i is often taken to be unity. Then the partial m_z is the moment produces for a unit load P_i , where P_i can be a unit load or unit moment [Cook and Young, 1985]. For the case described by Equation 5.2, P_i is a unit moment and thus the partial m_z is equal to one.

Since none of the terms of this integral are functions of x , the solution is quite simple, and after simplification is represented in the form:

$$\alpha = \frac{M}{E} \left(\frac{L_1}{I_1} + \frac{L_2}{I_2} \right). \quad (5.3)$$

The deflection(v_y) of these beams is found using a similar approach, using again Castigliano's Second Theorem. While neglecting shear effects, the deflection takes the form:

$$v_y = \int_0^{L_2} \frac{M_z m_z}{EI_2} dx + \int_{L_2}^{L_1+L_2} \frac{M_z m_z}{EI_1} dx. \quad (5.4)$$

All the variables in Equation 5.4 remain the same as in Equation 5.3, except for the dummy moment(m_z) which becomes a function of x because P_i is in this case a unit load in the y -direction, as described in Equation 5.5:

$$m_z = \frac{\partial M_z}{\partial P_i} = \frac{\partial M_z}{\partial P_y} = x \quad (5.5)$$

The solution to this integral is:

$$v_y = \frac{M_z}{2E} \left[\frac{L_1^2}{I_1} + \frac{L_2(2L_1 + L_2)}{I_2} \right]. \quad (5.6)$$

The bending stiffnesses K_v and K_α of the fictitious beams are introduced as:

$$K_\alpha = \frac{M_z}{E\alpha}, \quad (5.7)$$

and

$$K_v = \frac{M_z r}{E v_y}. \quad (5.8)$$

The stiffnesses K_v and K_α are similar to the bending stiffnesses k_v and k_α introduced in the previous chapter, except they contain E and r which reduce the number of variables in development. Combining Equations 5.7 and 5.3, after simplification yields:

$$\frac{1}{K_\alpha} = \frac{L_1}{I_1} + \frac{L_2}{I_2}. \quad (5.9)$$

Similarly by combining Equations 5.8 with 5.6 yields:

$$\frac{1}{K_v} = \frac{1}{2} \left[\frac{L_1 (L_1 + 2L_2)}{I_2} + \frac{L_2^2}{I_1} \right]. \quad (5.10)$$

From Strength of Materials, the Section Modulus of a beam in bending is classically defined as:

$$\mathcal{S} = \frac{I}{c} = \frac{M}{\sigma_{max}}, \quad (5.11)$$

where I is the moment of inertia of the beams cross section, c is the maximum distance from the plane of bending to the outside edge, or half the beam height for a rectangular beam. However, because the section modulus can be calculated from the real hinge, it is convenient to transform Equation 5.11 into:

$$\frac{1}{\mathcal{S}} = \frac{h_1}{2I_1} \quad (5.12)$$

By looking at Equations 5.1, 5.9, 5.10, and 5.12, it is seen that there are 4 equations to solve for the 4 geometric parameters of the fictitious hinges namely: L_1 , L_2 , h_1 , and h_2 .

The first parameter is found from Equation 5.12, since it is all in terms of h_1 it takes the form:

$$h_1 = \sqrt{\frac{6\mathcal{S}}{b}} \quad (5.13)$$

The parameter L_1 is found by solving Equation 5.9 for h_2 and by solving Equation 5.1 for L_2 , the results of which are substituted into Equation 5.10. The closed form solution for L_1 then takes the form:

$$L_1 = \frac{rbh_1^3}{12} \left(\frac{\frac{2}{K_v} - \frac{1}{K_\alpha}}{r - \frac{bh_1^3}{12K_\alpha}} \right) \quad (5.14)$$

Then the parameter L_2 can be found from the modified form of 5.1, which takes the form:

$$L_2 = r - L_1. \quad (5.15)$$

Finally the parameter h_2 is found from modified form of Equation 5.9, and takes the form:

$$h_2 = \left(\frac{\frac{L_2}{b}}{12K_\alpha - \frac{L_1}{h_1^3}} \right)^{1/3} \quad (5.16)$$

This concludes the development of the Equivalent Beam Methodology. It yields the geometry of fictitious beams that, when used in combination, have the equivalent stiffness and section modulus of a real flexure hinge. A flexure hinge can then be modelled using beam elements with a low number of DOF. This gives rise to computational efficient and accurate prediction of the deflection and angle of rotation of the hinge end-point, and the maximum bending stress of a flexure hinge for a moment loading.

5.3 Comparison to 3-D Finite Element Results

In this section the EBM is compared to a 3-D finite element hinge, presented in the previous chapter. First the equivalent beams of the EBM method will be found, based on the 3-D finite element model presented in Chapter 4. Following this, the EBM hinge will be compared to the 3-D finite element model under three different loading conditions.

5.3.1 Sizing Beams for the EBM

In order to be consistent with the theme of this thesis, the hinge type and geometry used in the 3RRR mechanism will be mapped by the EBM. From the 3-D hinge model presented in Chapter 4, the lateral deflection and angle of rotation can be found for a given load, as well the maximum stress in the y -direction, which is the maximum principal stress. The hinge radius is 1 *mm*. With this information, the EBM model can be applied.

Note that in the development presented in the above section the length of the hinge was assumed to be in the x-direction; however, in the 3-D finite element model hinge length is in the y-direction, as such v_x is used in the calculation of K_v .

The input parameters for the EBM were obtained from the 3-D finite element model discussed in Chapter 4. The lateral deflection(v_x) was taken from the nodal solution at $y = r$. The rotation angle was obtained from the end of the link, since it is assumed α remains constant along the its length. Finally, the maximum stress in the y direction is found from the nodal results of the finite element model. With the above mentioned values, the process of the EBM was completed, the results of which are summarized in Table 5.1.

Table 5.1 Calculation of the EBM geometry from the 3-D finite element data

Hinge Properties	FEM Data	Calculated Values	EBM Values
$b = 10 \text{ mm}$	$\sigma_{ymax} = 219.4 \text{ MPa}$	$\mathcal{S} = 91.18 \text{ mm}^3$	$h_1 = 0.740 \text{ mm}$
$r = 1 \text{ mm}$	$v_x = 1.665 \text{ } \mu\text{m}$	$K_v = 1.144 \text{ mm}^3$	$h_2 = 1.14 \text{ mm}$
$t = 0.8 \text{ mm}$	$\alpha = 2.558 \text{ mrad}$	$K_\alpha = 744.6 \text{ mm}^4$	$L_1 = 0.250 \text{ mm}$
$M = 0.2 \text{ N} \cdot \text{m}$	—	—	$L_2 = 0.750 \text{ mm}$
$E = 105 \text{ GPa}$	—	—	—

With real solutions to the EBM geometry, a model made of beam elements was created to test against the 3-D finite element hinge model.

5.3.2 Result Comparison

In order to test the validity of the EBM, the results of three cases, based on loading type, are compared. The first case is one which used a pure bending moment for the loading type. The second used combined moment loading with a force in the x-direction. The final case involved the use of a force in the x-direction only.

The symmetry in the y-direction used in the 3-D finite element model of Chapter 4 is only valid for moment loading. Any lateral force applied to the model results

in unrealistically high stresses and deformation at the constrained node of the hinge centre. In order to compare the results a new constraint strategy was employed to the 3-D and EBM models. The xy-face of the 3-D model and the EBM model are shown in Figure 5.2. Note that the 3-D model has over 47,000 active DOF, while the EBM model has only 18.

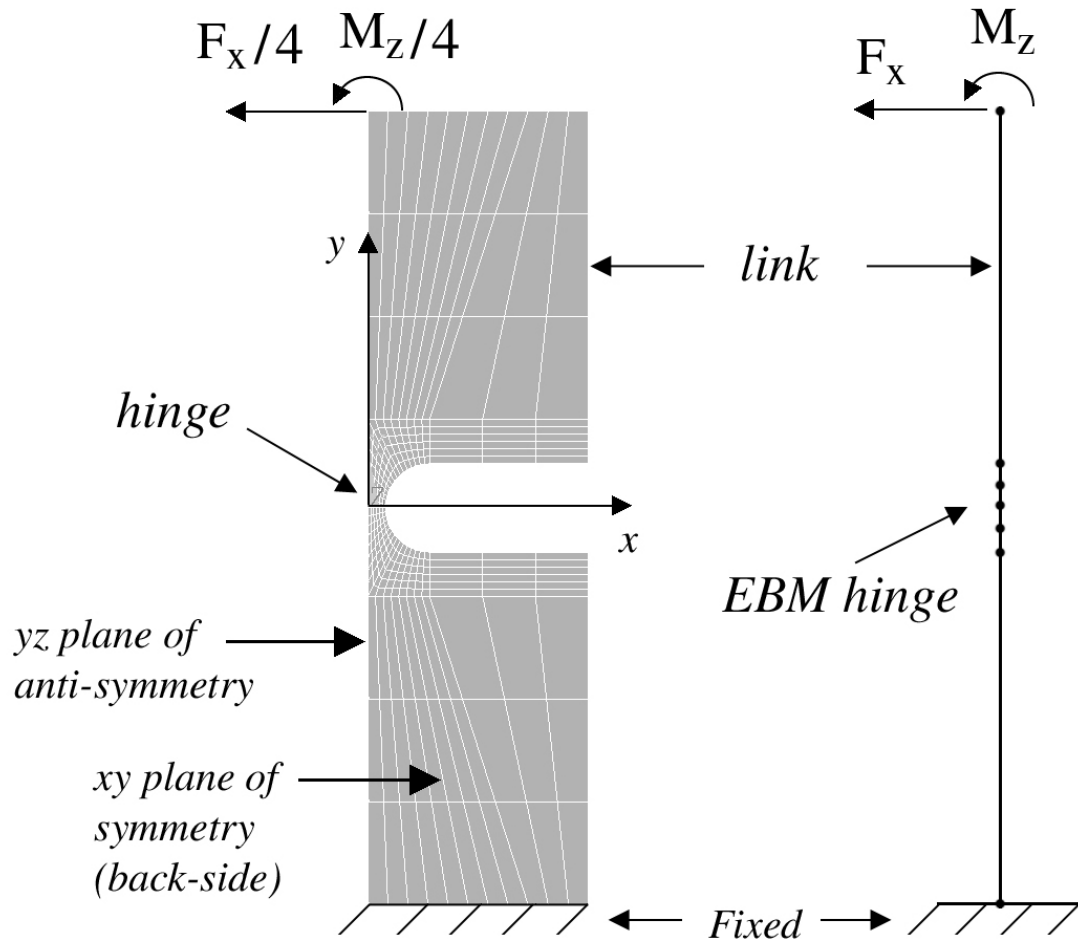


Figure 5.2 Modified model set-up to test the validity of EBM

The ANSYS scripts used to build the modified 3-D finite element model and the EBM model are presented in Appendix B. Also note, that the model of the EBM took about 5 minutes to set up compared to the hours needed to build the 3-D model; further, the EBM model takes fractions of a second to solve compared to the minutes required to solve the 3-D model.

After the completion of the EBM model of the hinge, the three loading cases were applied. Case 1 involved loading the models with a couple moment in the z -direction of quantity $0.2 N \cdot m$. As shown in Table 5.2 there is almost complete agreement between the results.

Table 5.2 A comparison of the EBM model to the 3-D model of a right circular hinge, with a $0.2 N \cdot m$ couple moment load in the z -direction

Model Parameter	EBM Result	3-D Hinge Result	% Difference
σ_{ymax}	219.4 MPa	219.2 MPa	0.1%
u_y	-46.4 μm	-46.0 μm	0.8 %
α_z	-5.15 mrad	-5.11 mrad	0.8 %

The fact that there is good agreement should not come as a surprise, as this was loading that the EBM was based on. The difference between the two models is attributed to some coupling between the link and the hinge that has been neglected in the development phase of the EBM. That said, these results are considered extremely good considering the EBM model has an ultra low number of DOF. The number of active DOF is roughly proportional to the computational time required to solve a model.

In case 2, a couple moment in the z -direction of $0.1 N \cdot m$ was applied as well as a force of $-12 N$. Table 5.3 shows a comparison of the EBM model to the finite element model.

The results of Table 5.3, shows that the EBM hinge is still predicting the end-point displacement and maximum stress developed in the hinge extremely well. This would suggest that for the constraints and loading conditions specified in these models, the deflection of the hinge is a result of the bending due to the applied or developed moment at the centre of the hinge, and that shear effects are negligible.

Table 5.4 shows the results of the case 3, in which a force of $-24 N$ was applied in the x -direction. Because this case involves no applied moment what-so-ever, the results

Table 5.3 A comparison of the EBM model to the 3-D model of a right circular hinge, with a $0.1 N \cdot m$ couple moment in the z-direction and a $-12 N$ load in the x-direction

Model Parameter	EBM Result	3-D Hinge Result	% Difference
σ_{ymax}	228.1 MPa	228.0 MPa	0.1%
u_y	-48.4 μm	-48.1 μm	0.5 %
α_z	-5.36 mrad	-5.32 mrad	0.8 %

show that shear effects are in fact negligible.

Table 5.4 A comparison of the EBM model to the 3-D model of a right circular hinge, with a $-24 N$ load in the x-direction

Model Parameter	EBM Result	3-D Hinge Result	% Difference
σ_{ymax}	236.9 MPa	236.7 MPa	0.1 %
u_y	-50.4 μm	-50.2 μm	0.3 %
α_z	-5.57 mrad	-5.52 mrad	0.8 %

Again the results indicate that the EBM model predicts the end-point of the hinge extremely well. It should be noted that the maximum stress in the y-direction presented in Tables 5.3 and 5.4, are taken at the hinge centre at its thinnest portion. Higher stresses are reported on the portion of the model, where the first EBM beam links to the second. This is because the developed moment due to the force in the x-direction is greater at this point. Because the hinge is not actually that thin at this point in the model, this greater stress can be considered to be fictitious.

To ensure that the shear effects are in fact negligible, one final test was completed. The length of link(l) was varied from 1 mm to 8 mm and loaded with a force in the x-direction of 24 N. As the link length is decreased, the moment arm to the hinge centre is also decreased, which causes the effects of shear to become increased. At each of the test cases the resulting deflection, angular rotation, and maximum stress was compared between the 3-D model and the EBM model. Plane stress and plane

strain 2-D models were also created and used for comparative purposes.

As the link length was varied, the EBM model still performed very well. Figure 5.3 shows how the ratio of angular rotation of EBM model(α^{ebm}), the 2-D plane stress(α^σ) and the 2-D plane strain model(α^ϵ) to the rotation of the 3-D model(α^{3D}) vary with link length.

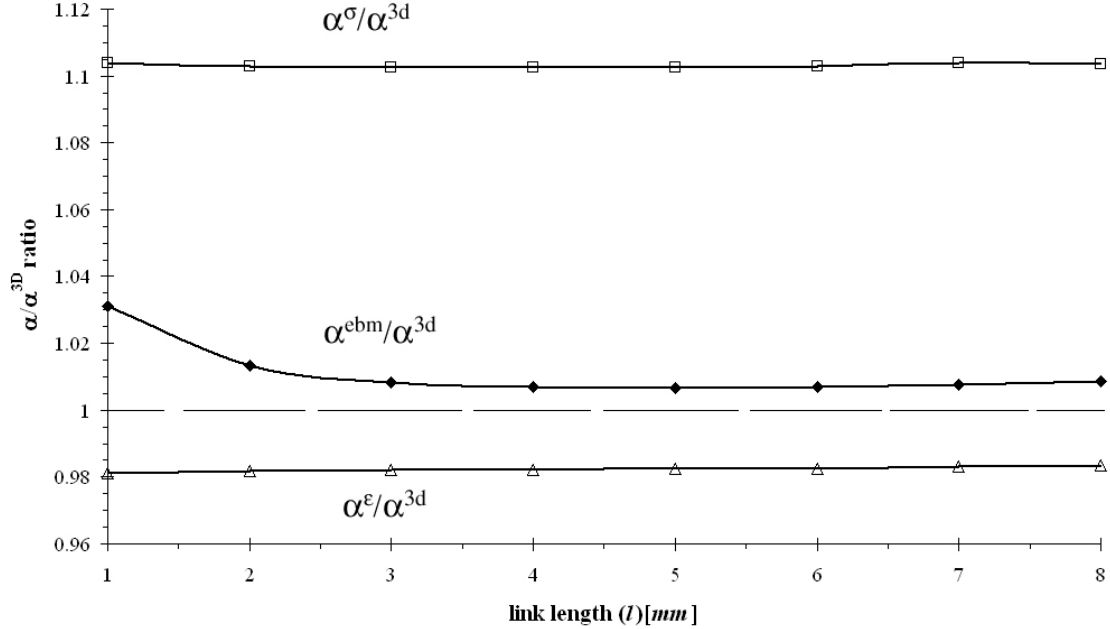


Figure 5.3 Comparing the angular rotation of the 3-D model to the EBM, plane stress and plane strain models

This shows that effects of shear are negligible for reasonable link lengths. Even when the link length is equal to the radius r of the hinge, the results are still quite reasonable, the ratio of rotation is only slightly higher than 1.2, which is comparable to the plane strain accuracy. The EBM model performs better than any of the other 2-D models for link lengths greater than 2.

Because the EBM model of the hinge has so few DOF compared to its 3-D counterpart it opens up many exciting possibilities for future research. One possibility includes hinge optimization and topographical optimization of the 3RRR mechanism. Also dynamic and modal analysis are also a possibility if the mass of the

hinge and links are matched in the same manner that the stiffnesses are. Finally one great advantage of the EBM method is the accurate prediction of deflection and stress at a low computational cost. The next chapter tests the robustness of the EBM hinges, by way of a complete finite element model of the 3RRR mechanism with a low number of DOF.

Also, note that the EBM is equally applicable to different types of flexure hinges, such as elliptically and corner filleted. Further, the EBM can be used with experimental data to find the necessary input parameters. This is a good indication of its high level of robustness for use in compliant mechanism design.

5.4 Conclusion and Recommendations

In this chapter, the development of the EBM was presented. The EBM seeks to accurately predict the 3-D deflection of the right circular hinge at its end point and the maximum stress at the hinge's centre for a given moment loading. The EBM accomplishes the prediction by replacing the 3-D structure of the hinge with fictitious beams of equivalent stiffness, section modulus and length, which when loaded achieve the same deflection and maximum stress.

Finite element testing revealed that an EBM model of a hinge similar to that found in the 3RRR mechanism predicts the behaviour extremely well, for a variety of loading conditions. The test also confirmed that within the constraints of the test, shear effects are negligible in the deflection of the hinge.

The EBM is also applicable for use with other hinge types and/or experimental data.

Chapter 6

Simulation Experimentation of the Equivalent Beam Methodology

6.1 Introduction

The main goal of this thesis is to complete an accurate finite element model of the 3RRR mechanism with a low number of DOF. In Chapter 4 it was shown that stress-strain behaviour of the right circular flexure hinge is completely 3-D. That said, it was shown that for the present thickness of the flexure hinge used in the 3RRR mechanism, the plane-strain assumption will achieve results within two percent of the 3-D results.

In Chapter 5 the Equivalent Beam Methodology was developed to allow for accurate modelling of a flexure hinge, without having to deal with the necessity of a large number of DOF dedicated to each flexure. The method was developed for the explicit purpose of increasing the ease of FEM modelling of compliant mechanisms and also to allow for the possibility of more advanced FEM solutions such as modal and optimization analysis.

This chapter is dedicated to the testing of the EBM on the 3RRR mechanism. To do

so, a model built with beam elements, which include those described by the EBM, is compared to a 2-D planar model of the 3RRR mechanism. The planar model will be solved under two assumption, first by assuming the plane-strain state and second assuming the plane-stress behaviour. The EBM model will be considered valid if the results from it lie between the results of the aforementioned plane states.

Ideally, the EBM model would be compared directly to a 3-D model of the 3RRR mechanism. An accurate 3-D model is not feasible at this point in time, because the academic license of ANSYS has a limit to the number of nodes. An accurate 3-D model would definitely exceed the imposed node ceiling.

Following this section, this chapter will contain the following sections: a description of the models, the method of analysis, the results, and the concluding remarks.

6.2 Model Description

As discussed in Chapter 2, the original 3RRR finite element model by Zou [2000] had some inherent problems which spawned the research of this thesis. In the original 3RRR finite element model, the actuators were modelled as pure displacements at the portion of the compliant mechanism which interfaces with the piezoelectric actuators, called the PZT blocks. Further, the transverse direction was assumed to be perfectly constrained. These assumption, inherently imply that the PZT actuators are infinitely stiff, and hence the physics of the model is somewhat unrealistic. Further this method of simulating the PZT actuators tends to over-constrain the model.

In this study, the 3RRR mechanism is actuated by force and the PZT blocks are free to deflect in the transverse direction. This is an oversimplification of the actuator; however, if both the planar and EBM models are actuated in the same way, the comparison will be meaningful.

Also in this study, the centrepiece of the compliant mechanism is assumed to be completely rigid. As such the ends of the first hinge are fixed, where the compliant linkages meet with the centrepiece. The centrepiece then does not have to be modelled at all. Details about the 2-D planar model and the EBM model follow.

The material properties of all of the models were the same. For the compliant links and hinges (brass), Young's Modulus is 105 *GPa* and Poisson's Ratio is 0.33. The end effector (steel) was modelled with a Young's Modulus of 200 *GPa* and a Poisson's Ratio of 0.3.

6.2.1 2-D Planar 3RRR Model

This subsection describes the planar model of the 3RRR mechanism. The model is similar to the model created by Zou [2000]; however, a new meshing strategy was used. The hinges were meshed with a mapped technique identical to the meshing used in the flexure hinge study, as shown in Figure 6.1. The rest of the 3RRR mechanism was meshed with 6 node (*Plane 2*) triangular elements. This allows for easier meshing of the areas between the flexure hinges.

Specifying either the plane-stress or plane-strain state is accomplished by setting a key-option of the plane elements. Note that the above mentioned behaviours are only applied to the hinges. The links of the 3RRR mechanism are always under a plane-stress state.

Another change was applied to the model; specifically, the end effector was changed from a triangular steel plate to a number of steel beams using beam elements. This was done because the rotational DOF information can be taken directly from the nodal solution. Also the end effector is interfaced to the compliant mechanism using beam elements. The advantage of this is that the rotational information of the end effector is preserved and easily attained from the beam element interface.

Figure 6.2 shows how the model is actuated, denoted by forces F on the PZT blocks

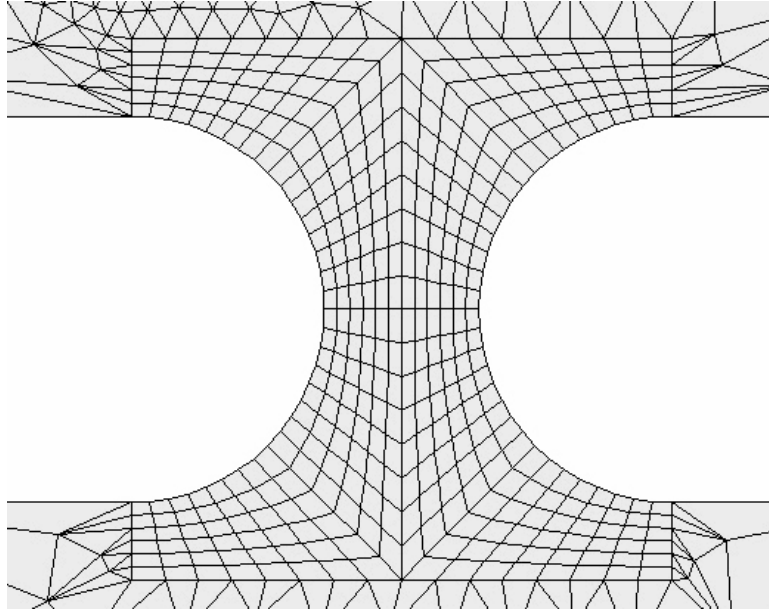


Figure 6.1 Mapped Meshing of the Hinges of the Planar Models

1, 2 and 3. Small yet stiff beam elements were also attached to the edge of the PZT blocks where the forces are applied. This ensures that the load is evenly distributed to the PZT block.

Note the absence of the compliant centre-piece and that the compliant arms are fixed at the end. Even with the centre-piece removed this model still has over 46,500 active DOF. The ANSYS script used to create this model can be seen in Appendix C.

6.2.2 EBM 3RRR Model

The EBM model of the 3RRR mechanism is built entirely with beam elements (Beam 3). All the elements used are assumed to have a depth of 10 *mm*. The flexure hinges are modelled with beam elements as sized by the EBM in Chapter 5.

Regarding the other portions of the compliant mechanisms, the links between the flexure hinges are modelled as beams based on their respective dimensions. As the end-points of the flexure hinges that interface with the central portion are fixed identical to what was done in the planar model.

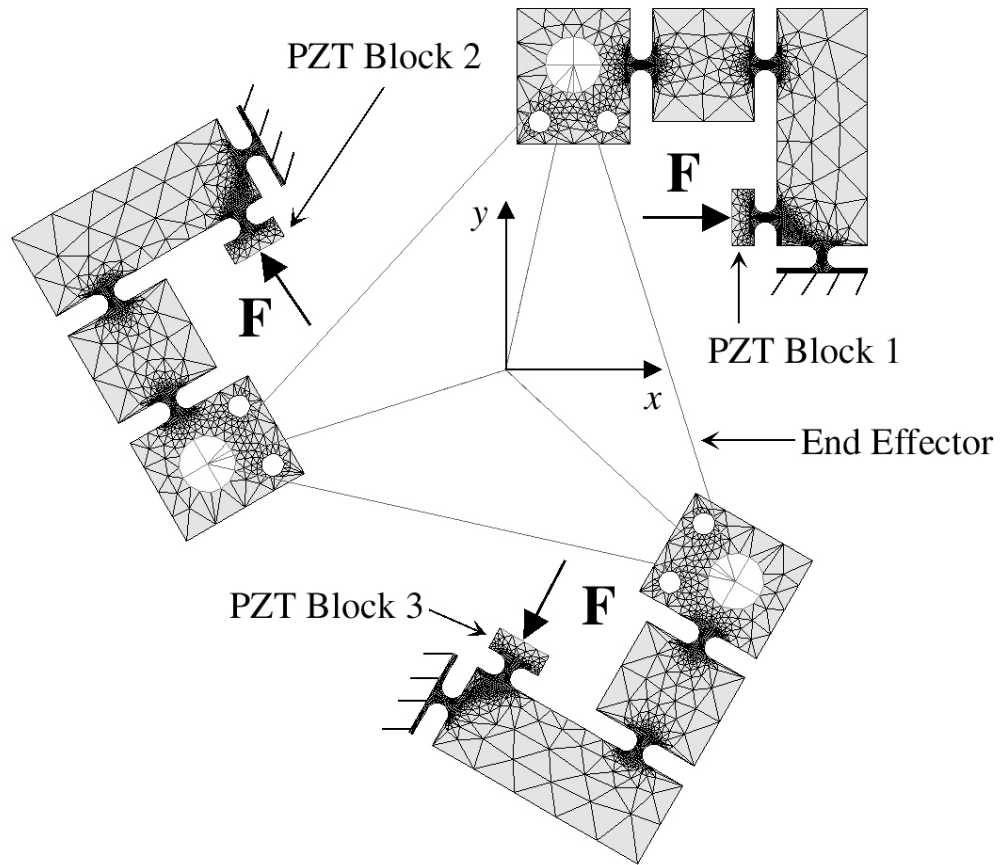


Figure 6.2 The graphical representation of the planar 3RRR finite element model

Beams and consequently beam elements, as described in Chapter 3, are inherently one dimensional. As such an offset is created when beams do not meet end to end. For instance, consider the portion of the model as shown in Figure 6.3. With beam elements super-imposed, it is clear that the model is not continuous. This offset is easily taken into account by introducing intermittent beam elements with stiffnesses equivalent to that of the missing link.

The EBM 3RRR model is shown in Figure 6.4. The 2-D planar 3RRR model is ghosted in the figure to aid in the visualization. The EBM 3RRR model has 291 active DOF, approximately 160 times less than its planar counterpart. The ANSYS

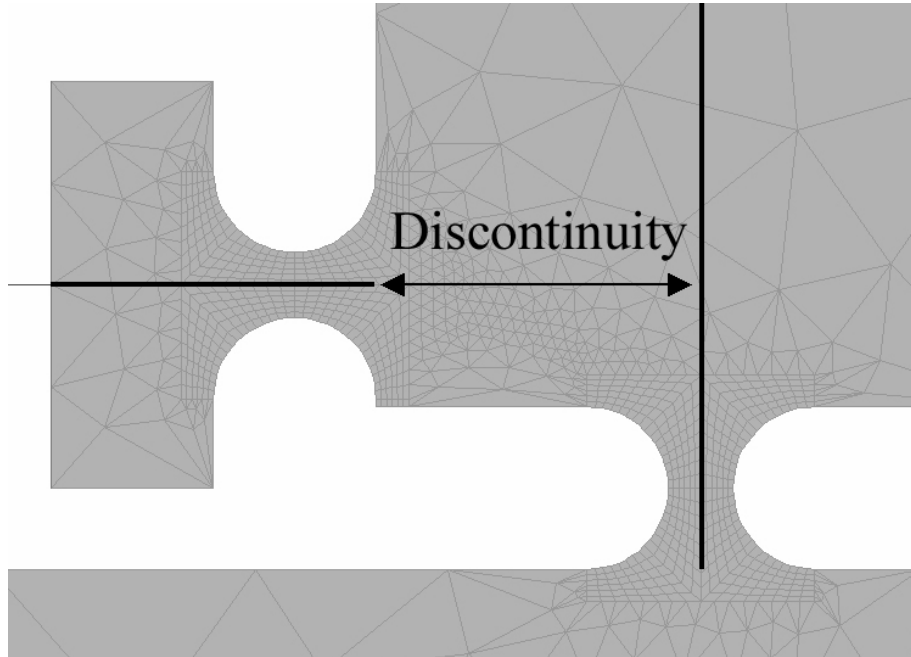


Figure 6.3 Discontinuous nature of beam element model

script used to create this model can be seen in Appendix C.

6.3 Method of Analysis

The objective of this chapter is to test the validity of the EBM-3RRR model; however, the difference between assuming a plane-stress and plane-strain behaviour is also of interest. In order to compare the models, three load cases were used. In all the cases a constant load of 250 N was applied to the PZT blocks. The load cases differed by the combination in which the PZT blocks are loaded, they are as follows:

1. PZT block 1 is loaded
2. PZT blocks 1 and 2 are loaded
3. PZT blocks 1, 2, and 3 are loaded

Of interest from the models is the end effector's position in the x- and y- directions, as well as the yaw angle rotation, and the maximum stress developed in the models

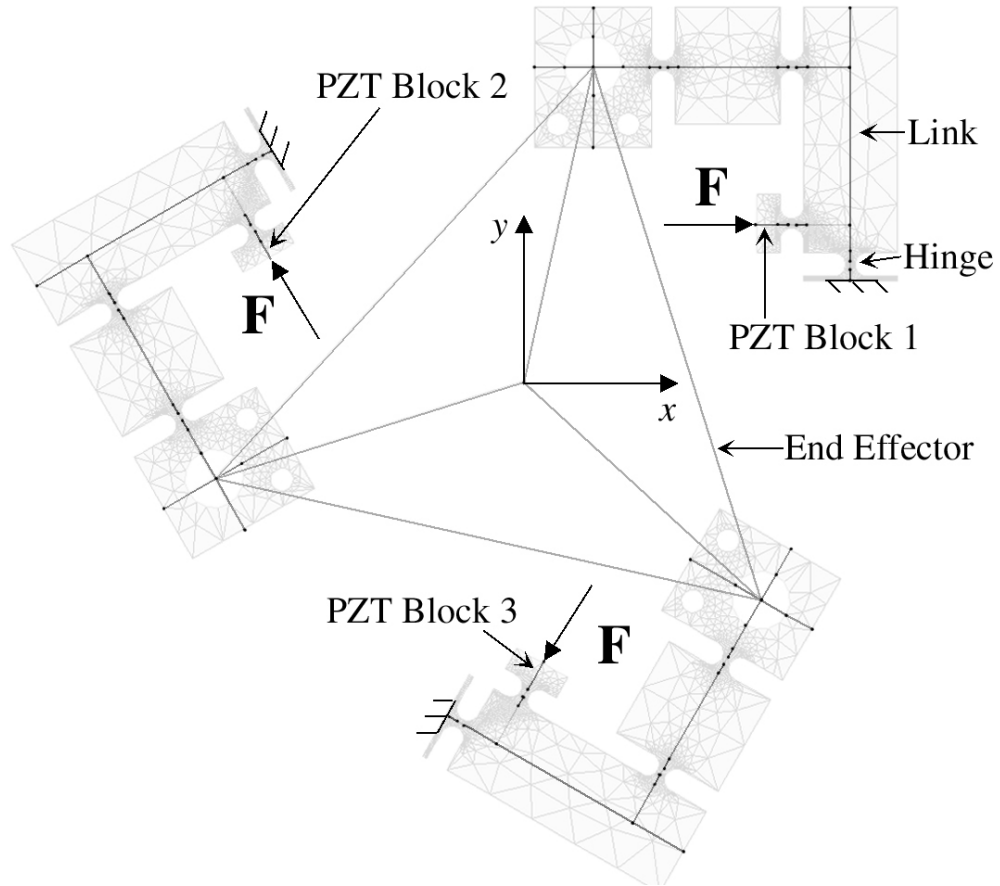


Figure 6.4 The graphical representation of the EBM 3RRR finite element model

after loading.

Also the deformation of the 3RRR mechanism models was compared graphically after each test case. Again the EBM will be considered valid if the results lie between the planar solutions assuming either the plane stress or plane strain state.

6.4 Results and Discussion

By graphical comparison, it is seen that the deformation of the EBM model of the 3RRR mechanism is almost identical to that of the plane strain model, as shown in Figure 6.5.

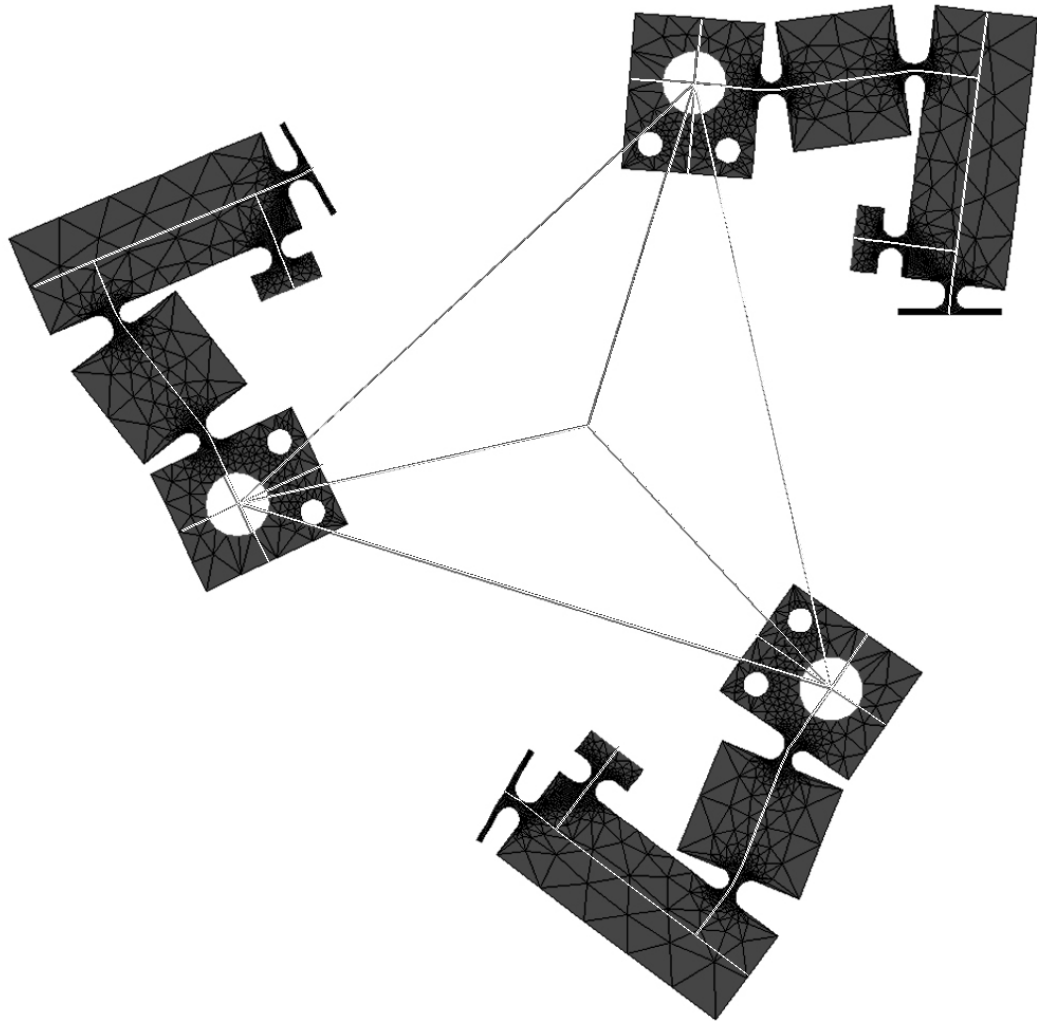


Figure 6.5 Same Modes of Deflection of the EBM and Plane Strain 3RRR Model

Figure 6.5 shows Load Case 3. The figure is actually a combination of two plots taken from ANSYS. The displacement scaling of these plots is 50 fold.

The end effector degree of freedom information and the maximum stress developed in the models is shown in Table 6.1.

Table 6.1 Comparison of Displacement and Rotation of End Effector and Maximum Equivalent Stress in each Respective Model

Load Case	Result	EBM	plane-strain	plane-stress
1	$v_x \mu m$	32.5	31.8 (-2.13%)	35.6 (+9.5%)
1	$v_y \mu m$	-0.40	-0.49	-0.53
1	$\theta mrad$	-0.56	-0.55 (-1.76%)	-0.62 (+9.85%)
1	$\sigma_{eqv} MPa$	191.1	188.7 (-1.27%)	189.1 (-1.06%)
2	$v_x \mu m$	16.6	16.3 (-1.63%)	18.2 (+9.96%)
2	$v_y \mu m$	27.9	27.3 (-2.30%)	30.5 (+9.34%)
2	$\theta mrad$	-1.13	-1.11 (-1.76%)	-1.24 (+9.85%)
2	$\sigma_{eqv} MPa$	316.4	307.7 (-2.75%)	308.4 (-2.53%)
3	$v_x \mu m$	≈ 0	≈ 0	≈ 0
3	$v_y \mu m$	≈ 0	≈ 0	≈ 0
3	$\theta mrad$	-1.69	-1.66 (-1.76%)	-1.86 (+9.85%)
3	$\sigma_{eqv} MPa$	232.4	227.6 (-2.07%)	228.2 (-1.84%)

The most relevant end-effector DOF results of the EBM model fall between the results of the plane strain and plane stress model. Further, the relative errors, as shown in brackets when considered significant, agree well with the results presented in Chapter 4. In that chapter it was shown that the stiffness of a hinge assuming the plane strain state are approximately 1.8 per cent higher than the 3-D stiffness, and that a hinge assuming the plane stress state were approximately 8.6 per cent lower.

The maximum stresses in the EBM model are roughly 2 per cent greater than either of the plane results. This also agrees well with what was discovered in the flexure hinge study. Though not explicitly reported in this thesis, the stress results of the 2-D plane hinges were approximately 2 per cent lower than the 3-D hinge results.

This validates that the EBM is an accurate and low DOF way of modelling flexure hinges, as components for compliant mechanisms. The EBM beams interface nicely with other beam elements, which also model the links in a very accurate way. The implication of this is an accurate model of the 3RRR mechanism with a very low number of DOF.

There are still some refinements which can be made to the EBM 3RRR model. First, the physical behaviour of the piezo electric actuators should be examined, and an accurate model of them should be incorporated into the 3RRR model. Second, when experimental results are available, they should be compared, so that the appropriate ‘tweaks’ can be made to the 3RRR model.

Other pursuits may involve topographical optimization of the 3RRR mechanism, as well as optimization of the stiffnesses of individual hinges in the compliant arms. Dynamic simulation and modal analysis may also be applied to the 3RRR mechanism model, in order to discover more about the systems behaviour. As well, the EBM is conceivably applicable for use in a real time control environment (i.e. time to build and solve EBM model is less than 1 second on a 800 MHz Processor).

6.5 Recommendations and Conclusions

In this chapter it was again shown that EBM is an accurate way to model flexure hinges. Used in conjunction with other beam elements to describe the links, the behaviour of the 3RRR mechanism can be accurately predicted.

The results were excellent. First the number of DOF was decreased from 46,500 in the 2-D plane models, to 291 in the 1-D EBM model (a decrease of 160 times!). Second, it was shown that the EBM model gave results which were between the 2-D planar models assuming either the plane stress (≈ 9.5 percent more stiff) or plane strain state (≈ 1.3 percent less stiff). This not only agrees well with theory and with what was shown in Chapter 4, but also verifies that the EBM 3RRR model gives

excellent predictions of the 3-D behaviour of the system.

Future work includes incorporating accurate actuator models into the 3RRR mechanism model. And tweaking the EBM model once experimental results are achieved. Also to be considered in the future, are the optimization, dynamic, and modal analyses which are feasible with the EBM-3RRR model.

Chapter 7

Conclusion and Proposed Future Work

7.1 Research Objectives

This research presented in this thesis was focused on the finite element analysis of a specific micro-positioning system, called the 3RRR mechanism. Though the research was aimed at a specific device, the conclusions are applicable to all micro-positioning systems which use compliant mechanisms that employ flexure hinges as the link between input and output.

The Research objective, as stated in Section 1.4, was to create an accurate finite element model of the 3RRR mechanism with a small number of degrees of freedom. In order to meet this objective, several goals were conceived, namely to:

Goal 1 Complete a finite element study on flexure hinges; in particular, to understand their true 3-D behaviour.

Goal 2 Develop an accurate model of a flexure hinge that accurately accounts for the physical behaviour, namely the slope and deflection at the flexure's endpoint.

Goal 3 Create a finite element model of the 3RRR Mechanism based on flexure model in Goal 2, and test against experimental and other finite element models (such as 2-D and 3-D).

7.2 Literature and Theory Review

The first step taken to meet the goals of this thesis, was to do an extensive literature review. In order to complete useful research, this back-ground check was required to understand the state of finite element analysis in the micro-positioning field.

It became apparent that most micro-positioning systems use compliant mechanisms to deliver the input motion or force to the end-effector, which is used to do some useful work on an independent entity. Compliant mechanisms differ from conventional mechanisms, in that they have no ‘moving’ parts and yet they can produce motion in a very precise manner.

Compliant mechanisms use relatively large scale deflections to change the input motion. They are composed of rigid portions which are connected with flexure hinges. Flexure hinges are an integral part of most compliant mechanisms.

The literature also revealed a number of things with regard to finite element modelling. It appeared that most of the work in this field was aimed at completing forward kinematic solutions for the compliant mechanisms. The solutions, for the most part, were based on the Pseudo-Rigid-Body-Model, which model the rigid portions as rigid links, and the flexures as torsional springs.

The stiffness assigned to these torsional springs was based on the work presented by Paros and Weisbord [1965]. This ‘seminal work’ was designed for use at a previous time, a time when the ‘micro computer’ was in its infancy. Because of the time at which that work was completed, it was necessary to have a relatively easy way to calculate an estimate for the compliance of the flexure hinges. Using an inherent plane-stress assumption they essentially treated the flexure as a beam in bending.

However, depending on the flexure depth, this assumption is invalid. This is due to the fact that at relatively large depths the flexure begins to act like a plate in bending, under an inherent plane strain state.

Many researchers in this field were willing to continue using this simplified approach to model flexure hinge compliance(or stiffness). Some planar analyses were done on flexure's and compliant mechanisms. However, no one mentioned which planar behaviour they were using and often times there was a sentiment the finite element method was too cumbersome for flexure and compliant mechanism design.

This fact in particular spawned the work of Chapter 3, in which an extensive review of the theory of elasticity, beam theory, and the finite element method were presented.

7.3 Flexure Hinge Study

Chapter 4 presented the results of research aimed at better understanding the nature of flexure hinges. Three models were built and compared using the finite element program ANSYS. These models included: a very accurate 3-D model, and two planar models, one assuming the plane-stress state and the other assuming the plane strain state. It was shown that the stress-strain behaviour of the 3-D model is governed by plane strain in the interior and plane stress at the free surfaces. For the present geometry of the hinges found in the 3RRR mechanism, the plane strain state is a better approximation of their behaviour, as the resulting stiffness is approximately 2 per cent greater than the 3-D stiffness.

Also in this chapter it was shown at what depth to hinge thickness ratio one can assume the hinge is 'thin' or 'thick'. 'Thin' implies that plane-stress is a valid assumption, while 'thick' implies that plane-strain is a valid assumption. Using a threshold of 2 per cent, it was concluded that the plane stress state is valid if the hinge in question has a b/t ratio less than 2, plane strain is valid when b/t is greater than 12.5, and that for b/t ratios greater than 2 and less than 12.5 the behaviour is

not accurately described by either the plane strain or plane stress state.

7.4 Equivalent Beam Methodology

In Chapter 5 the Equivalent Beam Methodology was developed. The aim of the EBM was to accurately predict the deflection and stress developed in a flexure hinge for a given bending load, regardless of its b/t ratio, and doing so with a small number of DOF. To do so, two beams of arbitrary length and heights were used to simulate the desired deflection and stress. The method was designed for use in the finite element method.

It was shown in this chapter that the EBM works extremely well. The number of DOF were reduced from over 47,000 in the 3-D model, to 18 DOF using the EBM model. The results were within 0.2 per cent for various loading combination including bending moments and transverse loads.

7.5 Comparing the 1-D EBM model to the 2-D Plane Finite Element Models of the 3RRR Mechanism

In Chapter 6, 3 different models of the 3RRR Mechanism were compared. The models included two planar, one assuming a plane-strain state and the other a plane-stress state, and one model based on the EBM. The EBM model contained hinges that had equivalent stiffness to the 3-D hinge model.

The results of this Chapter showed that the EBM model results of end effector deflection and rotation were between the two plane models, agreeing well with theory. This shows that the EBM can be used to model the hinge stiffness in a system, with very good accuracy and a low number of DOF.

7.6 Proposed Future Work

Proposed future work in this area is as follows:

1. Completion of a finite element analysis of the piezoelectric actuators.
2. Incorporating the EBM model with the proposed piezoelectric actuator model to develop an accurate model of the 3RRR mechanism with a small number of DOF, and compare the results of which to experimental data when available.
3. Completing topographic optimization and optimization of individual hinges of the 3RRR mechanism to increase the work space of the 3RRR mechanism
4. Dynamic Simulation and Modal Analysis using the EBM model with incorporated PZT actuators.
5. Investigate the possibility of using the EBM model for model-based control of the actual 3RRR mechanism.

References

Ferdinand P. Beer and E. Russel Jr. Johnston. *Mechanics of Materials*. McGraw-Hill Inc., 1981.

S. Bi, G. Zong, R. Liu, and S. Wang. “Accuracy Analysis of the Serial-Parallel Micromotion Manipulator”. In *SMC’97 International Conference on Systems, Manufacturing and Cybernetics – Computational Cybernetics & Simulation*, pages 2258–2263, Hyatt Orlando, Florida, October 1997.

S.H. Chang and B.C. Du. “A precision piezodriven micropositioner mechanism with large travel range”. *Review of Scientific Instruments*, 69(4):1785–1791, Apr. 1998.

Robert Davis Cook and Warren Clarence Young. *Advanced Mechanics of Materials*. Macmillan Publishing Company, 1985.

E Furukawa and M. Mizuno. “Piezo-Driven Translation Mechanisms Utilizing Linkages”. *Int. J. Japan Soc. Prec. Eng.*, 26(1):54–59, Mar. 1992.

E. Furukawa, M. Mizuno, and T. Hojo. “A Twin-Type Piezo-Driven Translation Mechanism”. *Int. J. Japan Soc. Prec. Eng.*, 28(1):70–75, Mar. 1994.

P. Gao, S-M. Swei, and Z. Yuan. “A new piezodriven precision micropositioning stage utilizing flexure hinges”. *Nanotechnology*, 10:394–398, Mar. 1999.

M. Goldfarb and J.E. Speich. ”A Well-Behaved Revolute Flexure Joint for Compliant Mechanism Design”. *Transactions of the ASME*, 121:424–429, September 1999.

C. Gosselin, S. Lemieux, and J-P Merlet. “A new architecture of planar three-degree-of-freedom parallel manipulator”. In *IEEE International Conference on Robotics and Automation*, pages 3738–3743, Minneapolis, Minnesota, April 1996.

A. Hara and K. Sugimoto. “Synthesis of Parallel Micromanipulators”. *Transaction of the ASME*, 111:34–39, March 1989.

I. Her and J.C. Chang. ”A Linear Scheme for the Displacement of Micropositioning Stages with Flexure Hinges”. *Transactions of the ASME*, 116:770–776, September 1994.

- L.L. Howell and A. Midha. “A Method for the Design of Compliant Mechanisms with Small-Length Flexural Pivots”. *ASME Journal of Mechanical Design*, 116: 280–290, March 1994.
- L.L. Howell and A. Midha. “Parametric Deflection Approximations for End-Loaded, Large-Deflection Beams in Compliant Mechanisms. *ASME Journal of Mechanical Design*, 117(1):156–165, 1995.
- L.L. Howell, A. Midha, and T.W. Norton. “Evaluation of Equivalent Spring Stiffness for Use in a Pseudo-Rigid-Body Model of Large-Deflection Compliant Mechanisms”. *ASME Journal of Mechanical Design*, 118(1):126–131, 1996.
- B.D. Jensen, L.L. Howell, D.B. Gunyan, and B.A. Salmon. “The Design and Analysis of Compliant mem Using the Pseudo-Rigid-Body Model”. In *Micro-electomechanical Systems (MEMS) 1997, presented at the 1997 ASME International Mechanical Engineering Congress and Exposition*, volume DSC-Vol. 62/HTD-Vol. 354, pages 119–126, Dallas, Texas, November 1997.
- C.B. Ling. Not available. *Trans. ASME*, 74:141, 1952.
- N. Lobontiu, J.S.N. Paine, E. Garcia, and M. Goldfarb. “Corner-Filletted Flexure Hinges”. *Transactions of the ASME*, 123:346–352, September 2001.
- S.M. Lyon, P.A. Erikson, M.S. Evans, and L.L. Howell. “Prediction of the First Modal Frequency of Complinat Mechanisms Using the Pseudo-Rigid-Body Model”. *Journal of Mechanical Design*, 121:309–313, June 1999.
- A. Midha, T.W. Norton, and L.L. Howell. “On the Nomenclature Classification, and Abstractions of Compliant Mechanisms”. *Transactions of ASME*, 116:270–279, March 1994.
- S. Moriyama, T. Haradam, and A. Takanashi. “Precision X–Y Stage with a Piezo-driven Fine-table”. *Bull Japan Soc. of Prec. Eng.*, 22(1):13–17, Mar. 1988.
- J.M. Paros and L. Weisbord. ”How to Design Flexure Hinges”. *Machine Design*, 37:151–156, November 1965.
- K.M. Ragulskis, M.G. Arutunian, A.V. Kochikian, and M.Z. Pogosian. “A Study of Fillet Type Flexure Hinges and Their Optimal Design”. *Vibration Engineering*, 3:447–452, 1989.
- Y. Rong, Y. Zhu, Z. Luo, and X. Liu. “Design and Analysis of Flexure-Hinge Mechanism used in Micro-Positioning Stages”. *Manufacturing Science and Engineering*, PED-Vol. 68(2):979–985, 1994.
- CTF Ross. *Finite Element Methods in Engineering Science*. Ellis Horwood Limited, 1990.

J.W. Ryu, D. Gweon, and K.S. Moon. “Optimal Design of a Flexure Hinge based $XY\theta$ Wafer Stage”. *Precision Engineering*, 21:18–28, 1997.

B.A. Salamon and A. Midha. “An Introduction to Mechanical Advantage in Compliant Mechanisms”. *Journal of Mechanical Design*, 120:311–315, June 1998.

F.E. Scire and E.C. Teague. “Piezodriven 50- μm Range Stage with Subnanometer Resolution”. *Rev. Sci. Instrum.*, 49(12):1735–1740, December 1978.

S.T. Smith, V.G. Badami, J.S. Dale, and Y. Xu. “Elliptical Flexure Hinges”. *Rev. Sci. Instrum.*, 68(3):1474–1483, March 1997.

E.C. Teague, R.D. Young, F. Scire, and D. Gilsinn. “Para-flex Stage for Microtopographic Mapping”. *Rev. Sci. Instrum.*, 59(1):67–73, January 1988.

W. Xu and T. King. “Flexure Hinges for Piezoactuator Displacement Amplifiers: Flexibility, Accuracy, and Stress considerations”. *Precision Engineering*, 19:4–10, 1996.

W. Xu and T.G. King. “Mechanical Amplifier Design for Piezo-actuator Applications”. Technical Report 1/5, The Institution of Electrical Engineers, Savoy Place, London, WC2R OBL, UK, 1995.

S. Zhang and E. Fasse. “A Finite-Element-Based Method to Determine the Spatial Stiffness Properties of a Notch Hinge”. *Journal of Mechanical Design*, 123:141–147, March 2001.

Jing Zou. Micro-motion systems study. M.sc., University of Saskatchewan, Saskatoon, Saskatchewan, Canada, 2000.

Appendix A

Flexure Hinge Models

A.1 Introduction

This appendix contains the ANSYS scripts which will generate the models described in Chapter 4. The comments to the code appear after the “!” symbol. The models presented in this Appendix include, the 3–D model and the 2–D model of the hinge.

A.2 3–D Hinge Model

```
/Title,3D Hinge Study
/PREP7
!!! Hinge Dimension Setup in metres
*set,b,0.005 ! Half Hinge Depth Usually 0.005
*set,t,0.0004 ! Half Hinge Thickness
*set,r,0.001 ! Hinge Radius
*set,h1,0.008 ! Rigid Length
*set,w,0.005 ! Half Rigid Width

!!! Micro Strength Fibers
*set,rm,.00001
*set,pi,acos(-1)

!!! Loading 1/4 Desired Load
*set,m1,0.05 ! N*m 0.05 for Case 1 0.025 Case 2, 0 Case 3
```

*set,f1,0 ! N : 0 for Case1; -3 for Case 2, -6 Case 3

!!! Mapped Meshing Div-Sizes

!!! Changeable

*set,l1,6 ! Bottom Area 1 !!! Converged Values

*set,l4,8 ! Top of Area 1

*set,l5,8 ! Left of Area 1

*set,l6,3 ! Bottom of Area 2

*set,l9,8 ! Right of Area 3

*set,l12,12*b/.005 ! Depth of All

*if,l12,LT,1,THEN

*set,l12,1

*endif

*if,l12,GT,31,Then

*set,l12,31

*endif

!!! Dependent Do not change

*set,l3,l1 ! Right Area 1

*set,l2,l4+l5 ! Fillet

*set,l7,l1 ! Right of Area 2

*set,l8,l6 ! Top of Area 2

*set,l10,l4+l8 ! Top of Area 3

*set,l11,l9 ! Left of Area 3

ET,1,SOLID95 !!! Element Type 1 !!!

KEYOPT,1,1,0 !!! Main Element Used

KEYOPT,1,5,1 !!! in Model

KEYOPT,1,6,0

KEYOPT,1,11,0

ET,2,BEAM4 !!! Element Type 2 !!!

KEYOPT,2,2,0 !!! Elements Used to Distribute

KEYOPT,2,6,0 !!! Load evenly on Model

KEYOPT,2,7,0

KEYOPT,2,9,0

KEYOPT,2,10,0

! Real Constants for Beams

! area,Iy,Iz,ty,tz,J

R,1,1E-12*pi*rm*rm,2E3*pi*rm*rm*rm*rm/4,2E3*pi*rm*rm*rm*rm/4,1E-6*2*rm,1E-6*2*rm,0,

RMORE,0,2E3*pi*rm*rm*rm*rm/2,0,0,0,0,

ET,3,SHELL93 !!! Element Type 3 !!!

KEYOPT,3,4,0 !!! Temporary Element Used

KEYOPT,3,5,0 !!! In meshing process

KEYOPT,3,6,0

```
!!! Material Properties
mp,ex,1,105E9 !!! For Brass
mp,nuxy,1,0.33 !!! Young's Modulus
mp,ex,2,1E21 !!! For Fictional Elements
mp,nuxy,2,0.3
```

```
!!! Setting Element type 3, material 1
type,3
mat,1
```

```
!!! Setting up KeyPoints and Meshing
```

```
!!! Area 1
k,,
k,,t,0
k,,t+r,r
k,,t+r,0
l,1,2
larc,2,3,4,r
kdele,4
k,,t+r,r+r
k,,0,r+r
l,3,4
l,4,5
l,5,1
lesize,1,,l1
lesize,2,,l2,1.2
lesize,3,,l3
lesize,4,,l4
lesize,5,,l5,!0.6
al,1,2,3,4,5
amap,1,1,2,3,4
```

```
!!! Area 2
```

```
k,,w,r
k,,w,r+r
l,3,6
l,6,7
l,7,4
al,3,6,7,8
lesize,6,,l6
lesize,7,,l7
lesize,8,,l8
amesh,2
```

```
!!! Area 3
```

```
k,,w,r+h1
k,,0,r+h1
l,7,8
```

```
1,8,9
1,9,5
lesize,10,,110
lesize,9,,19
lesize,11,,111
al,4,8,9,10,11
amap,3,5,7,8,9
```

```
Type,1
mat,1
```

```
!!! Extruding 3D solid
k,,0,0,b
l,1,10
lesize,12,,112,!0.2
vdrag,1,2,3,,12
aclear,all
```

```
!!! Reinforcing top with fictitious elements
!!! Results in evenly distributed load
```

```
type,2
mat,2
real,1
nselect,s,loc,y,r+h1
nselect,r,loc,z,0
*get,testx,node,0,count
*get,maxx,node,0,mxloc,x
nselect,s,loc,y,r+h1
nselect,r,loc,x,0
*get,testz,node,0,count
*get,maxz,node,0,mxloc,z
*dim,nlx,,(testx+1)/2
*dim,nlz,,(testz+1)/2
```

```
*do,k,1,(testz+1)/2,1 !!! Creating Beam Elements For Top
*do,i,1,(testx+1)/2,1
nselect,s,loc,y,r+h1
nselect,r,loc,z,(k-1)*2*maxz/(testz-1)
nselect,r,loc,x,(i-1)*2*maxx/(testx-1)
*get,nlx(i),node,0,num,max
*enddo
nselect,all
*do,j,1,(testx-1)/2,1
e,nlx(j),nlx(j+1)
*enddo
*enddo
```

```
*do,k,1,(testx+1)/2,1 !!! Creating Beam Elements For Top
```

```

*do,i,1,(testz+1)/2,1
nset,s,loc,y,r+h1
nset,r,loc,x,(k-1)*2*maxx/(testx-1)
nset,r,loc,z,(i-1)*2*maxz/(testz-1)
*get,nlz(i),node,0,num,max
*enddo
nset,all
*do,j,1,(testz-1)/2,1
e,nlz(j),nlz(j+1)
*enddo
*enddo

!!! Getting Top and Center Node Number
nset,s,loc,y,r+h1
nset,r,loc,x,0
nset,r,loc,z,0
*get,unno,node,0,num,max

nset,s,loc,x,0 !!! Fixing Center Node
dsym,asym,x
nset,s,loc,z,0
dsym,symm,z
nset,s,loc,y,0
dsym,symm,y
!nset,r,loc,x,0
!nset,r,loc,z,0
!d,all,all
nset,all
fini

!!! Solution Environment
/solu
/pbc,all,,0
ANTYPE,STATIC,NEW
F,unno,mz,m1
F,unno,fx,f1
solve
fini

!!! Post1 Environment
/post1
PLNSOL,S,y,1,1
nset,s,y
!!! Reading Results into Scalar Parameters
*get,symax,sort,0,max
*get,theta,node,unno,rot,z
*get,disp,node,unno,u,x
fini

```

A.3 2–D Plane Hinge Model

```
/Title, 2D Hinge Study
/prep7
!!!!!!!!!!!!!!!!!!!!!!!!!!!!!!!!!!!!!!!!!!!!!!
!!!!!! Changeable Portion of Model !!!!!!!
!!!!!!!!!!!!!!!!!!!!!!!!!!!!!!!!!!!!!!!!!!!!!!

*set,flag,2 !!! 0 for plane stress, 2 for plane strain, 3 pstress w thick

!!! Hinge Dimension Setup in m
!*set,b,0.005 ! Half Hinge Depth
*set,t,0.0004 ! Half Hinge Thickness
*set,r,0.001 ! Hinge Radius
*set,h1,0.008 ! Rigid Length
*set,w,0.005 ! Half Rigid Width

!!! Micro Strength Fibers
*set,rm,.00001
*set,pi,acos(-1)

!!! Loading 50X Desired Load
*set,m1,10 ! N*m 10 for Case 1 5 Case 2, 0 Case 3
*set,f1,0 ! N : 0 for Case1; -600 for Case 2, -1200 Case 3

!!! Mapped Meshing Div-Sizes
!!! Changeable
*set,l1,6 ! Bottom Area 1 !!! Converged Values
*set,l4,8 ! Top of Area 1
*set,l5,8 ! Left of Area 1
*set,l6,3 ! Bottom of Area 2
*set,l9,3 ! Right of Area 3

!!! Dependent Do not change
*set,l3,l1 ! Right Area 1
*set,l2,l4+l5 ! Fillet
*set,l7,l1 ! Right of Area 2
*set,l8,l6 ! Top of Area 2
*set,l10,l4+l8 ! Top of Area 3
*set,l11,l9 ! Left of Area 3

!!!!!!!!!!!!!!!!!!!!!!!!!!!!
!!!! Elements !!!!
!!!!!!!!!!!!!!!!!!!!!!!!!!!!
```

```

ET,1,PLANE82
KEYOPT,1,3,flag !!! 0 Plane Stress, 3 Plane Strain
KEYOPT,1,5,0
KEYOPT,1,6,0
R,1,1 !!! If thickness for plane strain is desired

```

```

ET,2,BEAM3
KEYOPT,2,6,0
KEYOPT,2,9,0
KEYOPT,2,10,0

```

```

! Real Constants for Beams
! area,Izz,height,shearz,istrn,addmas
R,2,pi*rm*rm,pi*rm*rm*rm*rm/4,2*rm,0,0,0

```

```

!!! Material Properties
mp,ex,1,105E9 !!! For Brass
mp,nuxy,1,0.33 !!! Young's Modulus
mp,ex,2,1E25 !!! For Fictional Elements
mp,nuxy,2,0.3

```

```

mat,1
type,1
real,1
!!! Setting up KeyPoints and Meshing
!!! Area 1
k,, !!! Key Points in mm Dimensions !!!
k,,t,0
k,,t+r,r
k,,t+r,0
l,1,2
larc,2,3,4,r
kdele,4
k,,t+r,r+r
k,,0,r+r
l,3,4
l,4,5
l,5,1
lesize,1,,l1
lesize,2,,l2,1.2
lesize,3,,l3
lesize,4,,l4
lesize,5,,l5,0.6
al,1,2,3,4,5
amap,1,1,2,3,4

```

```

!!! Area 2
k,,w,r
k,,w,r+r
l,3,6
l,6,7
l,7,4
al,3,6,7,8
lesize,6,,l6
lesize,7,,l7
lesize,8,,l8 amesh,2

```

```

!!! Area 3
k,,w,r+h1
k,,0,r+h1
l,7,8
l,8,9
l,9,5
lesize,10,,l10
lesize,9,,l9
lesize,11,,l11
al,4,8,9,10,11
amap,3,5,7,8,9

```

```

*dim,test,,1,1 ! Number of nodes on top
*dim,maxx,,1 ! Furthest top node x
*dim,maxy,,1 ! Y Distance to last node on centerline
*dim,test2,,1 ! Number of nodes along y upto 2

```

```

nselect,s,loc,y,r+h1
*get,test(1),node,0,count
*dim,nl1,,(test(1)+1)/2
*get,maxx(1),node,0,mxloc,x

```

```

*do,k,1,(test(1)+1)/2,1
nselect,s,loc,y,r+h1
nselect,r,loc,x,(k-1)*maxx(1)/((test(1)+1)/2-1)
*get,nl1(k),node,0,num,max
*enddo
nselect,all

```

```

type,2
mat,2
real,2
*do,k,1,(((test(1)+1)/2)-1),1
e,nl1(k),nl1(k+1)
*enddo
allsel

```

```
nselect,s,loc,y,0
dselect,s,symm,y
nselect,s,loc,x,0
dselect,s,asym,x
nselect,r,loc,y,0
d,all,all
nselect,all
```

!!! Getting Top and Center Node Number

```
nselect,s,loc,y,r+h1
nselect,r,loc,x,0
*get,errno,node,0,num,max
allselect
fini
```

```
/solu
/psbc,all,,0
ANTYPE,STATIC,NEW
F,errno,mz,m1
F,errno,fx,f1
eplot
solve
fini
```

```
/post1
PLNSOL,S,y,1,1
nselect,s,y
*get,symax,sort,0,max
nselect
*get,theta,node,errno,rot,z
*get,disp,node,errno,u,x
fini
```

Appendix B

EBM Verification Models

B.1 Introduction

This appendix contains the ANSYS scripts which will generate the models described in Chapter 5. The comments to the code appear after the “!” symbol. The models presented in this Appendix include, the 3–D model and the EBM model of the hinge.

B.2 3–D Verification Model

```
/Title,3D Hinge Study
/PREP7
!!! Hinge Dimension Setup in m
*set,b,0.005 ! Half Hinge Depth Usually 0.005
*set,t,0.0004 ! Half Hinge Thickness
*set,r,0.001 ! Hinge Radius
*set,h1,0.008 ! Rigid Length
*set,w,0.005 ! Half Rigid Width
*set,mm,1E-3

!!! Micro Strength Fibers
*set,rm,.00001
*set,pi,acos(-1)

!!! Loading 1/4 Desired Load
```

```
*set,m1,0.00 ! N*m 0.05 for Case 1 0.025 Case 2, 0 Case 3
*set,f1,-6 ! N : 0 for Case1; -3 for Case 2, -6 Case 3
```

```
!!! Mapped Meshing Div-Sizes
!!! Changeable
*set,l1,6 ! Bottom Area 1 !!! Converged Values
*set,l4,8 ! Top of Area 1
*set,l5,8 ! Left of Area 1
*set,l6,3 ! Bottom of Area 2
*set,l9,3 ! Right of Area 3
*set,l12,12*b/.005 ! Depth of All
*if,l12,LT,1,THEN
*set,l12,1
*endif
*if,l12,GT,31,Then
*set,l12,31
*endif
```

```
!!! Dependent Do not change
*set,l3,l1 ! Right Area 1
*set,l2,l4+l5 ! Fillet
*set,l7,l1 ! Right of Area 2
*set,l8,l6 ! Top of Area 2
*set,l10,l4+l8 ! Top of Area 3
*set,l11,l9 ! Left of Area 3
```

```
ET,1,SOLID95 !!! Element Type 1 !!!
KEYOPT,1,1,0 !!! Main Element Used
KEYOPT,1,5,1 !!! in Model
KEYOPT,1,6,0
KEYOPT,1,11,0
```

```
ET,2,BEAM4 !!! Element Type 2 !!!
KEYOPT,2,2,0 !!! Elements Used to Distribute
KEYOPT,2,6,0 !!! Load evenly on Model
KEYOPT,2,7,0
KEYOPT,2,9,0
KEYOPT,2,10,0
```

```
! Real Constants for Beams
! area,Iy,Iz,ty,tz,J
R,1,pi*rm*rm,1000*pi*rm*rm*rm*rm/4,1000*pi*rm*rm*rm*rm/4,2*rm,2*rm,0,
RMORE,0,1000*pi*rm*rm*rm*rm/2,0,0,0,0,
```

```
ET,3,SHELL93 !!! Element Type 3 !!!
KEYOPT,3,4,0 !!! Temporary Element Used
KEYOPT,3,5,0 !!! In meshing process
KEYOPT,3,6,0
```

```
!!! Material Properties
mp,ex,1,105E9 !!! For Brass
mp,nuxy,1,0.33 !!! Young's Modulus
mp,ex,2,1E21 !!! For Fictional Elements
mp,nuxy,2,0.3
```

```
type,3
mat,1
```

```
!!! Setting up KeyPoints and Meshing
!!! Area 1
k,, !!! Key Points in mm Dimensions !!!
k,,t,0
k,,t+r,r
k,,t+r,0
l,1,2
larc,2,3,4,r
kdele,4
k,,t+r,t+r
k,,0,t+r
l,3,4
l,4,5
l,5,1
lesize,1,,l1
lesize,2,,l2,1.2
lesize,3,,l3
lesize,4,,l4
lesize,5,,l5,
al,1,2,3,4,5
amap,1,1,2,3,4
```

```
!!! Area 2
k,,w,r
k,,w,t+r
l,3,6
l,6,7
l,7,4
al,3,6,7,8
lesize,6,,l6
lesize,7,,l7
lesize,8,,l8
amesh,2
```

```
!!! Area 3
k,,w,r+h1
k,,0,r+h1
l,7,8
```

```
1,8,9
1,9,5
lesize,10,,110
lesize,9,,19
lesize,11,,111
al,4,8,9,10,11
amap,3,5,7,8,9
```

```
Type,1
mat,1
```

```
!!! Extruding 3D solid
k,,0,0,b
l,1,10
lesize,12,,112
vdrag,1,2,3,,12
aclear,all
```

```
!!! Reinforcing top with fictitious elements
!!! Results in evenly distributed load
type,2
mat,2
real,1
nsel,s,loc,y,r+h1
nsel,r,loc,z,0
*get,testx,node,0,count
*get,maxx,node,0,mxloc,x
nsel,s,loc,y,r+h1
nsel,r,loc,x,0
*get,testz,node,0,count
*get,maxz,node,0,mxloc,z
*dim,nlx,,(testx+1)/2
*dim,nlz,,(testz+1)/2
*do,k,1,(testz+1)/2,1 !!! Creating Beam Elements For Top
*do,i,1,(testx+1)/2,1
nsel,s,loc,y,r+h1
nsel,r,loc,z,(k-1)*2*maxz/(testz-1)
nsel,r,loc,x,(i-1)*2*maxx/(testx-1)
*get,nlx(i),node,0,num,max
*enddo
nsel,all
*do,j,1,(testx-1)/2,1
e,nlx(j),nlx(j+1)
*enddo
*enddo

*do,k,1,(testx+1)/2,1 !!! Creating Beam Elements For Top
```

```

*do,i,1,(testz+1)/2,1
nselect,s,loc,y,r+h1
nselect,r,loc,x,(k-1)*2*maxx/(testx-1)
nselect,r,loc,z,(i-1)*2*maxz/(testz-1)
*get,nlz(i),node,0,num,max
*enddo
nselect,all
*do,j,1,(testz-1)/2,1
e,nlz(j),nlz(j+1)
*enddo
*enddo

!!! Expanding xz plane of symmetry VSYMM,Y,all, , , ,0,0
nummrg,all,0.001*mm,0.001*mm,low
NUMCMP,NODE

!!! Getting Top and Center Node Number
nselect,s,loc,y,r+h1
nselect,r,loc,x,0
nselect,r,loc,z,0
*get,unno,node,0,num,max

nselect,s,loc,x,0 !!! Fixing Center Node
dsym,asym,x
nselect,s,loc,z,0
dsym,symm,z
nselect,s,loc,y,-(r+h1)
d,all,all
nselect,all
fini

/solu
/pbc,all,0
ANTYPE,STATIC,NEW
F,unno,mz,m1
F,unno,fx,f1
solve
fini

/post1
PLNSOL,S,y,1,1
nselect,s,y
*get,symax,sort,0,max
nselect
*get,theta,node,unno,rot,z
*get,disp,node,unno,u,x

```

B.3 EBM Verification Model

```
/title, EBM Representation of Hinge
/prep7
! Parameter Declarations
*SET,h1,7.396346742E-4 ! height 1 of ebm
*SET,L1,2.4958891087E-4 ! length 1 of ebm
*SET,h2,1.11429533452E-3 ! height 2 of ebm
*SET,rr,1.0E-3 ! Radius of hinge required for ebm
*SET,L2,rr-L1 ! height 2 of ebm
*SET,h,0.007 ! Width of rigid portion 1
*SET,w,10E-3 ! Width of rigid portion 2
*SET,b,10E-3 ! Depth of 3RRR mechanism

!!! Elements
ET,1,BEAM3
KEYOPT,1,6,1
KEYOPT,1,9,0
KEYOPT,1,10,1

!!! Reals
R,1,h1*b,h1*h1*h1*b/12,h1, , , , ! Reals ebm 1
R,2,h2*b,h2*h2*h2*b/12,h2, , , , ! Reals ebm 2
R,3,w*b,w*w*w*b/12,w, , , , ! Rigid link 1

!!! Material Properties
mp,ex,1,105E9 ! E for 3RRR
mp,nuxy,1,0.33
mp,dens,1,8750

n,1,,-rr-h
n,2,,-rr
n,3,,-L1
n,4,,
n,5,,L1
n,6,,rr
n,7,,rr+h

mat,1
type,1
real,3
e,1,2
real,2
e,2,3
```

```
real,1  
e,3,4  
e,4,5  
real,2  
e,5,6  
real,3  
e,6,7  
finish
```

```
/solu  
d,1,all,0  
f,7,mz,0  
f,7,fx,-24  
solve  
fini
```

```
/post1  
!!! This etable allow the user to see bending stress etable,sbyb,ls,3
```

Appendix C

3RRR Models

C.1 Introduction

This appendix contains the ANSYS scripts which will generate the models of the 3RRR mechanism as described in Chapter 6. The comments to the code appear after the “!” symbol. The models presented in this Appendix include, the 2–D model and the EBM model of the 3RRR mechanism.

C.2 2–D 3RRR Planar Model

```
/prep7
!!! Units in m,kg,N
!!! End-effector and PZT have to be scaled appropriately
!!! Because of the Unit Thickness applied to 3RRR for p-strain
!!! Parameters you may want to change !!!
!!! PZT Loads 0 - 250 N
*set,load1,250 !!! loading on PZT 1
*set,load2,250 !!! loading on PZT 2
*set,load3,250 !!! loading on PZT 3

*set,sb1,0 ! Stress Behavior switch: 0 pstress, 2 pstrain
!!! END of Changeable Parameters
```

```

*set,mm,1E-3 ! 1 mm
*SET,b,1 ! Scaled Depth for End Effector (10*original depth)
*set,b2,0.5 ! Scaled Depth for PZT actuator (10*original depth)
*SET,R,32E-3 ! Outer most Radius
*set,pi,acos(-1) ! PI
*set,l,9E-3 ! verticle distance from center to edge of main block
*SET,rr,1E-3 ! Radius of Hinge
*SET,h,10E-3 ! Width of rigid portion
*SET,t,0.8E-3 ! Thickness of hinge
*SET,g,(h-t-2*rr)/2 ! To center of radius for upper most hinges
*Set,w,8E-3 ! width of other rigid poriton
*SET,w2,5E-3 ! Width of PZT block
*SET,g2,(w-t-2*rr)/2 ! To center of radius for left most hinges
*SET,lab,17E-3 ! A verticle distance that defines distance from hinge 1 to 2
*SET,lbc,11E-3 ! A horizontal distance that defines distance form h 2 to 3
*SET,h1,l+rr+h/2+lab ! Time saver
*SET,h2,R-w-lbc ! Time saver
*SET,r0,4.5E-3 ! Offset to center of PZT block
*SET,h4,10E-3 ! End Effector Creation
*SET,pl,20E-3 ! Length of PZt
*set,rm,.0001 ! Micro Strength Fibers

```

!!! Elements

```

ET,1,PLANE82 ! Hinges
KEYOPT,1,3,sb1
et,2,plane2 ! Element for compliant mechanism
keyopt,2,3,0 ! ! Set to Plane Stress
ET,3,BEAM3 ! Element for End Effector
KEYOPT,3,6,1
KEYOPT,3,9,0
KEYOPT,3,10,0

```

!!! Real Constants

```

R,2,h4*b,h4*h4*h4*b/12,h4, , , ! Real for end effector
R,3,1E-12*pi*rm*rm,1E12*pi*rm*rm*rm*rm/4,1E-6*2*rm,0,0,0
R,4,b*w,b*w*w*w/12,w
R,5,b*w2,b*w2*w2*w2/12,w2
R,6,b*h,b*h*h*h/12,h

```

!! Material Properties

```

!! Compliant Mech
mp,ex,1,105E9
mp,nuxy,1,0.33
mp,dens,1,8.75E3

```

! End Effector

```

mp,ex,2,200e9
mp,nuxy,2,0.33

```

```

mp,dens,2,7.85E3

mp,ex,3,105E9 !!! For Fictional Elements
mp,nuxy,3,0

n, ! For end-effector later
!!! Building 1/4 of first hinge
k,1,r-g2,l
k,2,r-g2-rr,l+rr
k,3,r-g2,l+rr !!! Keypoint 3 for defining arc
k,4,r-g2-t/2-rr,l+rr
k,5,r-g2-t/2-rr,l-t/2
k,6,r-g2,l-t/2

larc,1,2,3,rr
l,2,4,6
l,4,5,8
l,5,6,8
l,6,1,6
lesize,1,,16

mat,1
type,1

al,1,2,3,4,5
amap,1,4,2,1,6
local,11,0,r-g2-t/2-rr,l+rr
csys,11

!!! Expanding to complete first hinge
arsym,x,1,,0
arsym,y,1,2,1,,0

!!! Merging nodes
nummrg,all,0.001*mm,.001*mm,low

!!! Generating other hinges for 1/3 of compliant mech
local,12,1,r-g2-t/2-r0,l+rr
csys,12
agen,2,1,4,1,,90,,0
csys,0
agen,1,5,8,1,-w/2-2*rr+r0,,,,1
agen,2,5,8,1,,lab+rr-r0,,0
agen,2,5,8,1,-lbc,lab+rr-r0,,0

k,58,R,l-t/2
k,59,R,l

```

k,60,R,l+2*rr
k,61,R,h1
k,62,R-w,h1
k,63,R-w-2*rr,h1
k,64,h2,h1
k,65,h2-2*rr,h1
k,66,h2-h-2*rr,h1
k,67,h2-h-2*rr,h1-h-2*mm
k,68,h2-2*rr,h1-h-2*mm
k,69,h2,h1-h
k,70,R-w-2*rr,h1-h
k,71,r-w-2*rr,l+r0+w2/2
k,72,r-w-2*rr-2*mm,l+r0+w2/2
k,73,r-w-2*rr-2*mm,l+r0-w2/2
k,74,r-w-2*rr,l+r0-w2/2
k,75,r-w,l+2*rr
k,78,pl,l+r0
k,80,r-w-2*rr-lbc-h/2,l+rr+lab
k,81,r-w-2*rr-lbc-h/2+3*mm,l+rr+lab-5*mm
k,82,r-w-2*rr-lbc-h/2-3*mm,l+rr+lab-5*mm
k,83,r-w+t/2,l+2*rr

l,1,59,4
l,59,58,6
l,58,6,4

al,5,65,66,67
amesh,17
csys,11
arsym,x,17
csys,0
l,12,60
l,60,61
l,61,62
l,62,28
l,33,9
l,22,83,4
l,83,17

!PZT offset
l,83,75,6
l,75,19,4

!!! First Link
lsel,s,,14,15
lsel,a,,18,21
lsel,a,,24

lsl,a,,,36,37
lsl,a,,,40,41
lsl,a,,,72,78
al,all
allsel

!!! Offset Area Created in First Link
al,25,77,79,80

!!! Upper Center
l,36,63
l,63,64
l,64,41
l,46,69
l,69,70
l,70,39
lsl,s,,,81,86,1
lsl,a,,,44,45
lsl,a,,,47,48
lsl,a,,,52,53
lsl,a,,,56,57
al,all
allsel

!!! Top Right
l,49,65
l,65,66
l,66,67
l,67,68
l,68,52
circle,80,2.5*mm
circle,81,1*mm
circle,82,1*mm

aclear,15,16
lsl,s,,,60,61
lsl,a,,,63,64
lsl,a,,,87,91
al,all
allsel
al,92,93,94,95
al,96,97,98,99
al,100,101,102,103
!!! Subtracting Boltholes
asba,22,23
asba,26,24
asba,22,25
!!! Remeshing Hinge

amap,15,43,42,49,51
amap,16,43,47,52,53

!!! PZT and mount

l,23,71
l,71,72
L,72,73,4
L,73,74
L,74,26
al,28,29,104,105,106,107,108,32,31
allsel

!!! Meshing

mat,1
type,2
!!! To change mesh-size
esize,5*mm
!!! First Link
lesize,76,,6
amesh,19
!!! Offset
type,1
amesh,20
!!! Top Center, Top Right and PZT mount
type,2
amesh,21
esize,,4
amesh,22
amesh,23
lsel,s,loc,x,pl
type,3
mat,3
real,3
lmesh,all
allsel
l,76,79,2
l,77,84,2
lsel,s,loc,x,r-lbc-2*rr-w-3/4*h,r-lbc-2*rr-w-1/4*h
lsel,r,loc,y,r-h/2+2.5*rr,r-h/2-2.5*rr
real,5
mat,2
lmesh,all
allsel

!!! generate entire 3rrr MECH using the egen command
nummrg,all,.001*mm,.001*mm,low

```

numcmp,node
Csys,1
egen,3,10000,all,,0,0,0,0,0,120
nummerg,all,.001*mm,.001*mm,low
numcmp,node
csys,0

```

!!! Shifting Element Coordinate System for PZTs 2 and 3

```
LOCAL,11,0,0,0,0,120, , ,1,1,
```

```
LOCAL,12,0,0,0,0,240, , ,1,1,
```

!!! Build the End-Effector

```

csys,0
nselect,s,loc,x,R-w-2*rr-lbc-h/2
nselect,r,loc,y,l+rr+lab
*get,en1,node,0,num,max
csys,11
nselect,s,loc,x,R-w-2*rr-lbc-h/2
nselect,r,loc,y,l+rr+lab
*get,en2,node,0,num,max
csys,12
nselect,s,loc,x,R-w-2*rr-lbc-h/2
nselect,r,loc,y,l+rr+lab
*get,en3,node,0,num,max
allsel
csys,0
type,3
real,2
mat,2
e,1,en1
e,1,en2
e,1,en3
e,en1,en2
e,en2,en3
e,en3,en1
eplot
finish

```

```

/solu
csys,0
nselect,s,loc,y,l-t/2
nselect,r,loc,x,r-w,r
d,all,all,0
csys,11
nselect,s,loc,y,l-t/2
nselect,r,loc,x,r-w,r
d,all,all,0
csys,12

```

```

nset,s,loc,y,l-t/2
nset,r,loc,x,r-w,r
d,all,all,0
csys,0
allsel
sbctran
csys,0
nset,s,loc,x,r-w-4*rr
nset,r,loc,y,l+r0
*get,f1,node,0,num,max
f,f1,fx,100*load1
csys,11
nset,s,loc,x,r-w-4*rr
nset,r,loc,y,l+r0
*get,f2,node,0,num,max
f,f2,fx,100*load2*cos(120/180*pi)
f,f2,fy,100*load2*sin(120/180*pi)
csys,12
nset,s,loc,x,r-w-4*rr
nset,r,loc,y,l+r0
*get,f2,node,0,num,max
f,f2,fx,100*load3*cos(240/180*pi)
f,f2,fy,100*load3*sin(240/180*pi)
allsel
csys,0
antype,static,new
time,0
solve
finish

/post1
get,yaw,Node,1,ROT,z
get,vy,node,1,u,y
get,vx,node,1,u,x

```

C.3 EBM 3RRR Model

```

/title, MMS as Beam Representation
/prep7
!!! Input by user !!!
!!! Piezo Loads !!!
!!! Input Force 0 - 250
*set,f1,250
*set,f2,250
*set,f3,250

```

```

! Parameter Declarations
*SET,h1,7.396E-4 ! height 1 of ebm
*SET,L1,2.496E-4 ! length 1 of ebm
*SET,h2,1.143E-3 ! height 2 of ebm
*SET,rr,1E-3 ! Radius of hinge required for ebm
*set,r3,1E-3
*SET,l2,r3-L1 ! height 2 of ebm
*SET,R,32E-3 ! Outer most point of 3RRR mech
*set,pi,acos(-1) ! PI
*set,l,9E-3 ! y-distance of first hinge
*SET,w2,5E-3 ! For Piezo Actuator
*Set,w3,2E-3 ! PZT block width
*SET,lab,17E-3 ! Veritcle Length from hinge 1 to 2
*SET,lbc,11E-3 ! Horizontal length from hinge 2 to 3
*SET,r0,4.5E-3 ! Offset for pzt mount from l
*SET,h3,8E-3 ! Width of rigid portion 1
*SET,h4,10E-3 ! Width of rigid portion 2
*SET,b,10E-3 ! Depth of 3RRR mechanism
*SET,q1,r3-rr
*SET,t,0.8E-3

!!! Elements
ET,1,BEAM3
KEYOPT,1,6,1
KEYOPT,1,9,0
KEYOPT,1,10,1

!!! Reals
R,1,h1*b,h1*h1*h1*b/12,h1, , , ! Reals ebm 1
R,2,h2*b,h2*h2*h2*b/12,h2, , , ! Reals ebm 2
R,3,h3*b,h3*h3*h3*b/12,h3, , , ! Rigid link 1
R,4,h4*b,h4*h4*h4*b/12,h4, , , ! Rigid link 2
R,5,b*w2,w2*w2*w2*b/12,w2, , , ! Real for PZT mount
R,6,w2*b,w2*w2*w2*b/12,w2,,,-8750*w2*b, ! Rigid link 1 with no mass
R,7,b*lbc,lbc*lbc*lbc*b/12,lbc, , , ! Real for End Effector
R,8,h4*b,h4*h4*h4*b/12,H4,,,-8750*h4*b, ! Real for massless Rigid 2

!!! Material Properties
mp,ex,1,105E9 ! E for 3RRR
mp,nuxy,1,0.33
mp,dens,1,8750

mp,ex,2,200E9 ! E for End Effector
mp,nuxy,2,0.33
mp,dens,2,7850

!!! Defining keypts

```

k,1,r-h3/2,l-q1
 k,2,r-h3/2,l-q1+l2
 k,3,r-h3/2,l-q1+l2+l1
 k,4,r-h3/2,l-q1+l2+2*l1
 k,5,r-h3/2,l-q1+2*l2+2*l1
 k,6,r-h3/2,l+r0
 k,7,r-h3+q1,l+r0
 k,8,r-h3+q1-l2,l+r0
 k,9,r-h3+q1-l2-l1,l+r0
 k,10,r-h3+q1-l2-2*l1,l+r0
 k,11,r-h3+q1-2*l2-2*l1,l+r0
 k,12,r-h3-2*rr-w3,l+r0
 k,13,r-h3/2,l+rr+lab
 k,14,r-h3/2,l+rr+lab+h4/2
 k,15,r-h3+q1,l+rr+lab
 k,16,r-h3-l2+q1,l+rr+lab
 k,17,r-h3-l2-l1+q1,l+rr+lab
 k,18,r-h3-l2-2*l1+q1,l+rr+lab
 k,19,r-h3-2*l2-2*l1+q1,l+rr+lab
 k,20,r-h3-lbc+q1,l+rr+lab
 k,21,r-h3-lbc-l2+q1,l+rr+lab
 k,22,r-h3-lbc-l2-l1+q1,l+rr+lab
 k,23,r-h3-lbc-l2-2*l1+q1,l+rr+lab
 k,24,r-h3-lbc-2*l2-2*l1+q1,l+rr+lab
 k,25,r-h3-lbc-2*rr-w2+2.5*rr,l+rr+lab
 k,26,r-h3-lbc-2*rr-w2,l+rr+lab
 k,27,r-h3-lbc-2*rr-w2-2.5*rr,l+rr+lab
 k,28,r-h3-lbc-2*rr-2*w2,l+rr+lab
 k,29,r-26*rr,r-h4/2+2.5*rr
 k,30,r-26*rr,r-h4/2-2.5*rr
 k,31,r-26*rr,r
 k,32,r-26*rr,r-h4-2*rr
 k,33,r-h3/2,l-t/2
 !!! Making all keypoints into nodes nkpt,all,all

!!! Making Elements type,1
 mat,1
 real,2
 e,1,2
 real,1
 e,2,3
 e,3,4
 real,2
 e,4,5
 real,3
 e,5,6
 real,6
 e,6,7

real,2
e,7,8
real,1
e,8,9
e,9,10
real,2
e,10,11
real,5
e,11,12
real,3
e,6,13
e,13,14
real,8
e,13,15
real,2
e,15,16
real,1
e,16,17
e,17,18
real,2
e,18,19
real,4
e,19,20
real,2
e,20,21
real,1
e,21,22
e,22,23
real,2
e,23,24
real,4
e,24,25
e,27,28
e,29,31
e,30,32
real,5
mat,2
e,25,26
e,26,27
e,26,29
e,26,30
mat,1
real,3
e,1,33

csys,1
!!! Generating entire 3RRR MEch !!!
egen,3,33,all,,0,0,0,0,0,,120

```
!!! Building End-Effector
```

```
n,100,0,0,0
```

```
mat,2
```

```
real,7
```

```
e,26,100
```

```
e,59,100
```

```
e,92,100
```

```
e,26,59
```

```
e,59,92
```

```
e,92,26
```

```
/solu
```

```
!!! Constraints
```

```
nsl,s,,33,99,33
```

```
d,all,all,0
```

```
allsel
```

```
!!! Applying Loads
```

```
f,12,fx,f1
```

```
f,45,fx,f2*cos(120/180*pi)
```

```
f,45,fy,f2*sin(120/180*pi)
```

```
f,78,fx,f3*cos(120/180*pi)
```

```
f,78,fy,f3*sin(240/180*pi)
```

```
!!! Solving
```

```
antype,static,new
```

```
solve
```

```
finish
```

```
/post1
```

```
etable,sbyt,ls,2
```

```
etable,sbyb,ls,3
```

```
*get,yaw,Node,100,ROT,z
```

```
*get,vy,node,100,u,y
```

```
*get,vx,node,100,u,x
```

```
fini
```